



MOMENTUM TRANSFER CONTINUUM BETWEEN PRESHAPE AND  
GRASPING BASED ON FLUIDICS

A THESIS SUBMITTED TO  
THE GRADUATE SCHOOL OF NATURAL AND APPLIED SCIENCES  
OF  
MIDDLE EAST TECHNICAL UNIVERSITY

BY

BARIŞ ÖZYER

IN PARTIAL FULFILLMENT OF THE REQUIREMENTS  
FOR  
THE DEGREE OF DOCTOR OF PHILOSOPHY  
IN  
ELECTRICAL AND ELECTRONICS ENGINEERING

OCTOBER 2012

Approval of the thesis:

**MOMENTUM TRANSFER CONTINUUM BETWEEN PRESHAPE AND  
GRASPING BASED ON FLUIDICS**

submitted by **BARIŞ ÖZYER** in partial fulfillment of the requirements for the degree of **Doctor of Philosophy in Electrical and Electronics Engineering Department, Middle East Technical University** by,

Prof. Dr. Canan Özgen  
Dean, Graduate School of **Natural and Applied Sciences** \_\_\_\_\_

Prof. Dr. İsmet Erkmen  
Head of Department, **Electrical and Electronics Engineering** \_\_\_\_\_

Prof. Dr. İsmet Erkmen  
Supervisor, **Electrical and Electronics Eng. Dept., METU** \_\_\_\_\_

Prof. Dr. Aydan M. Erkmen  
Co-supervisor, **Electrical and Electronics Eng. Dept., METU** \_\_\_\_\_

**Examining Committee Members:**

Prof. Dr. Erol Kocaođlan  
Electrical and Electronics Eng. Dept., METU \_\_\_\_\_

Prof. Dr. İsmet Erkmen  
Electrical and Electronics Eng. Dept., METU \_\_\_\_\_

Assoc. Prof. Dr. Duygun Erol Barkana  
Electrical and Electronics Eng. Dept., Yeditepe Univ. \_\_\_\_\_

Prof. Dr. Veysel Gazi  
Electrical and Electronics Eng. Dept., İKBU \_\_\_\_\_

Assist. Prof. Dr. Yiđit Yazıcıođlu  
Mechanical Engineering Dept., METU \_\_\_\_\_

**Date:** \_\_\_\_\_

**I hereby declare that all information in this document has been obtained and presented in accordance with academic rules and ethical conduct. I also declare that, as required by these rules and conduct, I have fully cited and referenced all material and results that are not original to this work.**

Name, Last Name: BARIŞ ÖZYER

Signature :



## ABSTRACT

### MOMENTUM TRANSFER CONTINUUM BETWEEN PRESHAPE AND GRASPING BASED ON FLUIDICS

Özyer, Barış

Ph.D., Department of Electrical and Electronics Engineering

Supervisor : Prof. Dr. İsmet Erkmen

Co-Supervisor : Prof. Dr. Aydan M. Erkmen

October 2012, 108 pages

This dissertation propose a new fluidics based framework to determine a continuum between preshaping and grasping so as to appropriately preshape a multi-fingered robot hand for creating an optimal initialization of grasp. The continuum of a hand preshape closing upon an object that creates an initial object motion tendency of the object based on the impact moment patterns generated from the fingers is presented. These motion tendencies should then be suitable for the proper initiation of the grasping task. The aim is motivated by human like behavior where we preshape and land on an object to initiate a certain grasping behavior without losing the continuum during the "preshaping to grasping" phases.

The continuity of momentum transfer phenomena is inspired by fluid dynamics that deals with fluid flow. We have adapted governing equations based on the physical principles of the fluid flow to generate momentum transfer from the robotic fingers, closing upon the object surface to fluid medium particles then from these fluid medium particles to the grasping object. Smoothed Particular Hydrodynamics (SPH)

which is a mesh free particle method and finite volume approximation is used to analyze fluid flow equations. The fingers of the robotic hand and object are modeled by solidified fluid elements and also can be compliance.

For evaluating the optimal grasp initialization of different hand preshape, we propose a decision support system consisting of artificial feed forward neural network based on the moment distribution on the object determines either : 1) given initial position and orientation of a robot hand, what preshape is suitable for generating a desired moment distribution on the surface of a given object in order to trigger a desired rotation in a desired direction when approaching with this preshaped hand or 2) given a predetermined hand preshape what initial position, orientation and hand aperture are suitable to generate a desired rotation upon approach and without causing the retroceding of the object.

Keywords: grasping, hand preshaping, multi-fingered robothand, computational fluid dynamics

## ÖZ

### AKIŞKAN DİNAMİĞİNE BAĞLI OLARAK ÖN-ŞEKİL VE KAVRAMA ARASINDAKİ MOMENTUM SÜREKLİLİĞİ AKTARIMI

Özyer, Barış

Doktora, Elektrik ve Elektronik Mühendisliği Bölümü

Tez Yöneticisi : Prof. Dr. İsmet Erkmen

Ortak Tez Yöneticisi : Prof. Dr. Aydan M. Erkmen

Ekim 2012, 108 sayfa

Bu tez, çok robot parmaklı robot eli ile bir nesneyi kavramak için nesne üzerine doğru hareket ederkenki elin aldığı ön şekli ile kavrama anındaki şekli arasındaki sürekliliği tanımlamak için akışkan tabanlı yeni bir çerçeve önermektedir. Elin ön şeklinin nesne yüzeyine doğru kapanırken parmaklar tarafından yaratılan moment örüntüsü, nesne hareket yönelimine neden olur. Bu hareket yönelimleri, nesneyi belir bir görev ile kavramak için yaklaşırken, harekete başladığı durumdaki el şekli ile uyumlu olması gerekmektedir. Amacımız, elin nesneyi belirli bir amaç ile kavramak için nesneye yaklaşırkenki almış olduğu şekillerin, hareket boyunca sürekliliğini kaybetmeden, insan davranışlarına benzer bir şekilde modellemesidir.

Momentum aktarımı fenomeninin sürekliliği, akışkanların akışını inceleyen akışkanlar dinamiği teorisinden esinlenmiştir. Biz, öncelikle parmaklar tarafından akışkan ortamdaki parçacıklara, sonra bu parçacıklardan nesne üzerindeki parçacıklara aktarılan momentumu yaratmak için akışkan akışını modelleyen fiziksel denklemleri kendi problemimize adapte ettik. Serbest örgü yöntemi olan hesaplamalı akışkanlar di-

namığı ve sonlu hacim yaklaşımı, akışkanlar akışı denklemlerini analiz etmekte kullanıldı. Parmaklar ve nesne katılaştırılmış akışkan parçacıkları ile modellendi. Bu parçacıklar aynı zamanda deforme edilebilir.

Farklı el ön şekillerinin en uygun şekilde kavramaya başlamasının hesaplanması için, biz nesne üzerinde yaratılan moment dağılımlarına bağlı olarak ileri yönlü beslenen, yapay sinir ağı içeren, karar destek sistemi önerdik. Denetleyici belirtilen iki durumu ifade eder 1) durumu ve yönelimi belirli olan robot elin hangi el şekli ile nesneye doğru yaklaşsın, nesneye verilmesi istenen hareket eğilimi istenilen yönde gerçekleşsin 2) daha önceden belirlenmiş el şekli ile hangi konum, yönelim ve el açıklığı ile yaklaşılmalı ki nesneye istenilen dönel hareket eğilimi verilebilsin.

Anahtar Kelimeler: nesne kavrama, el ön şekli, çok parmaklı robot el, hesaplamalı akışkanlar dinamiği

*To my lovely wife*

## ACKNOWLEDGMENTS

Firstly, I would like to express my deepest grateful to my thesis advisor Prof.Dr. İsmet Erkmen and coadvisor Prof.Dr. Aydan M. Erkmen for their extraordinary support and guidance during my thesis. They always encourage me attempt not only to learn the theory of control and robotics in engineering aspect but also to adapt different methodologies to robotic side. I am impressed by their innovative approaches to the challenging problem. For that reason, I have been able to look at the problems in different ways and become familiar with different research areas.

Thanks to my thesis committee, Prof. Dr. Erol Kocaođlan and Associate Prof. Dr. Duygun Erol Barkana, for all the meetings they guide and support my progress and also thanks to Prof. Dr. Veysel Gazi for attending my all meetings during my thesis and giving the motivation for hard times.

I would like to thank my friend Umut Tilki, Sebahattin Topal, Sedat Dođru and Akif Durdu, in the Mechatronic Laboratory for their brainstorming and collaboration. Aspecially, Umut and Sebahattin, we all share most of the hardworking times together in the laboratory. We have discussed on our research problems for hours and encouraged us to motivate all times.

I started doing doctorate thesis with my friends at the same time. We had good memories and shared beautiful times during this period. I would like to thank all Yılmaz Kalkan, Evren Ekmekçi, Atilla Dönük, Hayrettin Yüzer, Reyhan Tutuk, Feza Çarлак, Levent Bayındır, Alev Mutlu and Mert Kolaylı for their friendly support.

I would like to thank Mitsuo Kawato and Gordon Cheng for providing me a chance to work in Department of Humanoid Robotics and Computational Neuroscience Laboratories, ATR, Japan. It was a really important experience for me to be a part of the laboratory. I would like to thank also HRCN members Michael Mistry, Joshua G. Hale, Sang-Ho Hyon, Jun Morimoto, Ales Ude, Joseph Hart, Takamitsu Matsubara, Jan Moren and Jan Babic for their friendships. I would like to give special thanks to

Erhan Öztop with whom I closely worked in Japan. He always supported and helped me for everything.

My friends Aykut Erdem, Erkut Erdem, Ruken Çakıcı, Oğuzhan Oğuz, Hasan Basri Arifoğlu, thanks a lot for your being with me and friendships.

My parents Gülten and Yücel , as well as my elder sisters Arzu and Sevinç deserve spacial thanks for their kindness, love and encouragement through the years.

Finally, I would like to give my very special thanks to my wife Gülşah for her love, support and being always with me in hard times. In fact, this thesis cannot be completed without her.

# TABLE OF CONTENTS

ABSTRACT . . . . .	iv
ÖZ . . . . .	vi
ACKNOWLEDGMENTS . . . . .	ix
TABLE OF CONTENTS . . . . .	xi
LIST OF TABLES . . . . .	xiv
LIST OF FIGURES . . . . .	xv
CHAPTERS	
1 INTRODUCTION . . . . .	1
1.1 Motivation and Objective . . . . .	1
1.2 Methodology . . . . .	2
1.3 Contribution . . . . .	3
1.4 Outline Thesis . . . . .	4
2 LITERATURE SURVEY . . . . .	6
2.1 Human Grasping . . . . .	6
2.2 Robotic Grasping . . . . .	10
2.2.1 Anthropomorphic Robotic Grasping . . . . .	10
2.2.2 Intelligent Grasping in robots . . . . .	11
2.2.3 Analytical approach for robotic grasping . . . . .	12
2.2.4 Continuity of hand preshaping considering momentum transfer . . . . .	14
2.3 Underwater Robotics . . . . .	14
2.4 Fluidics in Robotics . . . . .	15
3 MATHEMATICAL BACKGROUND . . . . .	17



3.1	Fundamentals of computational fluid dynamics . . . . .	17
3.1.1	Continuity Equation . . . . .	20
3.1.2	Momentum Conservation . . . . .	20
3.1.3	Energy Conservation . . . . .	21
3.2	Finite Volume Method for Solving Governing Equations . . . . .	23
3.2.1	Domain Discretization . . . . .	23
3.2.2	Discretization of Governing Equation . . . . .	24
3.2.3	Discretization for Convection and Diffusion . . . . .	28
3.3	Solution of steady-State fluid flows . . . . .	29
4	<b>MOMENTUM TRANSFER FROM FINGERS TO OBJECT IN UNDERWATER</b> . . . . .	33
4.1	Analysis of Underwater Grasping . . . . .	33
4.2	Problem Definition . . . . .	34
4.3	Methodology . . . . .	36
4.3.1	Adapting computational fluid dynamics model to our problem . . . . .	36
4.3.2	Preprocessing . . . . .	38
4.3.3	Fingers Motion . . . . .	40
4.3.4	Object Motion . . . . .	40
4.3.5	Momentum transfer for different preshapes . . . . .	43
4.3.6	Simulation Results . . . . .	43
4.3.7	Examples of rotating motion tendencies of object . . . . .	52
4.3.8	Compliance fingers and object modeled as solidified fluid elements . . . . .	55
4.4	Sensitivity analysis . . . . .	58
4.5	Conclusion . . . . .	61
5	<b>APPROACH CONTROL FOR UNDERWATER GRASPING</b> . . . . .	62
5.1	Structure of the Approach Controller . . . . .	62
5.1.1	First Goal of the controller: Determining the robot preshape for a desired moment distribution on object . . . . .	63

5.1.2	Second Goal of the Controller: Determining the initial condition of the robot preshape towards triggering a desired moment distribution on a given object . . . . .	68
6	DIPPING FINGERS INTO THE WATER TOWARDS A FULLY IMMERSED OBJECT . . . . .	76
6.1	Problem Definition . . . . .	77
6.2	Smoothed Particle Hydrodynamics (SPH) Fundamentals . . . . .	78
6.3	Modeling Simple Two Fingers Preshapes . . . . .	81
6.3.1	Modeling Solid Objects . . . . .	83
6.3.2	Modeling our solid fluid interaction . . . . .	83
6.4	Simulations . . . . .	85
6.5	Conclusions . . . . .	94
7	CONCLUSION and FUTURE WORK . . . . .	95
7.1	Future Work . . . . .	97
	REFERENCES . . . . .	99
	CURRICULUM VITAE . . . . .	107

## LIST OF TABLES

### TABLES

Table 4.1	Momentum Distribution on the rotating square object . . . . .	52
Table 5.1	The error between desired and actual moment at the center of gravity of the square object. . . . .	65
Table 5.2	Constructing Data Set for Decision Support System . . . . .	66
Table 5.3	The error between desired and actual moment at the center of gravity of the square object for Figure 5.2(a) . . . . .	66

# LIST OF FIGURES

## FIGURES

Figure 2.1 The human hand preshapes apertures opening and closing during reaching to object [13]. . . . .	8
Figure 2.2 Human grasping classification proposed by Napier [19]. . . . .	9
Figure 2.3 Virtual finger model proposed for different human prehension [25].	10
Figure 3.1 Fluid particle at macroscopic length scale [96] . . . . .	18
Figure 3.2 Discretized computational domain by mesh [97] . . . . .	24
Figure 3.3 One dimensional grid domain . . . . .	25
Figure 3.4 Two dimensional grid domain . . . . .	26
Figure 3.5 Three dimensional grid domain [96] . . . . .	28
Figure 3.6 Staggered grid for two dimensional domain taken from [96] . . . .	31
Figure 4.1 Two dimensional grid representation of the fluid environment . . .	37
Figure 4.2 Solid object and manipulator . . . . .	39
Figure 4.3 Flow chart of the simulation . . . . .	42
Figure 4.4 represent the contours of velocity for square object in different time step (a) $t=0.02$ (b) $t= 0.18$ (c) $t=0.40$ . . . . .	46
Figure 4.5 Moment distribution (a) top and (b) bottom surfaces of the square object . . . . .	47
Figure 4.6 Total moment at the center of gravity of the square object . . . . .	48
Figure 4.7 Contours of velocity magnitude for circular object . . . . .	49
Figure 4.8 Total moment at the center of gravity of the circular object . . . . .	50

Figure 4.9 (a) represents velocity magnitude contours of different velocities of fingers landing on the object (b) moment of top and bottom surfaces of the object . . . . .	51
Figure 4.10 Contours of velocity magnitude for rotating square object . . . . .	53
Figure 4.11 Contours of velocity magnitude and total pressure for rotating square object at different time step from (a) to (e) . . . . .	54
Figure 4.12 Compliance of an object . . . . .	56
Figure 4.13 Finger compliance . . . . .	57
Figure 4.14 The total moment at the center of the square object for different finger velocities landing on an object . . . . .	59
Figure 4.15 The total moment at the center of the square object for different internal mesh size . . . . .	59
Figure 4.16 Velocity magnitude contour for different internal mesh size (a) 0.1 (b) 0.5 (c) 1 . . . . .	60
Figure 5.1 Samples of training for different object location (a) and (b) objects location changes along y-axis (c) and (d) object location changes along x-axis. . . . .	64
Figure 5.2 Analyzing data using back-propagation algorithm (a) momentum versus joint angles of the one link (b) momentum versus joint angles of the both two links . . . . .	67
Figure 5.3 Different orientation, preshape and aperture of fingers landing on the object . . . . .	70
Figure 5.4 Velocity magnitude contour for square object (a) desired moment distribution (b) actual moment distribution of best preshape (c) actual moment distribution of worse preshape . . . . .	71
Figure 5.5 Momentum distribution on top and bottom surfaces of the object (a) desired moment distribution (b) actual moment distribution of best preshape (c) actual moment distribution of worse preshape . . . . .	72
Figure 5.6 Error between the actual and desired output vectors . . . . .	73

Figure 5.7 3d velocity magnitude contour for cylindrical grasp (a) desired velocity magnitude contour motion tendencies of the object (b) actual velocity magnitude contour . . . . .	74
Figure 5.8 3d velocity magnitude contour for pinch grasp (a) desired velocity magnitude contour motion tendencies of the object (b) actual velocity magnitude contour . . . . .	75
Figure 6.1 1 DOF planar gripper . . . . .	82
Figure 6.2 The velocity vector for $i - th$ solidified particle on fingers . . . . .	84
Figure 6.3 Grid based listing neighbor particles . . . . .	86
Figure 6.4 Flow chart of Compressible SPH Program . . . . .	87
Figure 6.5 Fluidic environment including fluid particles represented by blue dots, robotic fingers red lines, objects black dots. It shows the particle positions during the fingers entry. The angle between the gripper $\theta$ is equal $80^0$ . . . . .	89
Figure 6.6 shows velocity fields of the particle upper side of the object at the end of the simulation. . . . .	90
Figure 6.7 (a) shows the magnitude and phase distribution of the velocity vectors applied on horizontal edge of the object. (b) shows the momentum around the center of gravity for each particle upper side of object . . . . .	91
Figure 6.8 Particle positions, phase, and magnitude of the velocity vectors and momentum around the center of gravity for different preshapes and position of the rectangular object. (a) Joint angle between the fingers is $80^0$ (b) shows the magnitude and phase distribution of the velocity vector on the object side(c) shows the momentum distribution around the center of gravity for each particle on the object side . . . . .	92
Figure 6.9 Particle positions, phase, and magnitude of the velocity vectors and momentum around the center of gravity for different preshapes and position of the rectangular object. (a) Joint angle between the fingers is $10^0$ (b) shows the magnitude and phase distribution of the velocity vector on the object side.(c) shows the momentum distribution around the center of gravity for each particle on the object side . . . . .	93

# CHAPTER 1

## INTRODUCTION

### 1.1 Motivation and Objective

Anthropomorphic dexterous multi-fingered manipulation of underwater objects requires planning of the approach orientation, aperture and velocity with a suitable hand preshape, much more than for an object outside the fluid medium. Any approach easily destabilizes an object suspended in fluid and imparts a motion to the object depending upon the preshape of hand, the approach initial distance and hand aperture together with the properties of the fluid medium. Taking a different perspective, in our work, we aim at triggering a motion on the object by the approaching phase of a preshaped robot hand that will be subsequently suitable to the initiation of a desired manipulation task after grasping. Consequently our specific objective in this thesis is to generate a desired moment distribution on an immersed object by the controlled approach of a hand preshape so that the generated moment triggers the desired object rotation and translation to be used as the initialization of the manipulation task of that object by the robot hand.

The literature abounds with works on the different phases of dexterous manipulation: grasp planning, approach, grasping and manipulation [1]-[4]. These works generally rely on heavy constraints brought to the grasping problem such as dexterity of the manipulator and object properties and provide solutions within this constrained framework [5]. However, last years have seen few attempts to bridge the everlasting gap between preshaping and landing on an object to grasp and manipulate [6]-[9]. Moreover, to the extent of our knowledge, no work has bridge this gap yet, within

the power of a single "preshaping to grasp" model. Our objective is to use fluidics to model momentum transfer phenomena and bridge within the continuum of a single model (namely fluid dynamics), all the phases from 1) preshaping of a multi-fingered hand during the approach of an object, 2) the initial momentum distribution generation on the object surfaces upon approach, leading to the preparation of the object for motion, 3) the actual landing of the fingers, initializing the task by the motion tendencies obtained from where the momentum transfer left off the approaching preshape now contacting the object.

## 1.2 Methodology

In this thesis, we propose a new fluidics based methodology to determine a continuum between preshaping and grasping so as to appropriately preshape a multi-fingered robot hand for creating an optimal initialization of grasp. We investigate the effects of impact forces and momentum transfer between different hand preshapes landing on an object. The continuity of momentum transfer phenomena is inspired by fluid dynamics that deals with fluid flows. The mathematical model of the fluid flows is based on three fundamental physical principles: conservation of mass, conservation momentum and conservation energy. By applying these principles to a fluid model, the governing equations of fluid dynamics are obtained. We have adapted the governing equations based on the physical principles of the fluid flows to generate the momentum transfer from the robotic fingers to the fluid medium then from the fluid medium to the grasping object. The fingers of the robotic hand and object are modeled by solidified fluid elements and thus can also be made compliant. Computational models are required to solve the governing equations otherwise these equations can not be solved analytically. Among these computational methods, Smoothed Particular Hydrodynamics (SPH) which is a mesh free particle method and finite volume approximation is used to analyze fluid flow equations. This approach provides a new model for analyzing the effect of the fingers motions landing on an object, firstly from fingers to the fluid medium and then from fluid medium to the object. We demonstrate a number of experiments for utilizing our fluidic based system on the different hand preshapes landing on the different objects. For evaluating the optimal grasp initial-



ization of different hand preshape, we propose a decision support system consisting of artificial feed forward neural network based on the momentum distribution on the object.

### **1.3 Contribution**

All the phases of grasping an object represented in the objective have not been handled in the literature within the continuum of a single model. Our contribution is to challenge bridging all the phases in a continuity using fluidics. Although our approach is valid for all environments, including air, in order to enhance the motivation and add visual value to our approach, we confine ourselves in this thesis to the approach of a preshaped robot hand towards an object suspended in an incompressible fluid medium such as water.

Robot hand and object are both immersed in the fluid medium. Momentum transfer from a preshaped multi-fingered hand to a fluid medium (air, water... etc.) and from the fluid medium to the object to be grasped within this medium always exist. The main issue is whether the fluid medium is incompressible or not and also whether the impact of the transferred momentum can influence the object so as to move it from its equilibrium way before contact. Dealing with approach to grasp an object suspended in incompressible fluid (here water) makes this momentum transfer critical even during a slow approach toward grasping. This criticality helps make our contribution visual which resides in the fluid based modeling of this momentum transfer from the phases of preshaping to approach, landing and grasping the object, all handled in a continuum within the same model.

Another advantage of our modeling perspective is to be able to model hand fingers and object as rigid (frozen) fluid elements. Consequently it is feasible within the model itself to enable soft object handling and flexibility in fingers so as to implement compliance in the grasp by relaxing this rigidity.

Moreover, we develop a neuro-controller that decides upon the hand preshape to be used for landing on the object, so that a desired moment distribution is created on the object during the approach. This decision is then carried out by initiating that hand

preshape from a given initial position and orientation. The controller also determines, in the case that a given hand preshape has to be adopted, what is the initial position, orientation and aperture of that given hand preshape so that a desired moment distribution is generated upon approach until the landing of the fingers on the object surfaces. This thesis specifically dwells with all these contributions, developing the momentum transfer model, generating the aforementioned controller, inserting compliance in the object, fingers whenever needed and demonstrates the performance of the proposed system. Sensitivity of the system is also analyzed within the perspective of the compliance.

The major contribution of this dissertation are summarized as follows:

- The development of the momentum transfer generated from the fingers upon landing on the object by adapting the continuity of the fluid flows and solid fluid interaction. This determines the momentum transfer continuum between preshaping and grasping of multi-fingered robot hand. This contribution provides optimal grasping strategies for robot hand before contacting an object.
- Modeling the initial effect of contact forces and moments onto the object that gives the initial rotation and translation tendencies due to momentum transfer upon impact.
- Generating the approach control system for grasping underwater in order to determine the optimal hand preshape for a given momentum distribution on the object surface.

#### **1.4 Outline Thesis**

In Chapter 2, the literature related with research on grasping by multi-fingered robot hand is reviewed. A brief overview of human grasping and anthropomorphic robotic grasping is presented. This includes analytical approaches of grasping, demonstrations of hand preshaping and fluidics in robotics.

Chapter 3 gives an overview of fundamental of computational fluid dynamics and finite volume approach for solving discrete governing equations, as a mathematical

for validation for our approach.

In Chapter 4, "Momentum transfer from preshape to grasping" concept is represented for initiating underwater the controlled motion tendencies on object to be grasped by the approach of a robot hand preshaped. We investigate, in this chapter, the effect of momentum transfer from the robot fingers to fluid medium, and from these medium to object surfaces that leads to rotational and translational motion tendencies. It includes also modelling of robot fingers and object as fluidic elements which rigidity can be relaxed to induce compliance.

In Chapter 5, we propose a novel concept of a controller that determines, given initial position and orientation of a robot hand, what hand preshape is suitable for generating a desired momentum distribution on the object surface. This chapter shows experimental results on how different hand preshapes initiated from different locations in the medium surrounding an object of different cross sections suspended in equilibrium in the fluid, affects its motion tendencies in terms of rotation and translation.

In Chapter 6, we model the dipping of the robot fingers into the water moving towards a fully immersed object in shallow water and demonstrate also the continuum of momentum transfer phenomena. Our proposed approach based on fluid particles is formalized and then demonstrated on experimental results through simulation. The methodology is inspired from water entry problem of free falling object. Smoothed particle hydrodynamics model (SPH) is used to simulate the general dynamic of fluid flows and momentum transfer between particles of different media. The fingers of the robotic hand are modeled by solidified fluid particles interacting with compressible surrounding fluids in which objects are defined as rigid-body solidified fluid particles. The interaction between the solid and fluid particles are represented. The developed model has been applied to the simulation of various simple robot hand preshaping and the generated momentum transfer profiles an object surface have been analyzed.

In Chapter 7, the thesis is concluded and provides suggestions for future work.

## CHAPTER 2

### LITERATURE SURVEY

The research on the grasping and manipulation of an object by multi-fingered robot hand have been studied in different aspect which is mostly inspired by biologically motivated model in the literature during the last decades. However, there is still a gap between preshaping and grasping in order to initialize hand preshaping. To close this gap, we use fluidic based approaches that provide the opportunity to analyze the effect of the momentum transfer for achieving successful grasping.

This chapter begins with a brief overview of some of the research on human grasping approaches in the literature. The model of human hand postures have been investigated by researchers to provide grasping strategies for robot hands. In the next section, we will review anthropomorphic robotic grasping that how human dexterity can be achieved by robotic manipulator. Next, the analytical approach for grasping an object is introduced. Finally, we will present briefly the works on the literature of fluidics in robotics.

#### **2.1 Human Grasping**

Human hands have great dexterity for grasping and manipulation of various shapes of an object. Thus, robotic researchers have been focused on biologically motivated approaches that can be used for complex grasping tasks by robot hand. In this section, we give an overview of human grasping including phases of human grasping and grasp taxonomies existent in the literature.

Human grasping can be described by two main phases: transportation and manipula-

tion [10]-[12]. Transportation means that the hand integrated with arm moves from initial position toward the desired target object [13]. On the other hand manipulation is adjusting hand postures under the applied forces to stabilize the object and undertake a task with it. While human hand is reaching to grasp an object, it adjusts hand preshapes before contacting on an object [11]. More research works [14]-[17] demonstrate that prehensile movement for human grasping need to coordinate that hand transport and preshape adjustment given in Figure 2.1. Preshape adjustments depend on feedback information from the environment based on human visual and sensing the object features. The object properties such as shape, size and weight called affordances also influence the grasping postures. Work in [14] represents an experimental study on hand movement over a curved trajectory while transportation to the target. This article specifies points on the trajectory called ‘via point’ that needs to be crossed during motion. The important finding in the experiment is that there is a delay for preshaping the hand into an appropriate grasping posture before passing the via point. The delay in hand apertures such as openings or closures uses the information of the hand transport to adjust the hand preshape. The studies that have investigated hand preshape also analyzed hand aperture which is the distance between the tips of the thumb and index finger [10]. This study shows that opening or closing hand aperture is based on the object size. In another study [15], the size of aperture of hand is found to be independent the object locations. These findings leads to the fact that hand preshapes are only based on distinctive properties of the object such as size and shape.

After the hand is preshaped, the grasp is applied to initialize closure phase. The grasping stage is relatively more complex than transportation because there are huge number of possibilities of hand preshapes in grasping an object. Grasping is basically considered as a set of fingers contacting the object with proper force distribution in order to stabilize the object under the control of hand movements.

In the literature, grasp taxonomies are achieved by classification of hand postures and have been studied in the field of rehabilitation and surgery. During the last decades, these grasp taxonomies have been applied in robotics and computer based simulations in order to provide different grasping strategies based on the object shape and manipulator types.

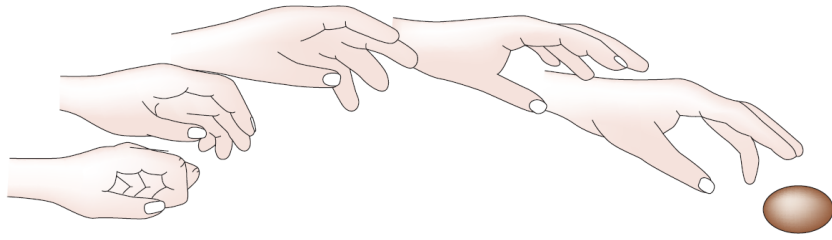


Figure 2.1: The human hand preshapes apertures opening and closing during reaching to object [13].

Primary studies on human grasping conducted by Schlesinger [18] classified human grasping into six different types: cylindrical, fingertip, hook, palmar, spherical and lateral. The taxonomy of Schlesinger classification is based on object surfaces such as cylindrical and spherical, hand surfaces such as fingertip, palmar and lateral and hand posture such as hook grasp. These classification is used to simplify the correlate between hand postures and object surfaces. However, achieving stable grasping which is needed to determine the necessary forces generated from the fingers are not considered in this study.

Later, the classification is extended by Napier [19] shown in Figure 2.2. That work classifies human grasping in two main groups: 1) power grasp 2) precision grasp. In the first group, the object can be held using palm and fingers. The stability and security is primarily considered in grasping an object. The contact area between object surfaces and hand postures is larger to achieving stable grasping in this case. On the other hand, thumb and the rest of four fingers can be used to hold the object for more complex task which determines the precision grasp. In this type of the grasp, dexterity is an important issue for grasping an object. Lyons [20] proposed definitions to determine three different grasp postures: encompass grasp, lateral grasp and precision grasp based on the shape and size of the object.

Followed by these researches, Cutkosky proposed a detailed taxonomy of human grasping based on the geometric properties of object such as shape and size to achieve prehensile movements[21]-[23]. These taxonomies have widely inspired robotic researchers nowadays. Power grasping and precision grasping proposed by Napier is

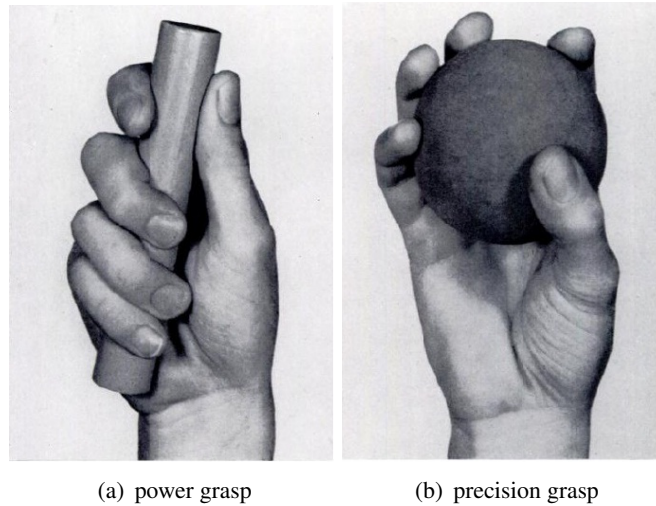


Figure 2.2: Human grasping classification proposed by Napier [19].

extended by subdividing the two coarse classes into different types of grasps. The relationship between object shapes, hand surfaces, hand shapes and forces are used to describe these grasp types. Task dependency in manipulation of objects have been considered to determine hand preshaping upon approach of an object to be grasped. Object geometry and manipulation task under appropriate forces is investigated to analyze and classify grasp choices. This is an important concept for robotic grasping because geometric properties of the object and task dependency are found to generate different hand preshaping and aperture types. As an instance, even if the task is same such that lifting an any object, the grasp type differs for different geometric properties of the object made of different material (glass or pencil)

Iberall [24],[25] and Arbib [26] proposed a virtual finger model that uses thumb and the rest for four fingers with palm to handle the opposite forces. In order to achieve successful grasping with human hand shown in Figure 2.3, the position of the virtual finger should be properly in coordination with the finger contacting the object. Three different hand preshapes are defined as pad opposition, palm opposition and side opposition as shown in Figure 2.3 from left to right [27]-[29]. The approximated contact points on object is determined by the virtual finger vectors represented as dashed lines. The opposition axis represented as solid line is required for achieving successful grasping. This proposed approach is used for generating different type of grasp posture.

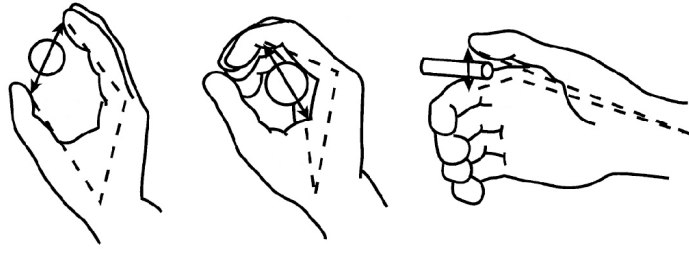


Figure 2.3: Virtual finger model proposed for different human prehension [25].

To summarize, when human hand approaches for landing on an object for given a task, it takes a hand preshape before contacting the object based on the object size and shape from visual feedback. Moreover, humans can reach for and grasp objects with a high level of flexibility and dexterity. Therefore, understanding human behavior is beneficial for robot skill transfer.

## 2.2 Robotic Grasping

The research study of grasping an object by robot hand has been conducted on many works over the last decades. This research area involves grasp analysis, synthesis and control schemes [30]. Recently, knowledge-based, control-based approaches and behavior based approaches that are comprised of biologically inspired approaches have been increasing interests for researchers.

### 2.2.1 Anthropomorphic Robotic Grasping

Anthropomorphism is basically defined as the dexterity of the robotic manipulator to observe and mimic human hand characteristics and dexterity. The dexterity is related to functionality of the manipulators [31]. In the literature, anthropomorphic manipulator exists with poor dexterity. They can perform very limited grasping tasks even if human like five- fingered robot hand have been developed during the last decades. Although it is difficult to gain dexterity close to humans in robots, anthropomorphism is a desirable goal in robotics, since human like robots will be involved in every part



of our lives, such as helping and assistance the disabled human, prosthetic arm and hand in medical fields.

In its most general sense, anthropomorphic robot grasping is divided into three main stages: object recognition, reaching for landing on that object and grasping like humans. Primarily the intrinsic properties of a target object such as location, size and shape have to be recognized [32]. Visuomotor system, widely that of a human, or mimicking human, encodes the object features and then generates a suitable hand preshaping shown in Figure 2.1 [13]. Hand preshaping and transporting are generally considered in the literature as two independent phases of reaching for landing on an object [33]. However, there is a continuous motion of the preshaped hand during reach, adjusting the hand aperture with respect to the object orientation and size while transporting the hand [10], [34]-[36]. Another approach proposed by Smeets uses minimum jerk hypothesis during orthogonal approach of finger and thumb to the surface of the target [37]. Minimum jerk hypothesis [38] represents mathematical model for the coordination of human planar two joint arm movement in order to determine the possible arm trajectories using dynamical optimization techniques. Moreover, the kinematic properties of arm transport based on the position and orientation of the target object and task have been studied considering force distribution among the fingers [39].

### **2.2.2 Intelligent Grasping in robots**

Although human can perform such a skillful grasping task easily, it is not easy to do so for robotic manipulators. One common way to obtain skillful robot behavior is to mimic human hand motion by motion capture system. There are several motion capture systems in order to get the human data. Data Glove and optic markers are widely used in the literature [40]-[43]. The motion capture system is equipped with several sensors. By the help of these sensors, the position and force information of the markers on the system are recorded. The human motion can be transferred to the robot in real time or offline after a series of data processing [44]. Recently, a large number of researches have focused on the popular studies known as learning by demonstration to achieve more complex task [45]. The tele-operation method that

indicate direct transmission of human dexterity is one way to teach complex task to robot [46]. In the process method, while the human hand can be used as master, robot is generally used as slave. Since the kinematic and dynamic properties of manipulator and human are different, the mapping procedure is used to transfer data. There are three different approaches to be used in mapping procedure in the literature. These are joint angle mapping, pose mapping and fingertip position mapping. Fingertip position mapping is more efficient than the others because the joint angles of manipulator can be calculated from the fingertip position by using inverse kinematic techniques. By the help of this technique, kinematic dissimilarities can be ignored. However, the sole use of tele-operation method or replicating the motion is not a suitable technique for learning the task by robot. The robot should be trained in order to give the answer of how to grasp an object within advanced intelligent control systems.

Robot have to be taught based on learning algorithms in order to perform and generate new biomimetic tasks. Reinforcement algorithm (RL) which is a well known algorithm, provides an optimal control methodology for generating new behaviors for robots. RL algorithm find a policy based on reward and punishment data received from environment. Although the dynamics of the system including manipulator and environment are not necessary to be known, the huge numbers of data collected from the task space give rise to inapplicable in real time learning systems [47]. Another approach, robot programming by demonstration, represented in [48] is that after human perform a task, system recognize the human grasping and then maps into manipulator. Here, the idea is to generate optimal grasping strategy based on the human demonstration. In addition to recognizing the human demonstration, object recognition and pose estimation combined by using visual and haptic feedback is used to generate the suitable grasping strategy in [49]-[52].

### **2.2.3 Analytical approach for robotic grasping**

A number of research which is inspired by human grasping have been studied during the last decades [53]-[58]. Traditionally, robotic grasping requires 1) determining the landing contact points or regions on the object surface [30], [59] 2) calculating finger position and palm direction determined from the hand posture via inverse kinematic

[60] 3) finding optimal forces and torques applied from the fingers to matching with the contact points [61]. The fundamental goal of grasping an object is to hold an object at the desired position for initializing the manipulation phase.

One approach taken by robotic researchers is to focus on stable grasping based on balancing external forces on a set of contact points on the object [62]. The capability of grasping an object have been tested by the concept of form and force closure [63]-[65]. Some researchers have focused on investigating the optimal grasp points on the object based on task, external forces and moments [66, 67]. In [68] and [70], the grasping force optimization problem is formulated based on a standard Euclidean gradient method and Dikin-type [68] recursion. M. Buss [69] proposed a gradient flow algorithm to optimize nonlinear friction forces constraints, which is equivalent to positive definite matrix, numerically tested on various friction models of point contact with Coulomb friction and soft contact. The studies have been carried out under the assumption that objects contact positions need to be fixed. However, in practice, position and orientation of the contact points on the object can be changed by exerting forces from fingers. Thus, the manipulator should generate a new strategy to grasp an object without sliding or deforming [71],[72]. J. Chen developed a control law to sliding and rolling contacts that satisfy asymptotically stability conditions of internal forces [73]. Zheng formulated dynamic control equations governing the motion of three fingered robot hand for three-dimensional space [71]. A.A. Cole has considered a control law for planar manipulators that achieve regrasping an object with sliding motion of the fingers [74]. A.M. Erkmén proposed a regrasping procedure as an optimal search problem based on genetic algorithm for five fingered robot hands [75]

As a summary, grasping an object is defined as a set of contact points on the surface of the object enclosed by an appropriate hand preshape. The robot hand has to reach contact points on object surfaces using inverse kinematics model matching these points with fingertips. Here, the problem is to find the optimal hand preshaping considering the applied forces and moments generated from the fingers in order to achieve successful grasping for a given task.

#### **2.2.4 Continuity of hand preshaping considering momentum transfer**

In addition to configure the appropriate hand preshaping, the momentum transferred to the robot during the pre-impact phase is another important issue for grasping an object [76]. However, momentum transfer from the approach to the landing and grasp initialization phase has not been considered in the literature for compressible fluid such as air since that medium absorbs most of the transfer to yield an object that seems to be unaffected by the hand approach momentum although its surfaces are bombarded by air particles. The same momentum transfer also exists for the case of incompressible fluids where this time, the phenomenon is visual and critical. The one case where this momentum transfer coupled to approach control is made visual in air when impaired human hand preshapes lead to loss of object stability due to momentum transfer upon landing, since disabled human who has prosthetic arm or hand, or those who cannot control their muscular and nervous system to realize a desired hand movement while approaching the object, gives uncontrolled, undesired motion tendencies to the object that has been just contacted [77]-[79]. At that time, a new grasping strategy is necessary to adjust hand preshapes for holding an object.

### **2.3 Underwater Robotics**

The robotic literature lacks to generally model the continuity of the phases between preshaping and grasping considering the momentum transfer phenomena. Our contribution in this thesis is to develop a fluidic based methodology to model this continuity and generate object motion tendencies. Since these object motion tendencies during the hand approach can be best made visual and demonstrated in incompressible fluid medium, we opt for water as the environment to which we apply our method. More specifically, we focus on momentum transfer between robot fingers modelled as solidified fluid particles to the water medium particles and from those particles to the object to be grasped, also suspended within water modelled as solidified fluid particles.

It is well known how difficult it is to manipulate an object with multi-fingered robot hands, underwater, because of the uncertainties in the control of the manipulator in the

fluid environment where the interaction between the manipulator and fluid medium needs to be modelled [80]-[82]. In the literature, most of the research works focus on the control of the manipulator via tele-operation in a master slave configuration [83],[84]. Due to the external disturbances such as drag forces, waves and currents and the continuity of the momentum transfer produced by the fingers, the operator remotely controls the manipulator and handles the disturbances by observing the object to be grasped at all phases of the approach and grasping. Several type of underwater manipulator has been designed to accomplish sophisticated operations [85]-[87]. The robot hand HEU Hand II and AMADEUS dextrous manipulator are such examples that have been developed with force sensors mounted at each fingertip for grasping objects in poorly visible fluid medium. A comprehensive survey for underwater robots can be found in [88].

## **2.4 Fluidics in Robotics**

In recent years, fluidic based approaches have been brought to the attention of more and more roboticists, especially in the field of coordination control in swarm robotics [89]. A new algorithm is presented to determine the localization of distributed swarm robots based on the fluid dynamics [90]. There is another work conducted by Shimizu points out the fact that the coherence of the swarm mobile robots is obtained without losing the connectivity of the shape in unstructured environment[91]. In the work [92], Kerr proposes a model based on the fundamentals of gas flow to obtain the obstacle avoidance for swarm mobile robots moving along the bounded region. Smoothed particle hydrodynamics (SPH) method which is basically a particle based model is used to control the motion of the swarm robots[93]. Unlike swarm robotics, SPH is used to imitate human hand preshapes in the correspondence problem where two different dynamic imitate each other [94]. We proposed and implemented a new model based on SPH for determining the continuum between preshaping and grasping [95]. Here, the computational fluid dynamic tool has been adapted for the simulation of the virtual environment, fluid flows and interaction between the fluidic medium and solid objects motions.

As a summary, the vast majority of approaches in the literature deals with the robotic

grasping problem after that contact occurs [62]-[72]. In fact, adjusting hand posture for grasping an object for a given manipulation task begins on pre-contact phase of grasp preparation like human grasping [8, 9]. However, It is missing in the robotic literature to model the continuity of the phases between preshaping and grasping. In this thesis, we focused on analyzing the momentum transfer as a continuum from approaching the object with a preshaped leading to bridge for transferring a momentum until object upon in underwater.

## CHAPTER 3

### MATHEMATICAL BACKGROUND

This chapter gives a brief overview of the mathematical background of the computational fluid dynamics for better understanding of the proposed approach in the next chapters. This chapter is adapted from the book [96] and survey [97] related with fundamentals of computational fluid dynamics . The equations are taken from the same book [96] by Versteeg.

#### 3.1 Fundamentals of computational fluid dynamics

Computational fluid dynamics is a numerical method in order to simulate and analyze the fluid flow. Basically, fluid flow is represented by the governing equations based on the three fundamental physical principles:

- Mass conservation
- Momentum conservation
- Energy conservation

The fundamental issue for describing these equations is that fluid is continuum. The continuum approach assumes that materials (fluids) are composed of molecules in a very small volume. The continuity of fluid flow is analyzed at macroscopic scales in terms of fluid variables; velocity, pressure, density and temperature. These variables are represented as a function of time.

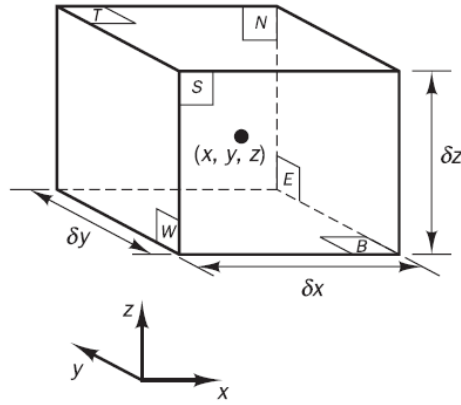


Figure 3.1: Fluid particle at macroscopic length scale [96]

A fluid particle is the smallest element of the fluid which is deformable and continuously distributed through the material. Figure 3.1 taken from [96] shows the such a infinitesimal fluid cell element at macroscopic scale. The fluid variables such as pressure denoted by  $p$ , density denoted by  $\rho$  are stored at the center of the particle  $(x, y, z)$ . The velocity vector  $\mathbf{u}$  of the particle are stored between the boundaries represented as N (North), S (South), E (East), W (West), T (Top), B (Bottom). For example,  $u$ -velocities along the  $x$ -axis are stored between W and E,  $v$ -velocities along the  $y$ -axis are stored between T and B boundaries.

There are two different type of equations, which are Eulerian and Lagrangian equations, to describe the fundamental physical governing equations. These equations cannot be solved analytically because of the nonlinearity. For that reason, the numerical solutions is necessary to analyze the fluid flow equations. Finite difference, finite element, finite volume method and particle based approach are used to approximate and discretize these governing equations. Before describing the discretization of the domain, we introduce how to derive these fundamental governing equations in Lagrangian form.

The time rate of change of fluid particle variables is obtained by using substantial derivatives represented by the following equation,



$$\frac{D\phi}{Dt} = \frac{\partial(\phi)}{\partial t} + \frac{\partial\phi}{\partial x} \frac{dx}{dt} + \frac{\partial\phi}{\partial y} \frac{dy}{dt} + \frac{\partial\phi}{\partial z} \frac{dz}{dt} \quad (3.1)$$

where  $dx/dt = u$ ,  $dy/dt = v$ ,  $dz/dt = w$  and then Eq.(3.1) is rewritten as

$$\frac{D\phi}{Dt} = \frac{\partial(\phi)}{\partial t} + u \frac{\partial\phi}{\partial x} + v \frac{\partial\phi}{\partial y} + w \frac{\partial\phi}{\partial z} = \frac{\partial(\phi)}{\partial t} + \mathbf{u} \cdot \text{grad}(\phi) \quad (3.2)$$

where  $\frac{D\phi}{Dt}$  represents the change of the fluid variables over time. This means that the time rate of change of fluid variables are caused by the movement across the boundaries per unit volume for each fluid particles.

In the case of mass conversion equation, the rate change of density  $\rho$  per unit volume for a fluid particle is obtained by the following equation,

$$\rho \frac{D\phi}{Dt} = \rho \left( \frac{\partial\phi}{\partial t} + \mathbf{u} \cdot \text{grad}(\phi) \right) \quad (3.3)$$

where the substantive derivative of  $\phi$  is multiplied by density  $\rho$ . Then the equation is rewritten as,

$$\begin{aligned} \frac{\partial\rho\phi}{\partial t} + \nabla(\rho\phi\mathbf{u}) &= \rho \left[ \frac{\partial\phi}{\partial t} + \mathbf{u} \cdot \text{grad}(\phi) \right] + \phi \left[ \frac{\partial\rho}{\partial t} + \nabla(\rho\mathbf{u}) \right] \\ &= \rho \frac{D\phi}{Dt} \end{aligned} \quad (3.4)$$

where the second term in the left hand side of the equation is zero because of the mass conversation. Therefore, the general of momentum and energy equation is obtained by replacing the quantity of  $\rho$  as below,

$$\begin{aligned}
x - \text{momentum} & \quad \rho \frac{Du}{Dt} = \frac{\partial \rho u}{\partial t} + \nabla(\rho u u) \\
y - \text{momentum} & \quad \rho \frac{Dv}{Dt} = \frac{\partial \rho v}{\partial t} + \nabla(\rho v u) \\
z - \text{momentum} & \quad \rho \frac{Dw}{Dt} = \frac{\partial \rho w}{\partial t} + \nabla(\rho w u) \\
\text{energy} & \quad \rho \frac{DE}{Dt} = \frac{\partial \phi E}{\partial t} + \nabla(\rho E u)
\end{aligned} \tag{3.5}$$

### 3.1.1 Continuity Equation

The continuity equation is derived from the mass conservation that represents the time rate of mass change is zero as the fluid particle moves along the flow. The equation is given by,

$$\frac{\partial \rho}{\partial t} + \nabla(\rho u) = 0 \tag{3.6}$$

where  $t$  is time,  $\rho$  is the density,  $u$  is the velocity,  $\nabla$  is the divergence operator represented as,

$$\nabla(\rho u) = \frac{\partial(\rho u)}{\partial x} + \frac{\partial(\rho v)}{\partial y} + \frac{\partial(\rho w)}{\partial z} \tag{3.7}$$

The sum of changes of the density and divergence velocity is equal to zero meaning that the change of mass of the fluid particles is constant over time along the fluid flow.

### 3.1.2 Momentum Conservation

The momentum conservation, Newton Second Law, refers that the total forces acting on the fluid particles is equal to the rate of change of fluid particle along the fluid flow. These forces is divided into two types: 1) surface forces such as pressure forces, viscous forces, gravity forces 2) body forces such as centrifugal force, and electromagnetic force. The continuity of the fluid flow are achieved by applying these forces on

the surface of the particles. Hence, the momentum governing equation is represented in terms of the body forces, pressure and viscous stress components as below,

$$\begin{aligned}
x - \text{momentum} \quad \rho \frac{Du}{Dt} &= -\frac{\partial p}{\partial x} + \frac{\tau_{xx}}{\partial x} + \frac{\tau_{yx}}{\partial y} + \frac{\tau_{zx}}{\partial z} + F_x \\
y - \text{momentum} \quad \rho \frac{Dv}{Dt} &= -\frac{\partial p}{\partial y} + \frac{\tau_{yy}}{\partial y} + \frac{\tau_{zy}}{\partial z} + \frac{\tau_{xy}}{\partial x} + F_y \\
z - \text{momentum} \quad \rho \frac{Dw}{Dt} &= -\frac{\partial p}{\partial z} + \frac{\tau_{zz}}{\partial z} + \frac{\tau_{xz}}{\partial x} + \frac{\tau_{yz}}{\partial y} + F_z
\end{aligned} \tag{3.8}$$

where  $p$  is the pressure,  $\tau$  is the viscous stress and  $F$  is the body forces. As an example, the notation of the  $\tau_{xy}$  refers the direction of the viscous stress from  $y$ -direction on a surface normal to the  $x$ -direction.

The viscous component of the equation (3.8) is computed as below,

$$\begin{aligned}
\tau_{xx} &= 2\mu \frac{\partial u}{\partial x} + \lambda \nabla u & \tau_{yy} &= 2\mu \frac{\partial v}{\partial y} + \lambda \nabla v & \tau_{zz} &= 2\mu \frac{\partial w}{\partial z} + \lambda \nabla w \\
\tau_{xy} = \tau_{yx} &= \mu \left( \frac{\partial u}{\partial y} + \frac{\partial v}{\partial x} \right) & \tau_{xz} = \tau_{zx} &= \mu \left( \frac{\partial u}{\partial z} + \frac{\partial w}{\partial x} \right) & & \\
& & \tau_{yz} = \tau_{zy} &= \mu \left( \frac{\partial v}{\partial z} + \frac{\partial w}{\partial y} \right) & &
\end{aligned} \tag{3.9}$$

where  $\mu$  is the molecular viscosity for linear deformations and  $\lambda$  is the coefficient for volumetric deformations.

### 3.1.3 Energy Conservation

The energy conservation equation is the third physical principle that is derived from the first law of thermodynamics. Consider the fluid particle moving along the fluid flow, the rate of change of energy of the fluid particle is equal to the rate of heat into the fluid particle and the rate work done on the particles due to the surface forces. The energy equation is defined as

$$\rho \frac{DE}{Dt} = -\nabla(pu) + \left[ \frac{\partial(u\tau_{xx})}{\partial x} + \frac{\partial(u\tau_{yx})}{\partial y} + \frac{\partial(u\tau_{zx})}{\partial z} + \frac{\partial(v\tau_{xy})}{\partial x} + \frac{\partial(v\tau_{yy})}{\partial y} + \frac{\partial(v\tau_{zy})}{\partial z} + \frac{\partial(w\tau_{xy})}{\partial x} + \frac{\partial(w\tau_{zy})}{\partial z} + \nabla(kgradT) + S_E \right] \quad (3.10)$$

where  $E$  is the energy defined as the summation of internal energy  $e$  and kinetic energy  $u^2/2$  as  $E = e + \frac{1}{2}(u^2 + v^2 + w^2)$ ,  $k$  is constant of heat flux,  $T$  is the heat,  $S_E$  body force vector.

As a summary, the governing Navier-Stoke equations of fluid flow can be derived in the form of developing finite volume method:

$$\text{Continuity} \quad \frac{\partial \rho}{\partial t} + \nabla(\rho u) = 0 \quad (3.11)$$

$$x - \text{momentum} \quad \frac{\partial(\rho u)}{\partial t} + \nabla(\rho u u) = -\frac{\partial p}{\partial x} + \nabla(\mu grad u) + F_x \quad (3.12)$$

$$y - \text{momentum} \quad \frac{\partial(\rho v)}{\partial t} + \nabla(\rho v u) = -\frac{\partial p}{\partial y} + \nabla(\mu grad v) + F_y \quad (3.13)$$

$$z - \text{momentum} \quad \frac{\partial(\rho w)}{\partial t} + \nabla(\rho w u) = -\frac{\partial p}{\partial z} + \nabla(\mu grad w) + F_z \quad (3.14)$$

$$\text{Energy} \quad \frac{\partial(\rho i)}{\partial t} + \nabla(\rho i u) = -p \nabla(u) + \nabla(k grad T) + F_i \quad (3.15)$$

$$\text{Equations of state} \quad p = P(\rho, T) \text{ and } i = i(\rho, T) \quad (3.16)$$

The governing equations of mass, momentum and energy can be defined in terms of a general scalar transport equations in the following form,

$$\frac{\partial(\rho \phi)}{\partial t} + \nabla(\rho \phi u) = \nabla(\Gamma grad(\phi)) + F_\phi \quad (3.17)$$

where  $\phi$  is the scalar quantity of general variable of fluid flow,  $\Gamma$  is the diffusion coefficient and  $F_\phi$  is the body forces. In order to obtain the governing equation mass, momentum and energy, the variable  $\phi$  is replacing with  $u, v, w, i$ . Equation (3.17) is an important equation to use the computational procedures in the finite volume method. The finite volume method is used for the discretization of conservation laws. In the finite volume method, the fundamental step of the finite volume method is the integration of Eq. (3.17) over a three dimensional control volume

$$\int_V \frac{\partial(\rho\phi)}{\partial t} dV + \int_V \nabla(\rho\phi\mathbf{u}) dV = \int_V \nabla(\Gamma grad(\phi)) dV + \int_V F_\phi dV \quad (3.18)$$

where the movement of the fluids inside the control volume  $V$  leads to the change of the control surface  $A$ . The volume integrals represent the total volume change of the entire Lagrangian control volume by using Gauss's divergence theorem given as below

$$\int_V \nabla(a) dV = \int_A \mathbf{n} \cdot a dA \quad (3.19)$$

where  $n$  is the normal vector of the  $a$  on the surface  $dA$ . The general transport equation is rewritten by applying the Gauss's divergence theorem,

$$\frac{\partial}{\partial t} \left( \int_V \rho\phi dV \right) + \int_A \mathbf{n} \cdot (\rho\phi\mathbf{u}) dA = \int_A \mathbf{n} \cdot (\Gamma grad(\phi)) dA + \int_V F_\phi dV \quad (3.20)$$

This equation represents the rate of change of the total amount of the fluid variable  $\phi$  in the control volume.

## 3.2 Finite Volume Method for Solving Governing Equations

In this part, we describe finite volume approximation that is used for both domain discretization and solve the general transport equation in the numerical simulations.

### 3.2.1 Domain Discretization

The computational domain should be generated in order to solve the nonlinear differential equation. The domain is discretized by using grid (mesh) of cells that divides the domain into smaller grids shown in Figure 3.2. Each cell centroid is enclosed by faces in two dimensions. The vertices of each faces are referred to as nodes. In three dimensions, faces are enclosed by edges. All fluid variables are stored at cell centers,

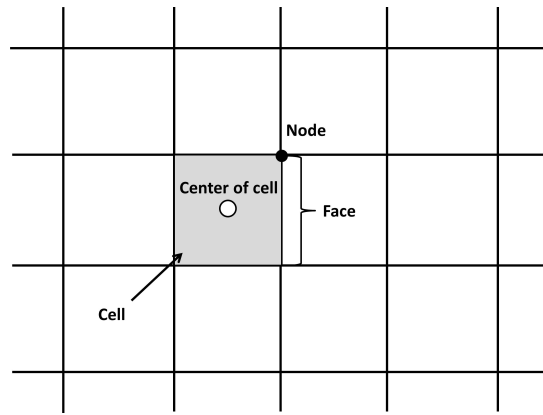


Figure 3.2: Discretized computational domain by mesh [97]

nodes and faces. There are different type of domain shape available such as rectangular, cubes and spheres. These shapes can be connected by structured or unstructured meshes in order to determine the complex geometries.

### 3.2.2 Discretization of Governing Equation

In numerical simulations, there are three fundamental approaches using to discretize the general transport equations. These approaches are finite difference, finite volume and finite element techniques. The finite volume method divides the domain into finite number of volumes. Each control volume is constructed around each cell using conservation of fluid variables  $\phi$  in discrete domain.

Let us consider the general transport equation 3.17. The first step is to generate the computational domain. In this part, governing equations over the control volume is derived for one dimensional, two dimensional and three dimensional domain. Consider a one dimensional domain shown in Figure 3.3. The discrete fluid variables  $\phi$  are stored at cell centroids denoted by P, and neighbors W (West) and E (East). The cell faces of P are denoted by w and e.

The second step is to discretize the general transport equation over a control volume. The discrete form of the integration of the governing transport equation over a control volume at nodal P is given as below

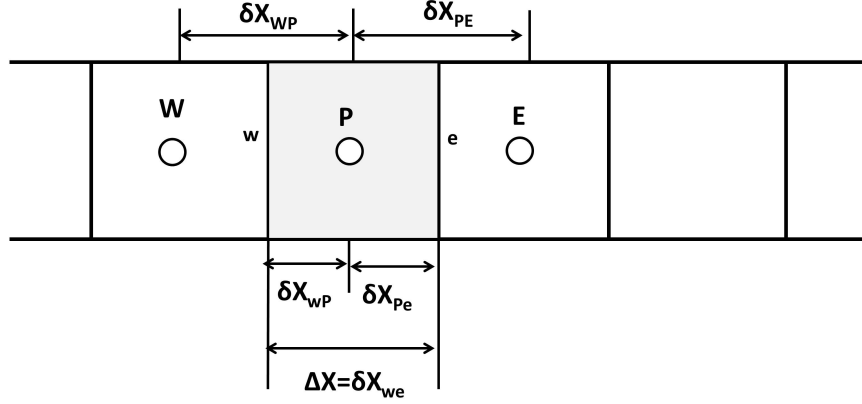


Figure 3.3: One dimensional grid domain

$$\int_{\Delta V} \frac{d}{dx} \left( \Gamma \frac{d\phi}{dx} \right) dV + \int_{\Delta V} S dV = \left( \Gamma A \frac{d}{dx} \right)_e - \left( \Gamma A \frac{d}{dx} \right)_w + \bar{F} \Delta V \quad (3.21)$$

where  $\Delta V$  is the volume,  $A$  is the area of the control volume face,  $\bar{F}$  is the average values of body forces over the control volume. Linear approximation is used to estimate the discrete fluid variables. Assume that the fluid variables  $\phi$  varies linearly between cell centroids. The equation (3.21) can be rewritten by the following form

$$\frac{\Gamma_e A_e (\phi_E - \phi_P)}{\delta x_{PE}} - \frac{\Gamma_w A_w (\phi_P - \phi_W)}{\delta x_{WP}} + F \quad (3.22)$$

This equation becomes

$$a_P \phi_P = a_W \phi_W + a_E \phi_E + F \quad (3.23)$$

where

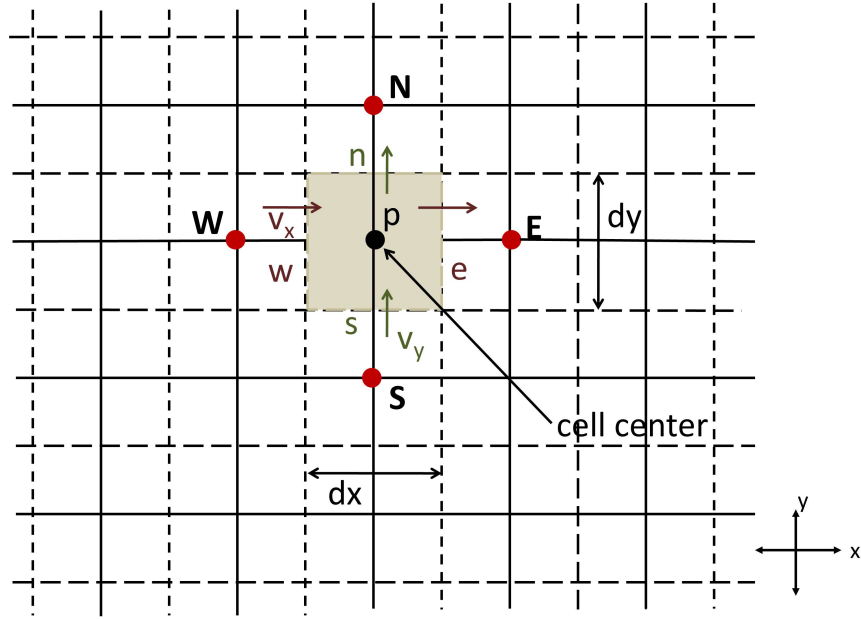


Figure 3.4: Two dimensional grid domain

$$\begin{aligned}
 a_W &= \frac{\Gamma_w}{\delta x_{WP}} A_w \\
 a_E &= \frac{\Gamma_e}{\delta x_{PE}} A_e \\
 a_P &= a_W + a_E \\
 F &= \tilde{F} \Delta x
 \end{aligned} \tag{3.24}$$

The final step is to solve the discretised governing equations. Solutions of these equations are obtained by iteratively. Iterative methods yield approximate solution of discrete variables  $\phi$  at nodal points applying repeated calculations until the convergence is achieved.

Two dimensional discrete domain is shown in Figure 3.4. The general transport equation integrated over the control volume for two-dimensional domain is given by

$$\int_{\Delta V} \frac{\partial}{\partial x} \left( \Gamma \frac{\partial \phi}{\partial x} \right) dx dy + \int_{\Delta V} \frac{\partial}{\partial y} \left( \Gamma \frac{\partial \phi}{\partial y} \right) dx dy + \int_{\Delta V} F_\phi dV = 0 \tag{3.25}$$



Equation (3.25) is discretized in form of the following equation

$$a_P\phi_P = a_W\phi_W + a_E\phi_E + a_S\phi_S + a_N\phi_N + F \quad (3.26)$$

where in addition to east and west neighbors, the nodal P has two more neighbors south (S) and north (N). The coefficients of the scalar quantities are represented as

$$\begin{aligned} a_W &= \frac{\Gamma_w A_w}{\delta x_{WP}} \\ a_E &= \frac{\Gamma_e A_e}{\delta x_{PE}} \\ a_S &= \frac{\Gamma_s A_s}{\delta y_{SP}} \\ a_N &= \frac{\Gamma_n A_n}{\delta y_{PN}} \\ a_P &= a_W + a_E + a_S + a_N \\ A_w &= A_e = \Delta y \quad A_s = A_n = \Delta x \end{aligned} \quad (3.27)$$

For three dimensional case shown in Figure 3.5, P nodes has six neighbors by adding bottom (B) and top(T) neighbors to two dimensional case. The discrete equation for the node P can be obtained as

$$a_P\phi_P = a_W\phi_W + a_E\phi_E + a_S\phi_S + a_N\phi_N + a_B\phi_B + a_T\phi_T + F \quad (3.28)$$

where the coefficient  $a_B$ ,  $a_T$  and  $a_\phi$  is obtained as the following equations

$$\begin{aligned} a_B &= \frac{\Gamma_b A_b}{\delta z_{BP}} \\ a_T &= \frac{\Gamma_t A_t}{\delta z_{PT} A_e} \\ a_P &= a_W + a_E + a_S + a_N + a_B + a_T \end{aligned} \quad (3.29)$$

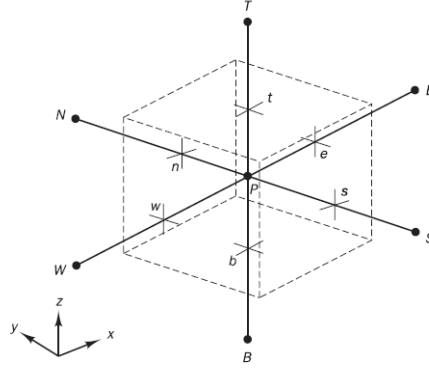


Figure 3.5: Three dimensional grid domain [96]

and the rest of the coefficient are the same with two dimensional case. We can write the discrete equations for one, two and three dimensional cases in general form by following equation

$$a_P \phi_P = \sum a_{nb} \phi_{nb} + F \quad (3.30)$$

where  $(nb)$  is the neighbor nodes,  $a_{nb}$  is the neighboring coefficients,  $\phi_{nb}$  are the fluid variables at the neighboring nodes and  $F$  is the force term.

### 3.2.3 Discretization for Convection and Diffusion

The effect of convection against to diffusion in fluid flow is important issue for the calculation the general transport equations. Diffusion of mass, momentum and heat is obtained due to the fluid particle motions. The steady convection-diffusion equation is obtained from the integration over a control volume of transport equation (3.17)

$$\int_A \mathbf{n} \cdot (\rho \phi \mathbf{u}) dA = \int_A \mathbf{n} \cdot (\Gamma \text{grad}(\phi)) dA + \int_V F_\phi dV \quad (3.31)$$

The flux balance is obtained by solving the equation (3.31) in a control volume along the fluid flow. The physical representation of the equation verify the fluid variable  $\phi$

are transferred into the fluid environment due to the convective flux given in the left hand side and diffusion flux and generation of the fluid variable in a control volume given in the right hand side the equation (3.31).

The discrete convection-diffusion equation for one dimensional case is represented by the following equation

$$a_P \phi_P = a_W \phi_W + a_E \phi_E \quad (3.32)$$

where the coefficients are

$$\begin{aligned} a_w &= D_w + \frac{F_w}{2} \\ a_e &= D_e - \frac{F_e}{2} \\ a_p &= a_e + a_w \\ D_w &= \frac{\Gamma_w}{\delta x_{WP}} & D_e &= \frac{\Gamma_e}{\delta x_{PE}} \\ F_w &= (\rho u)_w & F_e &= (\rho u)_e \end{aligned} \quad (3.33)$$

where F and D to represent the convective mass flux per unit area and diffusion conductance at cell faces. This approximation does not take into account the pressure gradient term as a body forces on the fluid particle. However, to develop our model, pressure gradient term which is important to for generating body forces in fluid flow, is used to calculate the momentum governing equation.

### 3.3 Solution of steady-State fluid flows

Let us consider the two dimensional laminar steady fluid flow. The momentum equation is derived from the general transport equation by following equation

x-momentum

$$\frac{\partial}{\partial x}(\rho uu) + \frac{\partial}{\partial y}(\rho vu) = \frac{\partial}{\partial x} \left( \mu \frac{\partial u}{\partial x} \right) + \frac{\partial}{\partial y} \left( \mu \frac{\partial u}{\partial y} \right) - \frac{\partial p}{\partial x} + F_x \quad (3.34)$$

y-momentum

$$\frac{\partial}{\partial x}(\rho uv) + \frac{\partial}{\partial y}(\rho vv) = \frac{\partial}{\partial x} \left( \mu \frac{\partial v}{\partial x} \right) + \frac{\partial}{\partial y} \left( \mu \frac{\partial v}{\partial y} \right) - \frac{\partial p}{\partial y} + F_y \quad (3.35)$$

continuity equation

$$\frac{\partial(\rho u)}{\partial x} + \frac{\partial(\rho v)}{\partial y} = 0 \quad (3.36)$$

Each momentum and continuity equations is obtained by replacing the variable  $\Phi$  in the general transport equation by  $u$ ,  $v$ ,  $w$  respectively.

In general fluid flow computations, pressure gradient term is not considered initially. The changes of the pressure is depended on the fluid flow. In the case of compressible flow, the changes in pressure are caused by the changes in density. Therefore, the pressure term is obtained from the density. On the other hand, if the flow is incompressible, the density is constant meaning that pressure is not effected from the density changes. In that case, the pressure is obtained from the flow field.

In this thesis, pressure-based algorithm that couples pressure and velocity, is used to solve iteratively the nonlinear equations of fluid flows. Initially, estimated pressure changes is calculated. Then the momentum equation is solved using this estimated pressure changes. The continuity equation is used to obtain real pressure values that update the velocity and pressure of the fluid variables. The iteration is in progress until the velocity and pressure variables are converged.

The momentum equations are discretized into staggered grid. The pressure is stored at cell centers  $P(I,Y)$  whereas the velocity is stored on the cell faces of shown in Figure 3.6.  $I$  and  $J$  refer to  $x$  and  $y$  directions. The cell faces are represented by lower case letters  $i$  and  $j$  in the  $x$ - and  $y$ -directions respectively. The  $u$ -velocities are stored at the  $e$  and  $w$  faces. For example  $e$  face is identified by  $(i + 1, J)$

The discretized momentum equation at the location  $(i,J)$  is given by

$$a_{i,J} u_{i,j} = \sum a_{nb} u_{nb} - (p_{I,J} - p_{I-1,J}) A_{i,J} + F_{i,J} \quad (3.37)$$

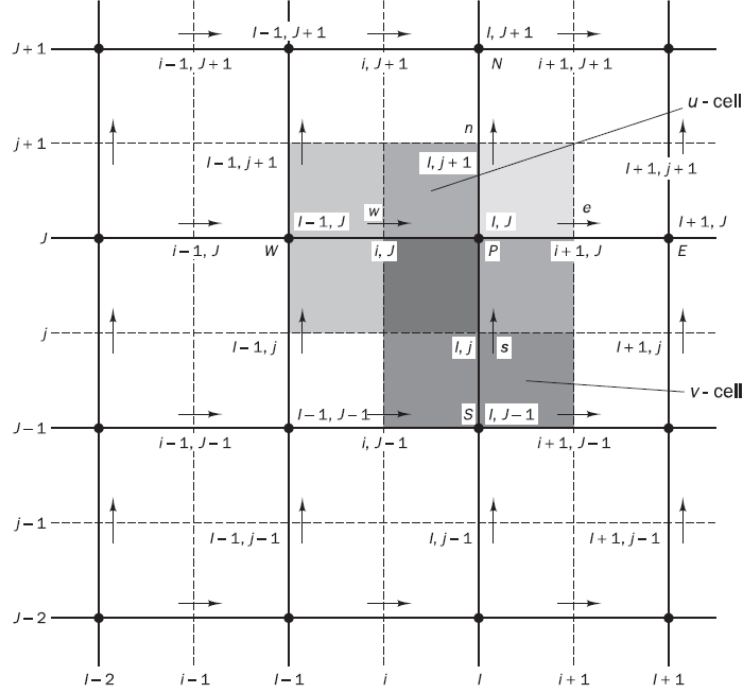


Figure 3.6: Staggered grid for two dimensional domain taken from [96]

where  $\Delta V$  is the volume of  $u$ -cell,  $F_{i,j} = \widetilde{F}\Delta V$  is the momentum body force term,  $A_{i,j}$  is the east or west cell face area of the  $u$ -control volume. E, W, N, S neighbors involved in  $\sum a_{nb}u_{nb}$  are  $i-1, j, i+1, j, i, j-1, i, j+1$ . The convective flux and the diffusive conductance coefficients are given as below,

$$\begin{aligned}
 F_w = (\rho u)_w &= \frac{F_{i,j} + F_{i-1,j}}{2} = \frac{1}{2} \left[ \left( \frac{\rho_{i,j} + \rho_{i-1,j}}{2} u_{i,j} \right) + \left( \frac{\rho_{i-1,j} + \rho_{i-2,j}}{2} u_{i-1,j} \right) \right] \\
 F_e = (\rho u)_e &= \frac{F_{i+1,j} + F_{i,j}}{2} = \frac{1}{2} \left[ \left( \frac{\rho_{i+1,j} + \rho_{i,j}}{2} u_{i+1,j} \right) + \left( \frac{\rho_{i,j} + \rho_{i-1,j}}{2} u_{i,j} \right) \right] \\
 F_s = (\rho v)_s &= \frac{F_{i,j} + F_{i-1,j}}{2} = \frac{1}{2} \left[ \left( \frac{\rho_{i,j} + \rho_{i,j-1}}{2} v_{i,j} \right) + \left( \frac{\rho_{i-1,j} + \rho_{i-1,j-1}}{2} v_{i-1,j} \right) \right] \\
 F_n = (\rho v)_n &= \frac{F_{i,j+1} + F_{i-1,j+1}}{2} = \frac{1}{2} \left[ \left( \frac{\rho_{i,j+1} + \rho_{i,j}}{2} v_{i,j+1} \right) + \left( \frac{\rho_{i-1,j+1} + \rho_{i-1,j}}{2} v_{i-1,j+1} \right) \right]
 \end{aligned} \tag{3.38}$$

$$\begin{aligned}
D_w &= \frac{\Gamma_{I-1,J}}{x_i - x_{i-1}} \\
D_e &= \frac{\Gamma_{I,J}}{x_{i+1} - x_i} \\
D_s &= \frac{\Gamma_{I-1,J} + \Gamma_{I,J} + \Gamma_{I-1,J-1} + \Gamma_{I,J-1}}{4(y_J - y_{J-1})} \\
D_n &= \frac{\Gamma_{I-1,J+1} + \Gamma_{I,J+1} + \Gamma_{I-1,J} + \Gamma_{I,J}}{4(y_{J+1} - y_J)}
\end{aligned} \tag{3.39}$$

After representing the discretized form of the  $u$ -momentum equation of the scattered grid domain, the discretized momentum equation for the pressure correction algorithm is obtained using the estimated pressure field to yield the estimated velocity components  $u^*$  and  $v^*$  as follows.

$$a_{i,J}u_{i,J}^* = \sum a_{nb}u_{nb}^* + (p_{I-1,J}^* - P^*I, J)A_{i,J} + Fi, J \tag{3.40}$$

$$a_{i,J}v_{i,J}^* = \sum a_{nb}v_{nb}^* + (p_{I,J-1}^* - P^*I, J)A_{J,j} + FI, j \tag{3.41}$$

where  $p'$  is the correction pressure and  $p^*$  is estimated pressure. The correct pressure is obtained by

$$p = p^* + p' \tag{3.42}$$

Then, the correct velocities  $u$  and  $v$  are calculated by the following equation,

$$u = u^* + u' \tag{3.43}$$

$$v = v^* + v' \tag{3.44}$$

The details of the derivation of the discrete momentum equations and the solution pressure-based algorithm are given in the sixth chapter of the reference [96].

## CHAPTER 4

# MOMENTUM TRANSFER FROM FINGERS TO OBJECT IN UNDERWATER

### 4.1 Analysis of Underwater Grasping

A fully immersed object, suspended in water can be rotated from distance by a pre-shaped robot hand approaching and closing upon the object prior to contacting it. Momentum transfer from robot fingers closing into a grasp, to the fluid medium particles, and from these particles to the object surface generates the motion tendencies of that object in terms of rotational and translational displacements. In this chapter, we build the infrastructure of the novel concept of a controller that will be introduced in Chapter 5 and which determines either : 1) given initial position and orientation of a robot hand, what preshape is suitable for generating a desired moment distribution on the surface of a given object in order to trigger a desired rotation in a desired direction when approaching with this preshaped hand or 2) given a predetermined hand preshape, what initial position, orientation and hand aperture are suitable to generate a desired rotation upon approach and, without causing the retroceding of the object. The desired object motion generated from distance by the approach of a hand preshape is to be used seamlessly for the subsequent manipulation of the object upon grasp. This infrastructure will be built through analyses of object motion tendencies imparted by robot hands approaching different objects, both immersed in water.

Towards this end, we propose in this chapter, a new model based on computational fluid dynamics, for determining the continuity in momentum transfer from robot hand fingers to the fluid medium, and to the object, until landing on that immersed object.

Our experimental results demonstrate how different hand preshapes initiated from different locations in the medium surrounding an object of different cross sections suspended in equilibrium in the fluid, affects its motion tendencies in terms of rotation and translation. This chapter also includes the modelling of robot fingers and object as fluidic elements which rigidity can be relaxed to induce compliance.

## **4.2 Problem Definition**

The primary objective of this work is to approach in a controlled manner, an object suspended within water by a preshaped robot hand so as to be able to generate a suitable the momentum transfer during this approach in order to induce a desired motion of the object. The momentum transferred from the preshaped approaching hand to the medium particles and from these particles to the surface of the object generates force and torque patterns that lead to object translation or rotation tendencies within any fluid medium, but especially in compressible fluids such as water. For that purpose, we adopt fluid dynamics to model the momentum transfer that bridges the phases of preshaping, approach and landing to grasp, initiating the motion tendencies of the object.

The main sub-objective of our primary goal is to generate a controller that determines which preshape is suitable to approach an object, given its size and shape together with the initial position and orientation of the robot hand, in order to induce a desired motion on the object. Similarly, given a predetermined hand preshape and object size, shape and location, the controller should be able to decide upon the aperture, the initial position and orientation of the preshaped hand from where the approach will begin so that a desired moment distribution is imparted to the object, generating desired motion tendencies. This controller will be the focus of Chapter 5.

Our objectives are motivated by human-like behaviors where we preshape our hands for landing on an object and initiate certain manipulation behaviour on that object without losing the continuum and thus, reducing the energy loss during transfer from preshaping to grasping phases. Learning to control our hand approach for imparting suitable motion tendencies to the object that will be used to initiate manipulation is a



critical issue in infancy and rehabilitation. However, this issue is still missing in the robotic literature that we contribute using fluidics in our approach. Our perspective of modelling the momentum transfer during the preshaped landing initiating motion tendencies on an object is best demonstrated for grasping a fully immersed object floating suspended in water. Although our method equally applies to any fluid medium, we concentrate in this work a water medium for better demonstration of our approach. Moreover, we use particle based fluid dynamics to model not only the momentum transfer between robot fingers medium particles and object but also model fingers and object as fluidic elements built from rigidly connected fluid particles which connectivity can further be relaxed to achieve any flexibility and compliance. This work also introduces this concept which is our second sub-objective. The characteristics of our problem of underwater grasping are based on the following assumptions:

- Both robot hand and object are fully immersed in a fluid medium.
- The object of variable but known features as size, shape and location is floating suspended in equilibrium in the fluid.
- The medium is modelled as incompressible fluid but fluid dynamics model can be adapted to any type of fluid.
- In order to be able to insert compliance in the grasp and/or enable material flexibility of fingers and/or object, the robot fingers and objects are modelled as solidified fluidic elements, where the rigidity parameter can be relaxed as desired.
- Momentum transfer from the fingers to fluid environment and then from environment particles to object surface is modelled within a single model as a continuum using computational fluid dynamic without the need for separate models.

This work provides simulation results on analyses of the interaction between the solidified fluidic elements, the fluid medium and the object surface through momentum transfer together with results on the developed controller. Finite volume discretization on a uniform grid meshing is used to solve the momentum governing equations in the fluidic environment as will be introduced in the upcoming section.

### 4.3 Methodology

This section introduces first the fluid dynamics modelling of the momentum transfer particles from the fluidic elements which are the robot fingers and object to the particles of the fluid medium. We will then demonstrate how we modelled fingers and objects as solidified fluidic elements that can incorporate flexibility and compliance whenever wanted. For the sake of completeness, we begin this section by introducing the mathematical background of computational fluid dynamics and its adaptation to our problem.

#### 4.3.1 Adapting computational fluid dynamics model to our problem

Computational fluid dynamics (CFD) is a sub-discipline of fluid mechanics that enables to model fluid flows by solving governing equations which are described by a set of differential widely known Navier- Stoke equations [99, 100].

$$\frac{\partial \rho}{\partial t} + \nabla \cdot (\rho \vec{v}) = 0 \quad (4.1)$$

$$\frac{\partial}{\partial t}(\rho \vec{v}) + \nabla \cdot (\rho \vec{v} \vec{v}) = -\nabla P + \nabla \cdot (\bar{\bar{\tau}}) + \rho \vec{g} + \vec{F} \quad (4.2)$$

where  $\rho$  is the density,  $P$  the pressure,  $\vec{v}$  the fluid velocity vector,  $\nabla$  the gradient operator,  $\rho \vec{g}$  the gravitational body force,  $\vec{F}$  external body force and  $(\bar{\bar{\tau}})$  the stress tensor. The first differential equation (4.1), which is the conservation of mass in Lagrangian form, is represented by density of fluid continuum in the control volume. The mass contained in the control volume remain constant over time. The momentum equation (4.2) is composed of pressure gradient and body forces with stress tensor. The stress tensor is represented as,

$$\bar{\bar{\tau}} = \mu[(\nabla \vec{v} + \nabla \vec{v}^T) - \frac{2}{3} \nabla \cdot \vec{v} I] \quad (4.3)$$

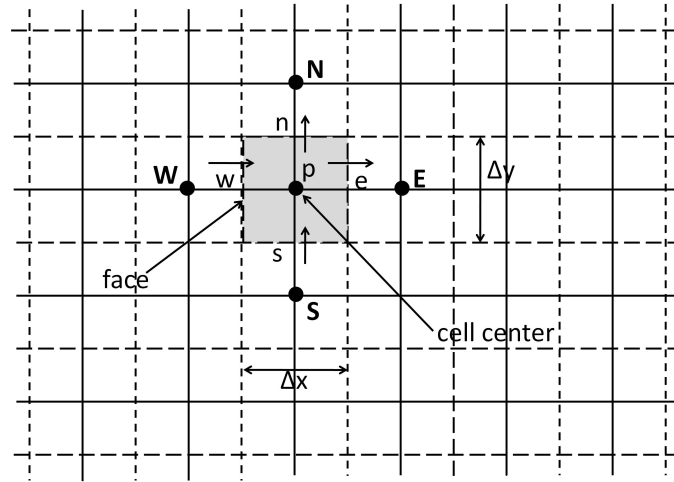


Figure 4.1: Two dimensional grid representation of the fluid environment

where  $\mu$  the molecular viscosity,  $I$  unit tensor. The equation underlines that the changes of momentum occur due to acting external body force on the entire fluid environment and those external body forces, which are relevant with the pressure gradient, affect the fluid motion of the medium. In our case, external body forces are generated by the closing hand fingers, hitting to medium particles. Since we deal with "approach to grasp" underwater, the fluid medium is modeled as incompressible.

The adaptation of the fluid model to our "approach to grasp" environment undergoing momentum transfer between particles is achieved by first discretizing the environment into grid (meshes) as shown in Figure 4.1. The fluid flow variables such as pressure and density are lumped to the center of mesh cells  $P$ , neighbored with four mesh cell centers denoted as east  $E$ , west  $W$ , north  $N$ , and south  $S$ . The fluid flow across the boundaries of the cells along the  $x$  and  $y$  directions are approximated by the pressure difference between two cells. The directional velocities represented as  $v_x$  along the  $x$ -axis is lumped at  $e$  and  $w$  boundaries and the velocity  $v_y$  along the  $y$ -axis is lumped at  $n$  and  $s$  boundaries of cell  $P$ . The momentum transfer between solid boundaries and fluid medium is calculated using dynamic mesh theory that models discrete fluid flow where the shape of the domain is changing with time [100]

The fluid flow governing equations (4.1,4.1) are numerically discretized by using finite volume method. The rate of change of the total amount of fluid characterized

as momentum in the control volume is represented as mass flux and pressure values at the surfaces of each finite volume of the fluid cells. The discrete momentum  $u$  is derived from the general transport equation integrating over the control volume using divergence theorem and represented along the  $x$  axis as providing by discretized model of the continuity of the velocity field of moving fluid particles:

The  $x$ -momentum equation is defined as

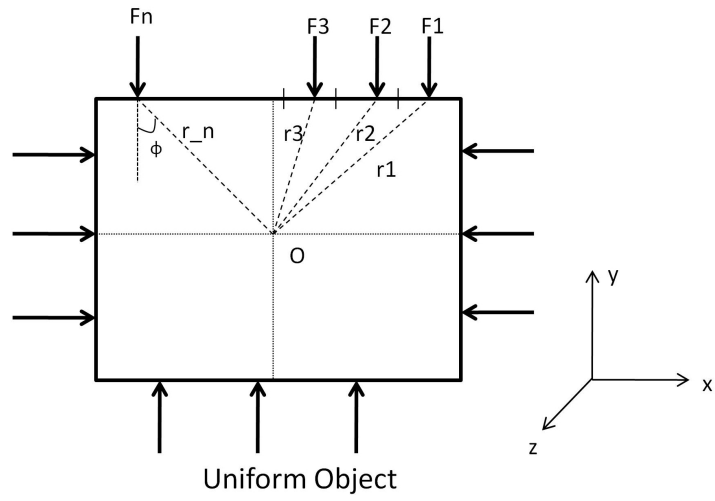
$$au = \sum_n a_n un + \sum p_f . A + F \quad (4.4)$$

where  $a$  and  $a_n$  are the diffusion coefficients of fluid particles,  $n$  is the neighbor boundaries of the center of the mesh cell  $P$ ,  $p_f$  the pressure applied in a direction perpendicular to area  $A$  of the cell volume for each fluid particle,  $F$  is the external forces which are generated in our problem by the solidified fluid particles of the fingers hitting the environment particles. The detailed information of the discretization of momentum equation can be found in [96]-[97] and Chapter 3.

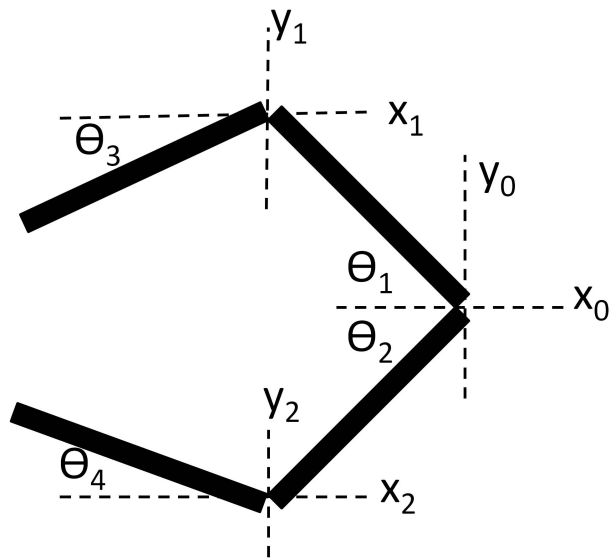
### 4.3.2 Preprocessing

The geometric model of the environment consisting of object to be grasped, manipulator fingers and medium have to be created in the preprocessing phase of our method.

- All this pre-processing phase, we model the objects and manipulator fingers as a rigid bodies made of solidified fluid particles while the medium is modeled as an incompressible fluid
- The boundary condition of the object and fingers are then stationary due to solidification but can be relaxed for compliance and then made to move.
- The fluidic environment is discretized into 2D or 3D meshes using Gambit 2.3 [98] which is the software used to build mesh models for computational fluid dynamic problems.



(a) Solid Object



(b) Manipulator with four joint angles

Figure 4.2: Solid object and manipulator

### 4.3.3 Fingers Motion

Two robot hands have been used in our approach, performing each, either planar grasp, equipped each with 2 fingers (planar approach to 2D grasp) shown in Figure 4.2(b) or volumetric approach to 3D grasp 5 fingers made up with 2 joints each which are revolute. The fingers undergo individually pitch motion within their own finger plane. Fingers are individually represented as solid bodies in our approach having a rigidity that can be relaxed to include flexible fingers in the grasp. The motion of the fingers in the reference frame  $k$  is generated by linear  $\vec{v}_k$  and angular  $\vec{w}_k$  velocities of the links at every discrete time step  $\Delta t$ .

$$\vec{x}_k^{n+1} = \vec{x}_k^n + \vec{v}_k \Delta t \quad (4.5)$$

$$\vec{\Theta}_k^{n+1} = \vec{\Theta}_k^n + \vec{w}_k \Delta t \quad (4.6)$$

### 4.3.4 Object Motion

Each surface on the object is partitioned into  $N$  surface particles (cells)  $p_i$  where  $i = 1, \dots, N$  shown as in Figure 4.2(a) rigidly attached to their neighboring cells. Each surface cell on the object is exposed to pressure generated by momentum transferred from the medium particles activated by the approaching robot fingers, yielding a total moment on the object which is lumped at its center of gravity, thus triggering object angular displacement with respect to that center of gravity. This total moment vector  $vecM_o$  about the center of the gravity is calculated as

$$\vec{M}_o = \sum_i^N \vec{r}_i \times \vec{F}_i \quad (4.7)$$

where  $r_i$  is the level arm of the applied force on a cell,  $N$  being the number of the particles. The force vector  $F_i$  at each center of the surface cells is generated from the applied pressure lumped to the center of  $i$

$$\vec{F}_i = P_i \cdot A \hat{n} \quad \text{where } i = 1, 2, 3 \dots N \quad (4.8)$$

where  $P_i$  is the center of the cell where pressure is lumped,  $A$  is the area of the cell,  $\hat{n}$  is the unit normal to the cell. Cells that are offset from the object center of gravity through a level arm  $r_i$  and therefore generate a rotation tendency on the object about its  $z$ -axis. The relationship between the angular momentum  $vecL$  and moment  $M_o$  at the center of the gravity of the object is

$$\vec{M}_o = \frac{d\vec{L}}{dt} \quad (4.9)$$

The angular momentum is expressed by the product of inertia tensor and angular velocity  $vecw$  in the direction of  $z$ -axis

$$\vec{L} = \hat{I} \cdot \vec{w} \quad (4.10)$$

The angular displacement denoted as  $\Phi_o$  of object around its origin is found as

$$\Phi_o = w \cdot dt \quad (4.11)$$

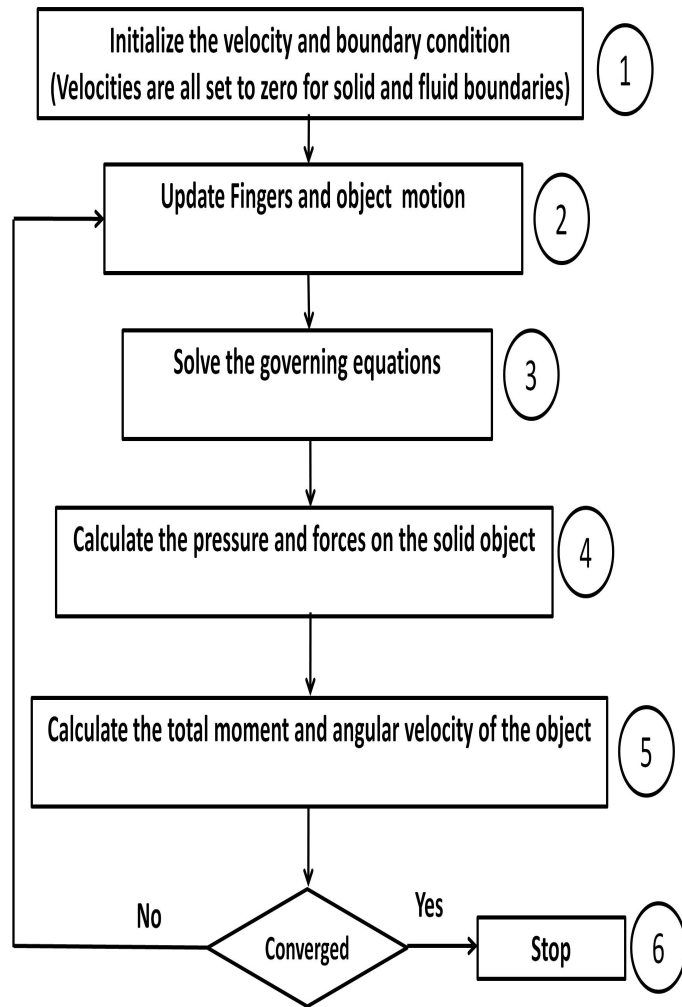


Figure 4.3: Flow chart of the simulation



### 4.3.5 Momentum transfer for different preshapes

Figure 4.3 provides a comprehensive view of our approach as a process flow chart. Simulation examples are all initiated with initial velocities of the fluid particles including fingers, object and medium all set to zero (step 1). Fingers begin to move towards the object surface by updating the angular velocities (step 2). At this stage, the solidified fluid particles interact each with the fluid medium particles causing a change in the velocity field of the fluid flow. The continuity governing equations and viscosity parameters are solved sequentially just after updating fingers motion (step 3). Then, the pressure and forces in the direction normal to solidified object particles are calculated (step 4). Before checking the convergence of the algorithm, the total moment vectors at the center of the gravity of the object are computed using the external forces generated from the fingers (step 5). This total moment vectors according to the hand preshapes are input and output training pairs of the ANN decision support system of the intelligent controller. The simulation ends when one of the finger contacts the object (step 6).

### 4.3.6 Simulation Results

In this section, we provide a series of examples to demonstrate the validity of our perspective and justify the algorithmic steps provided in Section 4.3.

Firstly, the proposed method of momentum transfer for different hand preshapes is discussed on experimental results. The effect of momentum transfer from the finger to different object such as square and circle object is represented. The experimental results demonstrate how different hand preshapes landing on the object affects its initial motion tendencies in the fluid medium. Secondly, our proposed approach is tested on the compliance fingers and object. In these experiments, rigid fluidic connections between the particles can be relaxed to induce compliance.

The numerical simulation based on "Fluent" commercial software package runs by solving the continuity and momentum governing equations for momentum transfer generated from the finger motions. The interaction between the fluid and solid boundaries has been performed using dynamic mesh method. The mesh spacing is taken as

0.5 units. A constant laminar viscosity term is used for more stable fluid motion. Unsteady fluid flow analysis has been performed to determine the structure of the dynamic mesh generated by finger motion. The boundary condition of the fingers, object and edges surrounding the environment are particles which connectivity is set as rigid in the result included in this section. The time step size for iteration used in the numerical simulation is kept 0.01 where total number of time step is set to 100. In order to get the desired convergent solution, the maximum iteration per time step size is fixed to 20, since this bound is found to be sufficient experimentally. User defined functions (UDF) coded in C are used to generate the finger motion in the fluid medium during the approach of the hand to the object. The *DEFINE\_CGMOTION* macro is used for creating the pitch motion of each finger that contribute to the transfer of momentum to fluid variables.

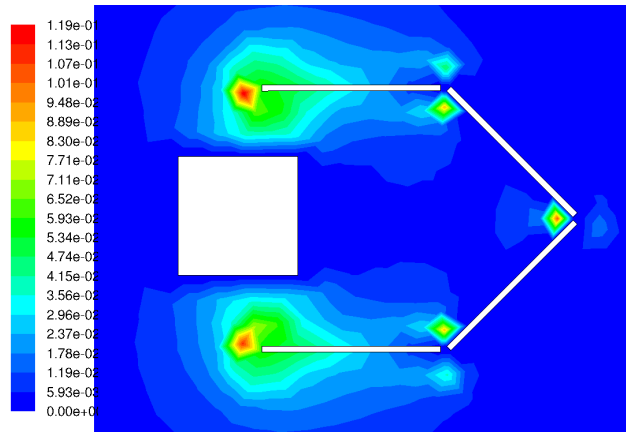
Figure 4.4 represents the momentum transfer velocity contours at three consecutive frames, the third one being the landing on the object. The color bar chart in the legend represents the magnitude of velocity of the fluid particles in the medium changing from blue that is the zero velocity to red that is the maximum velocity. In order to better demonstrate velocity contour changes, the object is assumed to be fixed with respect to the reference frame in this experiment. Figure 4.4(a)-4.4(c) show how momentum intensities increase depending upon the pressure generated on the object by the bombardment of medium particles activated by the closing of fingers. Figure 4.5 demonstrates the moment values on top and bottom surfaces of the object. There are four surface particles (cells)  $\beta_i$   $i = 1, \dots, 4$  on each surface of the object. The x-axis of the figure represents cell centers labelled from left to right for both cases. While the moment patterns on bottom surface given in Figure 4.5 represents the tendency of object rotational motion in the direction of counterclockwise, on top of the surfaces given in Figure 4.5(b) represents in the reverse direction of clockwise. The resultant moment at the center of gravity of the object is shown in Figure 4.6 which causes rotational motion tendencies along the z-axis. The curve indicates high negative moments in the first 6 iterations on the object which means that the object, if let free, would tend to move clockwise. The angular velocity of two fingers landing on the square object are same and set to 0.4m/sec.

Another experiment is represented in Figure 4.7 where the velocity magnitude con-

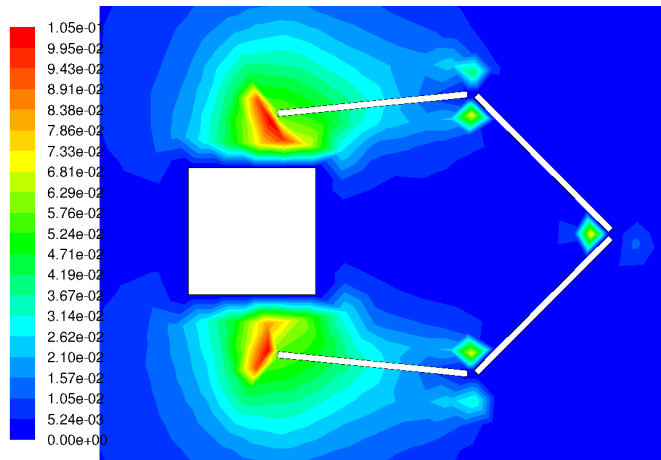
tours for circular object at different time step are shown. The initial position and joint angles of the fingers while landing on the circular object are kept the same as for the first experiment on the square object for comparative purposes. The circular object is divided into 16 surface particles (cells) as for the perimeter of the square object and the total moment with respect to its center of gravity is shown in Figure 4.8. The effect of the pressure forces on a circular object surface area has to be smaller in nature than the square object. We also see here that the total moment with respect to center of gravity of the circular object is comparatively less than that for the square object.

Let us consider another illustrative example of momentum transfer approaches of square object in Figure 4.9. In this case, the velocity of the Finger3 which is the upper side is set to  $0.4m/sec$  and the other one Finger4 velocity is set to  $0.2m/sec$ . Figure 4.9(a) shows the velocity magnitude contours at just before Finger3 contacting with the object. As seen from the velocity contour, the upper side of object is exposed to momentum forces more than bottom side that leads to counterclockwise motion tendencies of the object. If we look at the moment patterns on the object surfaces given in Figure 4.9(b), in this case the moment patterns are different than the previous examples given in Figure 4.6 because of the position of object and different velocity of the fingers. Comparing changes of the moment patterns in each case provides information about the importance of the initial position and orientation of the hand preshapes according to the object for creating desired motion tendency.

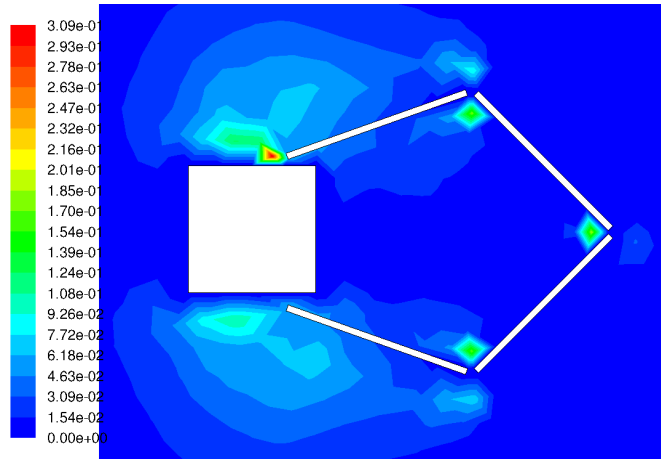
Another experiment is done to investigate the motion tendencies of the object in three dimensional case shown in Figure 5.7. The cubic object is landed by cylindrical hand preshape in this experiment. Our results for cylindrical hand preshape landing on the cubic object surfaces shows that the distribution of the moment patterns on the object surfaces changes motion tendencies according to the impact pattern applying at contact surface.



(a)

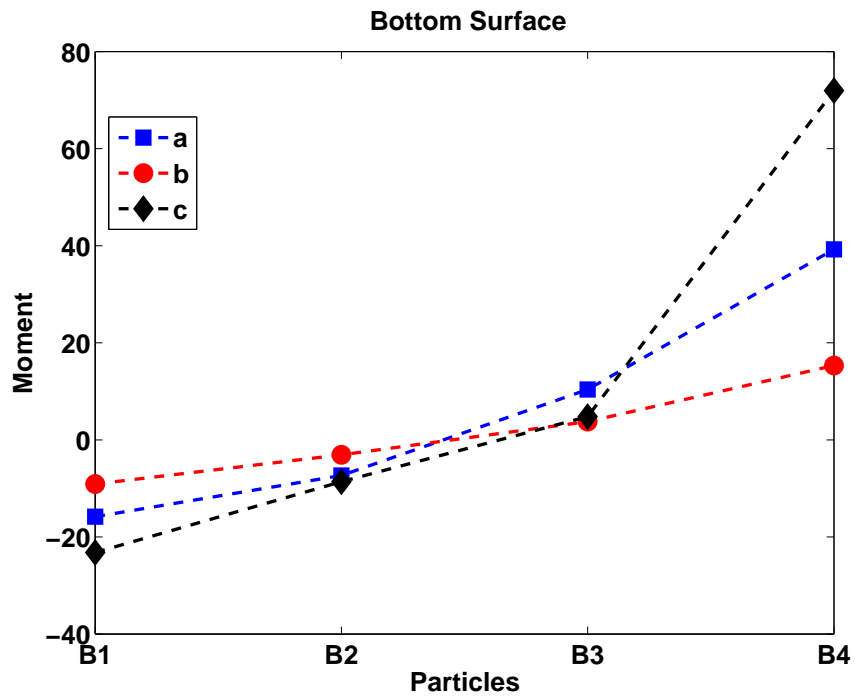


(b)

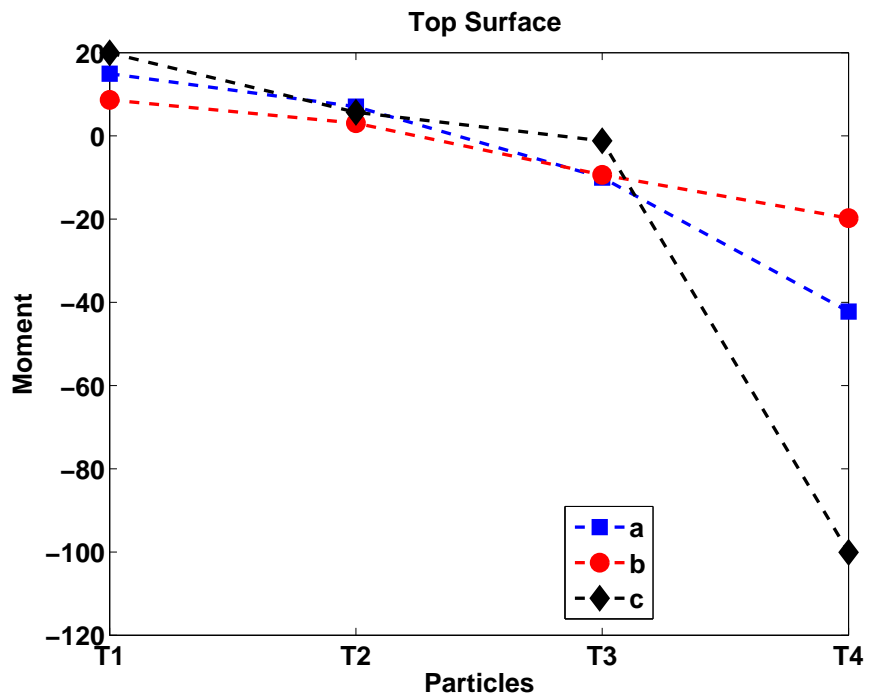


(c)

Figure 4.4: represent the contours of velocity for square object in different time step  
 (a)  $t=0.02$  (b)  $t=0.18$  (c)  $t=0.40$



(a)



(b)

Figure 4.5: Moment distribution (a) top and (b) bottom surfaces of the square object

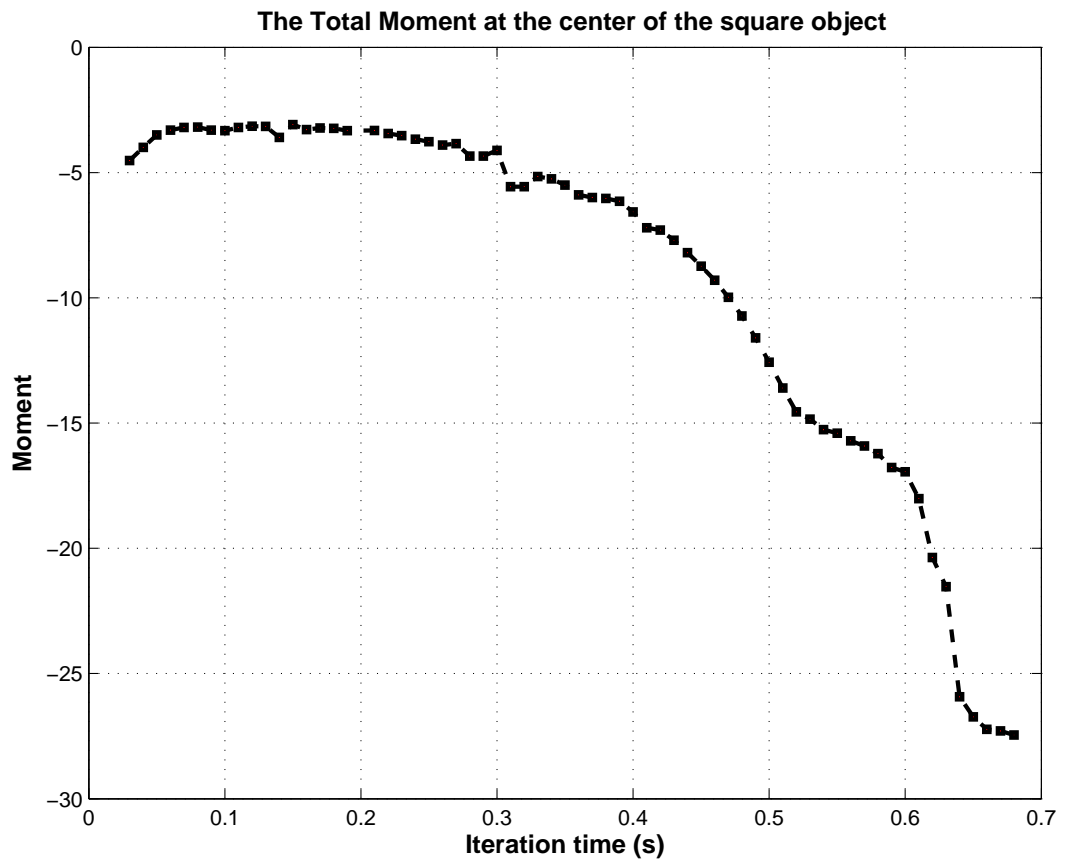
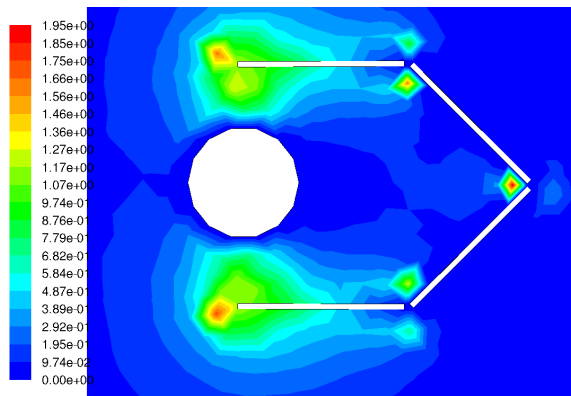
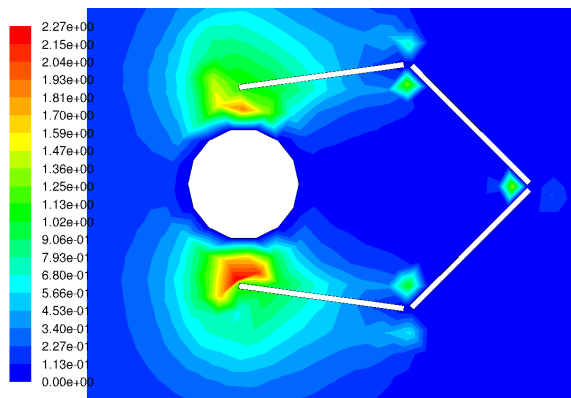


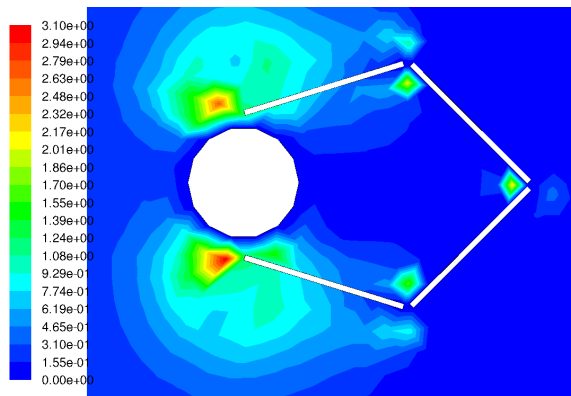
Figure 4.6: Total moment at the center of gravity of the square object



(a)



(b)



(c)

Figure 4.7: Contours of velocity magnitude for circular object

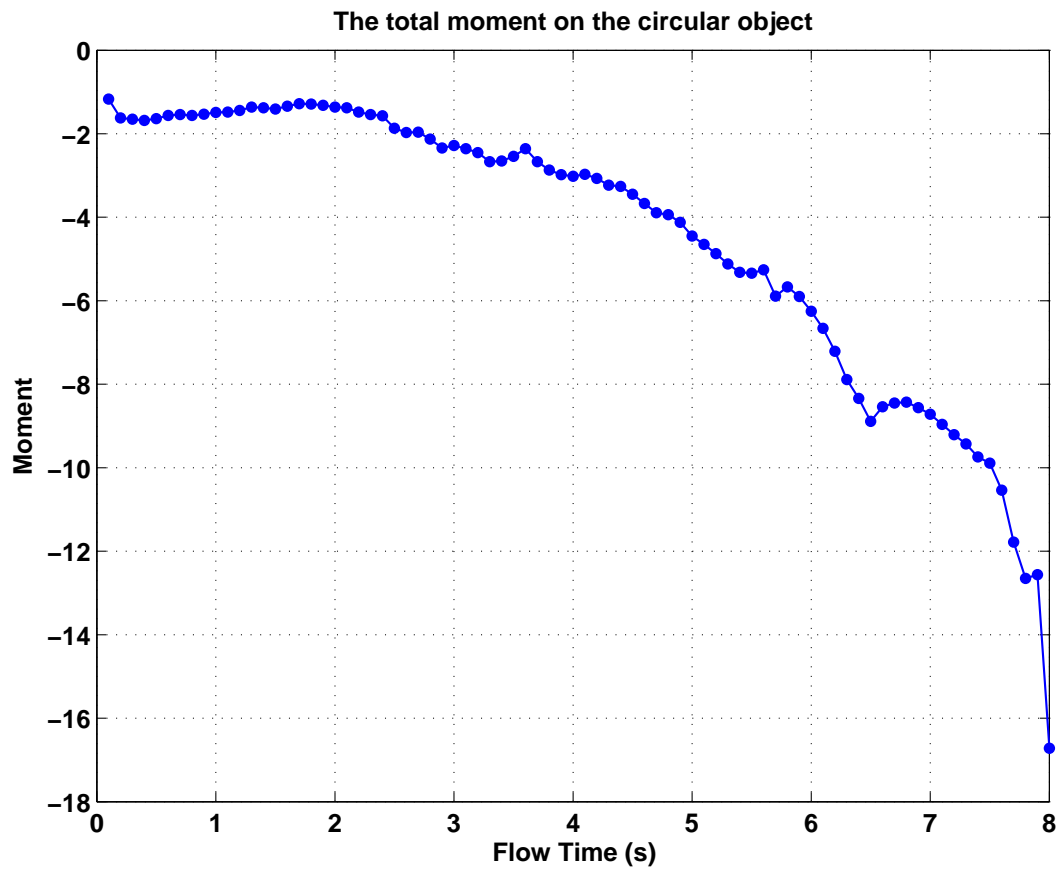
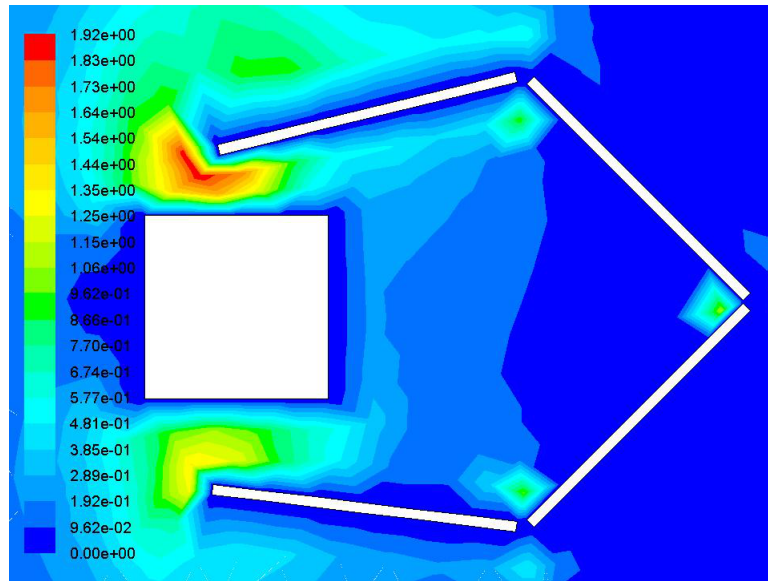
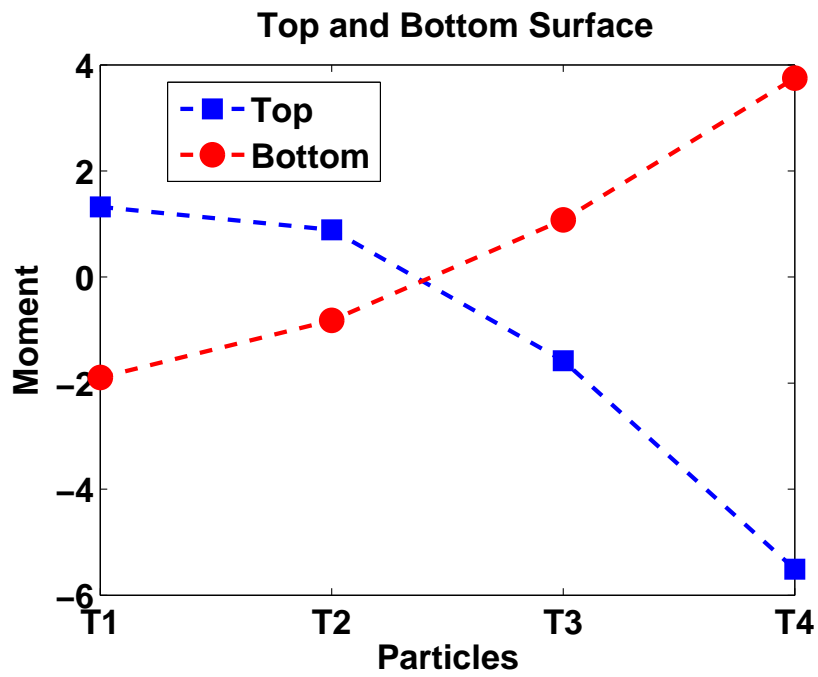


Figure 4.8: Total moment at the center of gravity of the circular object





(a)



(b)

Figure 4.9: (a) represents velocity magnitude contours of different velocities of fingers landing on the object (b) moment of top and bottom surfaces of the object

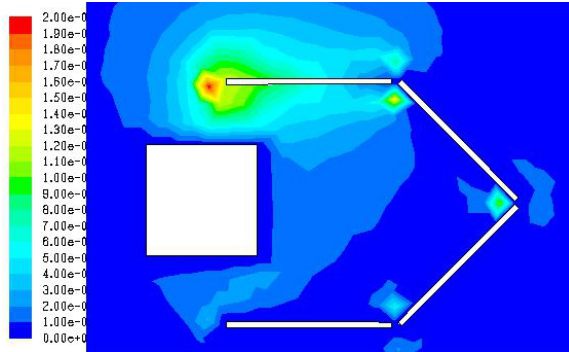
Table 4.1: Momentum Distribution on the rotating square object

Left Face	M1=13.3	M2=0.2	M3=-1.1	M4= -3.3
Bottom Face	M5=-15.4	M6=-17.6	M7=-19.8	M8= -22.1
Right Face	M9=3.5	M10=1.7	M11=-0.6	M12=-11.8
Top Face	M13=91.5	M14=82.5	M15=65.9	M16=74.1

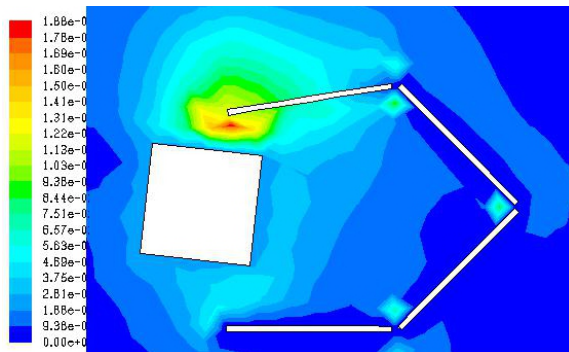
#### 4.3.7 Examples of rotating motion tendencies of object

Here, the object is left free to rotate. The effect of external forces from the fingers to fluidic medium and then from the medium to the object particles are calculated using equation (4.9). The perimeter of the square object shown to rotate in Figure 4.10 is composed of 16 cells, each surface partitioned into 4 discrete intervals. The total moment vector around the  $z$ -axis is calculated using equation (4.8). Table-4.1 represents the moment distribution on each object surface for each of the 4 surface cells and their individual contribution to total momentum vector causing rotation around  $z$  normal to the surface of the work, located at the center of gravity. The resultant momentum distribution on the square object yields a clockwise rotational motion tendency. The clockwise motion is accelerated, as seen for the intensity codes of the contours specially due to particle momenta on the upper surface of the object in Figure 4.10(c). The lower surface of the object exhibits a counter-clockwise moment distribution; but this moment distribution cannot counter balance the top surface distribution and the whole object rotates clockwise as in Figure 4.10(c).

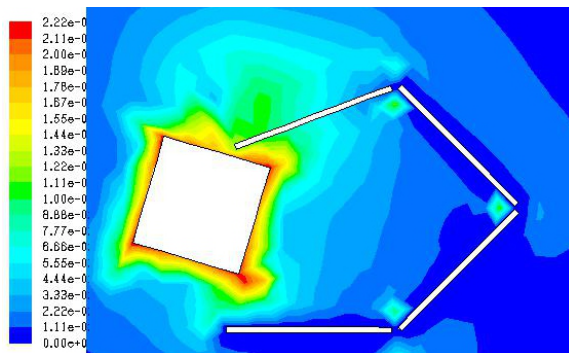
To give another illustrative example for rotating motion tendencies an object, let us consider two different finger movement in order to approach on the object as shown Figure 4.11. After Finger2 firstly lands on the object at a certain of time shown in Figure 4.11(a)- 4.11(c), Finger4 starts to movement in the reverse direction Figure 4.11(d). It can be shown that the movement of the fingers leads to different motion tendencies of the object.



(a)

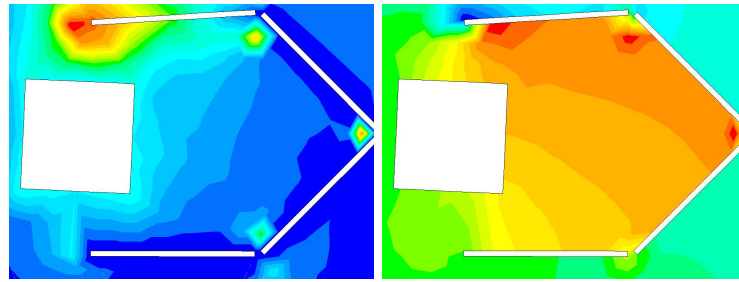


(b)

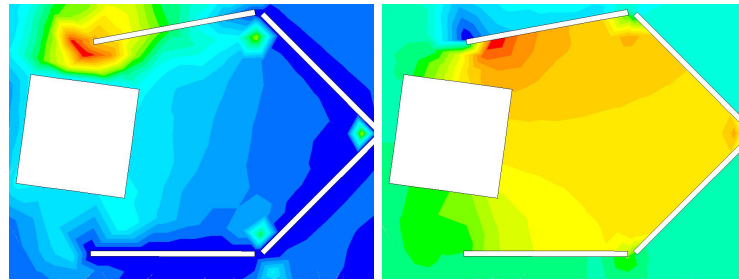


(c)

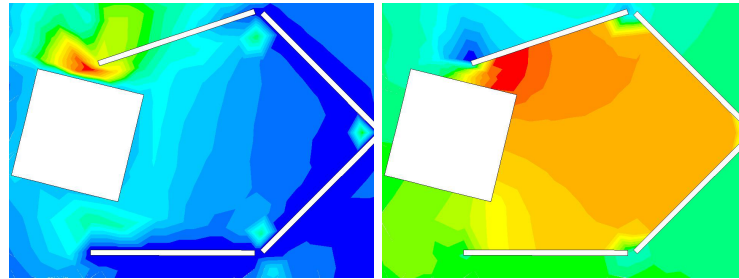
Figure 4.10: Contours of velocity magnitude for rotating square object



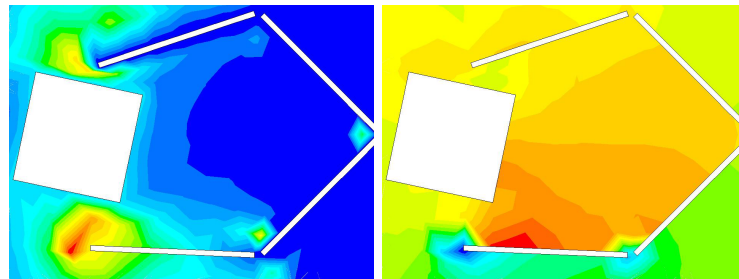
(a)



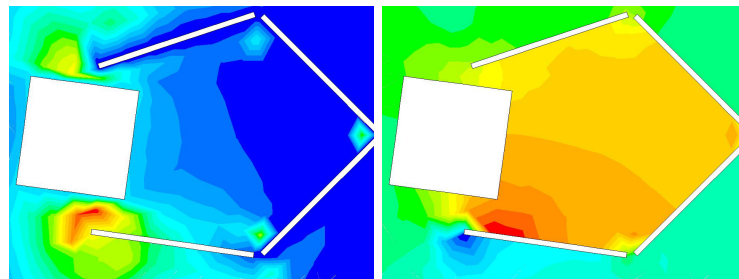
(b)



(c)



(d)



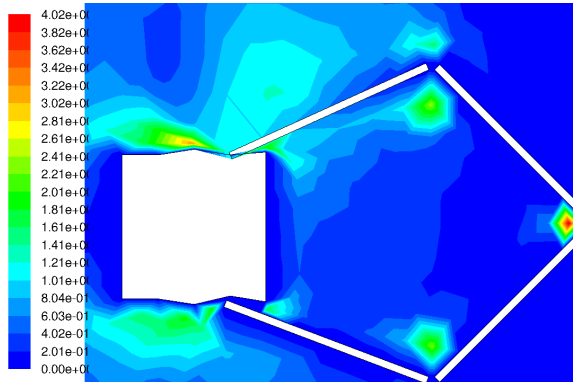
(e)

Figure 4.11: Contours of velocity magnitude and total pressure for rotating square object at different time step from (a) to (e)

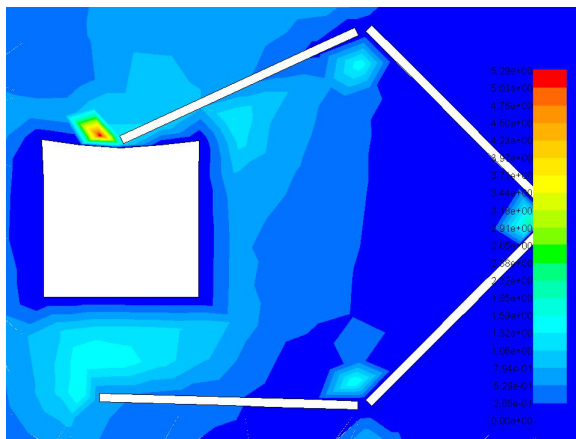
#### **4.3.8 Compliance fingers and object modeled as solidified fluid elements**

Modeling fingers and objects as solidified fluidic elements allows us to relax rigidity for momentum transfer analysis for the case of flexible fingers or deformable object towards compliant grasp. This section demonstrates such approaches to compliance beginning with deformable object. In order to analyze how object deforms from distance by the approach of a preshaped hand with rigid fingers, we decrease the rigidity values in the connectivity of particles forming each surface of the object, thus generating soft boundary fluid particles on the object surface. These soft boundary particles connected by springs to each other represent the surface cells that partition object surfaces into small entities. This structure allows object deformation in the virtual environment caused by forces on the object surface generated by rigid fingers approaching the object as shown in Figure 4.12(a). When fingers collide with the object surface, the object's deformation caused by the forces from the fingers naturally increases at the contact area. The deformation of the object is seen to increase with respect to increasing angular velocities of the fingers approaching the object.

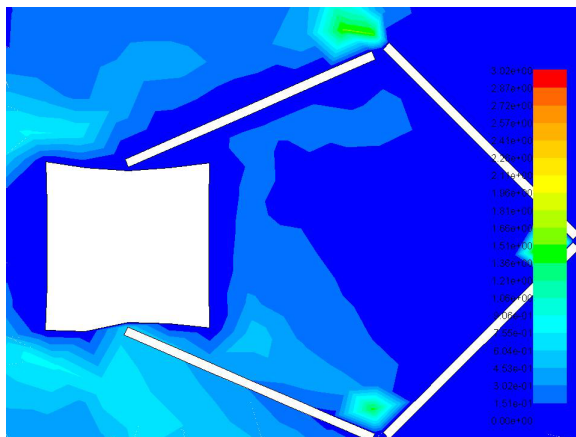
Moreover, our proposed method can be adapted to the case of rigid object approached by flexible fingers. The compliance of the fingers is also important for achieving stable grasping. The interaction between the fingertips and object surface is shown in Figure 4.13. Each finger is composed of four rigid cells. Two of them through the fingertips sides are allowed to relax to rigidity and the rest ones are still modeled as rigid fluid particles shown in Figure 4.13(b). The reaction forces exerted from objects surface to the fingertip at the contact region of the rigid object leads to the deformation of the fingers based on the stiffness constant determined by experimentally. The preliminary results show that the finger compliance can be determined by the continuity of the momentum transfer before contacting of an object that balance the disturbances and undesired external forces to grasp an object.



(a)

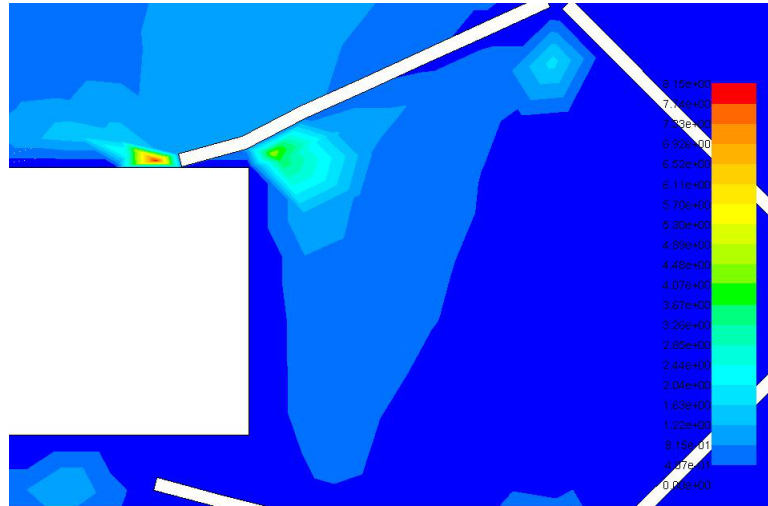


(b)

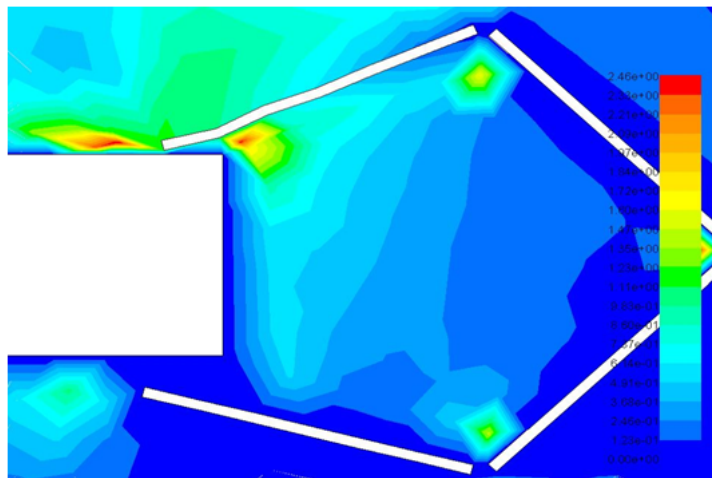


(c)

Figure 4.12: Compliance of an object



(a)



(b)

Figure 4.13: Finger compliance

#### 4.4 Sensitivity analysis

The sensitivity of the numerical simulation is investigated by setting different values of numerical parameters in the simulation. The performance of the system can be evaluated by means of adjusting different angular velocities of the fingers. The total moment vector at the center of gravity of the object according to different angular velocity of the finger approaching on the object is shown in Figure 4.14. In this case, the other computational parameters are not being changed. The initial position of the finger and object are same for both cases. Moreover, initial velocity of the fingers and object are set to zero. The total moment vector on the object pronouncedly increases after the setting the angular velocity of the finger as 0.4 rad/s. This is due to the fact that the external forces around the object may be increased compared to the angular velocity of the finger as 0.2 rad/s. It can be easily concluded that increasing the angular velocities of the fingers leads to more motion tendencies of the object.

To give another example, let us consider the velocity magnitude contour of the square object landing by fingers shown in Figure 4.16. The connectivity of the fluid medium particles changes according to the mesh size. The fluid environment is generated with three different internal mesh sizes. These three internal mesh sizes are specified as 0.1, 0.5 and 1 as shown in Figure 4.16(a)-4.16(c). The angular velocities of the fingers landing on the object are same for three of these cases. The initial position of the hand pre-shaping are same for all three cases. We can conclude from the figure that as the mesh internal size decreases, the momentum distribution on the object increases even if small changes occur of the fingers movement given in Figure 4.16(a). Moreover, the connectivity of the fluid particle increases by decreasing the mesh size as expected. Figure 4.15 shows the total moment at the center of the square object at different time steps. At the beginning of the simulation the total moment at center of the gravity of the object are comparatively similar. However, the rest of the simulation, as seen from the figure, the total moment at the center of the object in the case of the mesh size is given as 0.5 increases more than the others because of the higher connectivity of the fluid particles.



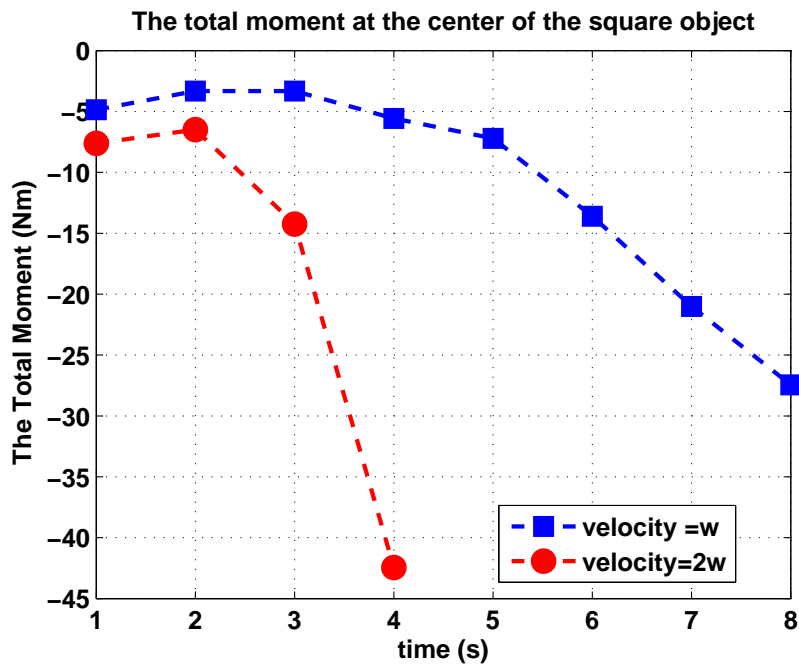


Figure 4.14: The total moment at the center of the square object for different finger velocities landing on an object

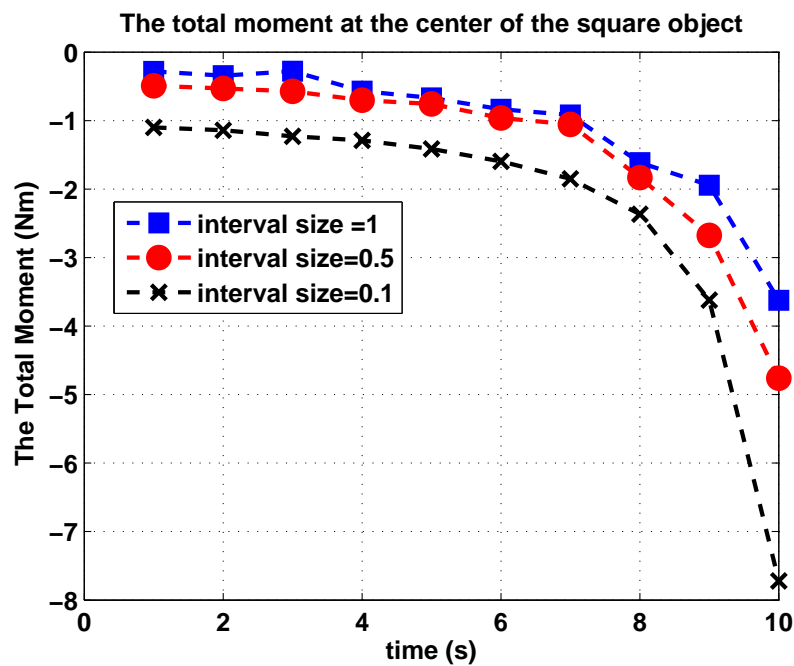
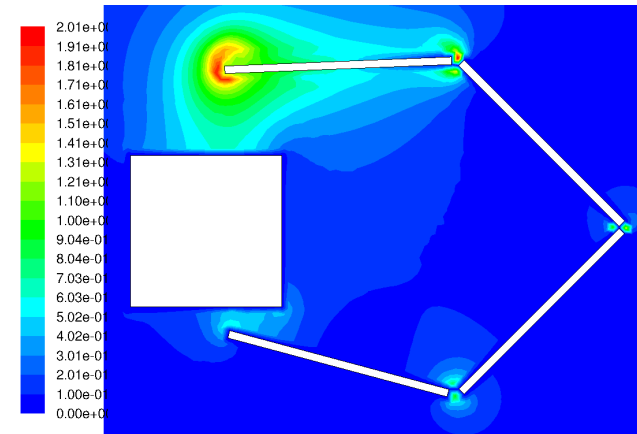
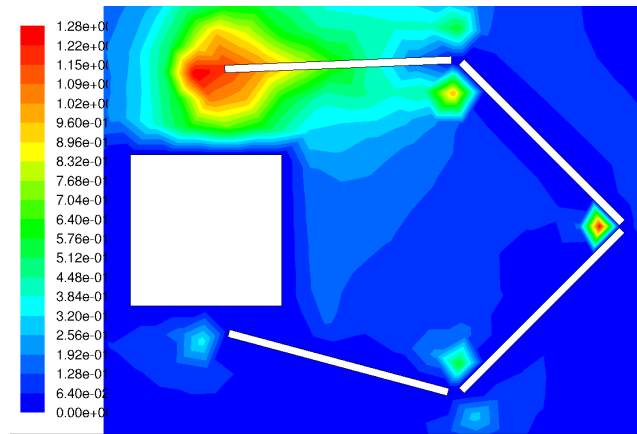


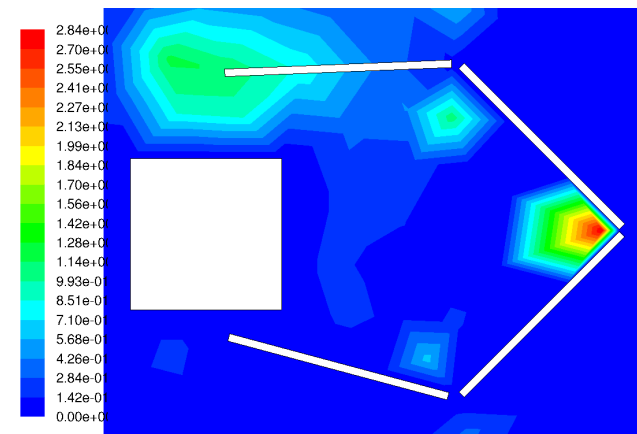
Figure 4.15: The total moment at the center of the square object for different internal mesh size



(a)



(b)



(c)

Figure 4.16: Velocity magnitude contour for different internal mesh size (a) 0.1 (b) 0.5 (c) 1

## 4.5 Conclusion

In this work, a new computational model for investigating the continuum between robot preshapes landing for grasping an object and thus generating the first object motion tendencies to be used in manipulation have been developed. The approach to grasp in a fluid medium has been found to generate the impact force patterns from robot fingers to medium particles and then from these medium particles to the object through analyses based on momentum transfer. We model the continuum of momentum transfer based on fluid dynamics by using finite volume method in order to provide visual simulations. Simulations not only demonstrate the motion tendency of object but also the deformation of the object during the approach of the robot hand just due to momentum transfer within the fluid medium whenever the rigidity of particle connections that model object surfaces is relaxed.

We have demonstrated our method on several examples including different hand preshapes and type of objects. It was shown that the object motion tendencies can be suitable for the proper initiation of the grasping task. The simulation results have supported the accuracy of the model that the continuity between the preshaping to grasping is crucial to initiate the manipulation phase.

## CHAPTER 5

### APPROACH CONTROL FOR UNDERWATER GRASPING

This chapter introduces the learning approach control infrastructure based on the decision support system that is trained to answer the following question during control of robot hand preshaping for grasping to manipulate an object for a given a task:

1. Which type of preshape the robot hand should take, so that for a given initial position and orientation underwater, the hand approach triggers upon impact, a desired moment distribution on the surfaces of an object of known size, location and orientation, so that desired object rotation and translation are obtained
2. From where and with what orientation and fingertip aperture should a given robot hand preshape begin approaching an object of known size, location and orientation, all immersed, such that a desired moment distribution is generated on the object surfaces to yield a desired motion tendency of the object.

#### 5.1 Structure of the Approach Controller

A neurocontroller is designed to generate the controlled approach of hand preshapes in order to trigger the desired object motion. The multilayer perceptron network, which consists of an input layer, hidden layer and output layer, is trained with back-propagation algorithm based on gradient descent method to minimize the mean square error between the desired and actual output of the network.

- Inputs to the system are the desired moment distribution to be generated by approaching fingers, object shape and initial position immersed in the fluid en-

vironment and for Case 1, the initial location and orientation of the robot hand that will begin to approach. For Case 2, this part is replaced by feature of the given preshape adopted by the robot hand.

- Outputs are for case 1, the joint angles of the robot hand fingers, determining the preshape and for case 2, the initial position, orientation of the palm of the preshaped hand.

### 5.1.1 First Goal of the controller: Determining the robot preshape for a desired moment distribution on object

In these experiments, the controller determines the hand preshapes to yield a desired moment distribution on an object that leads to a desired motion tendency. We assume that the initial condition of the hand in terms of position, orientation is given. The input set of the controller is the desired moment vector of the object directed around the z-axis, object location, shape and robot hand initial position and orientation described as  $\{x_1, x_2, x_3, \dots, x_N\}$  where  $[x_{i1}, x_{i2}, x_{i3} \dots, x_{in}]^T \in R^n$  is the feature vector of the  $i$ -th sample of the system represented by  $n$  dimensional vector and  $N$  is the number of the samples. The corresponding output sequence vector described as  $\{y_1, y_2, y_3, \dots, y_n\}$  where  $[y_{i1}, y_{i2}, y_{i3} \dots, y_{im}]^T \in R^m$  is the hand preshape in terms of joint angles represented by  $m$  dimensional vector. Figure 5.1 represents examples of four training input data for different object location. The input and output pairs shown in Figure 5.1 are described by

$$x_i = [M_x, M_y, M_z, Obj_x, Obj_y, Obj_z, R_x, R_y, R_z]^T \quad y_i = [\theta_1, \theta_2, \theta_3, \theta_4]^T \quad (5.1)$$

$$x_1 = [0, 0, -7.21, -5, -0.5, 1, 0, 0, 0]^T \quad y_1 = [45, -45, 158.17, 202.36]^T \quad (5.2)$$

$$x_2 = [0, 0, -5.04, -5, -0.5, 1, 0, 0, 0]^T \quad y_2 = [45, -45, 155.04, 205.24]^T \quad (5.3)$$

$$x_3 = [0, 0, -3.29, -5.5, 0, 1, 0, 0, 0]^T \quad y_3 = [45, -45, 156.03, 204.31]^T \quad (5.4)$$

$$x_4 = [0, 0, -6.13, -4.5, 0, 1, 0, 0, 0]^T \quad y_4 = [45, -45, 157.35, 203.67]^T \quad (5.5)$$

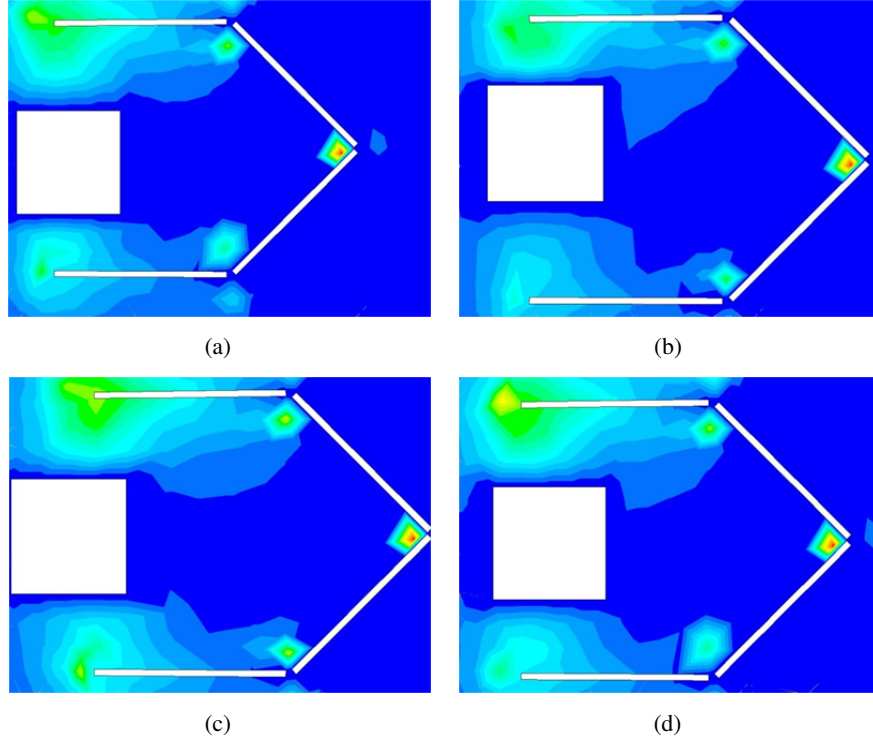


Figure 5.1: Samples of training for different object location (a) and (b) objects location changes along y-axis (c) and (d) object location changes along x-axis.

where  $M_x, M_y, M_z$  are moments,  $Obj_x, Obj_y$  are object locations along the  $x$  and  $y$  axis,  $R_x, R_y, R_z$  are the position of manipulator.  $x_1, x_2, x_3$  and  $x_4$  representing four different input pairs shows that object location changes along  $x$  and  $y$  axis without any rotation. The validation of the system is performed re-applying hand preshapes, obtained from the ANN outputs to the simulations with the same initial conditions. If we look at the error difference between the desired and actual moment shown in Table 5.1, the optimal hand preshaping configuration can be obtained at the desired moment values of  $-7.06$ .

In another experiment, we investigated the optimal hand preshaping where initial position and orientation of the hand preshaping is given for analyzing the effect of moment patterns generated from the fingers. The controller determines the optimal hand preshaping in joint space of the fingers represented as  $\Theta = [\Theta_1, \Theta_2, \Theta_3, \Theta_4]$ . The data set is constructed with 86 different hand preshape in same initial position and orientation according to object position. The input set of the controller is the desired moment vector of the object a given shape (here square) directed around the  $z$ -axis

Table 5.1: The error between desired and actual moment at the center of gravity of the square object.

Joint Angles		Actual Moment(AM)	Desired Moment(DM)	Error ( $ DM - AM $ )
$\Theta_4$	$\Theta_3$			
158.17	202.36	-7.21	-8.34	1.14
155.04	205.24	-5.04	-6.82	1.78
156.53	204.31	-3.29	-4.84	1.55
157.35	203.67	-6.13	-7.06	0.93

that is calculated just before contacting the fingers described as  $\{M_1, M_2, \dots, M_N\}$  where  $M_i \in R^3$  the  $i$ -th sample of the system and  $N$  is the number of the samples. The corresponding output sequence vector is the hand preshape represented by the feature vector in terms of joint angles. 86 samples are used to train the network. 36 different test moment vectors at the center of gravity of the square object are used to analyze the controller. The purpose of collecting data is to train neural network that is capable of generating optimal solution for new input data. The constructed data for the controller is given in Table-5.2. Figure 5.2(a) represents the actual and estimated joint angles of the finger according to the object momentum around the  $z$ -axis after the training the network. Figure 5.2(b) represents actual and estimated two joint corresponding to the total momentum on the object around the  $z$ -axis. The validation of the system is performed by re-applying hand prehapess, obtained from the ANN outputs to the simulations with the same initial conditions. In the case of approaching with different hand preshapes on the object causing similar motion tendencies on the object, the difference error increases as the joint angle  $\Theta_3$  varies between  $180^0$  and  $200^0$ . If we look at the error difference between the desired and actual moment shown in Table-2, the optimal hand preshaping can be obtained at the moment values of -7.924.

For three dimensional case, two different hand preshaping; cylindrical and pinch are used to land on the cubic object surface for analyzing the effect of moment patterns given in Figure 5.7 and Figure 5.8.

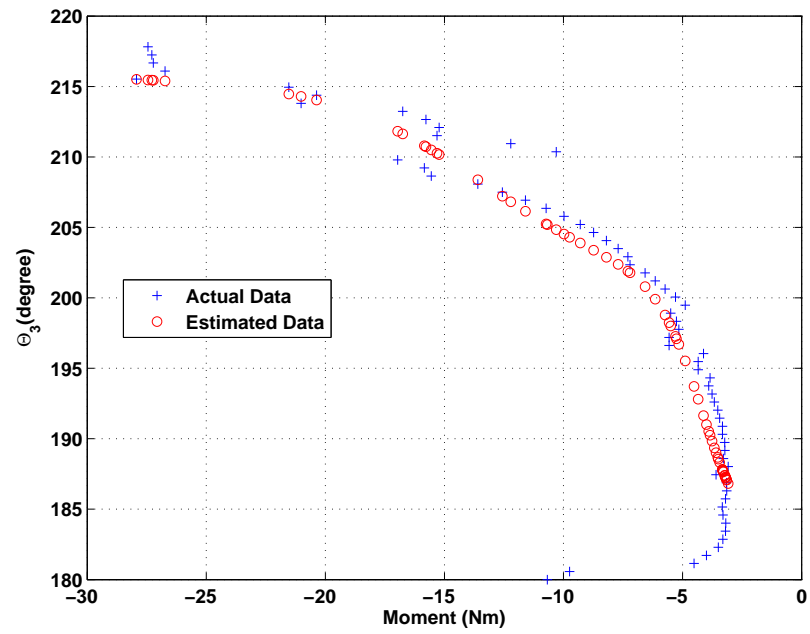
Table 5.2: Constructing Data Set for Decision Support System

	X				Y		
$n$	$\Theta_1$	$\Theta_2$	$\Theta_3$	$\Theta_4$	$M_x$	$M_y$	$M_z$
1	135	180	225	180	0	0	-10.68
2	135	180.57	225	179.81	0	0	-9.64
...	...	...	...	...	...	...	...
N	135	142.57	225	217.57	0	0	-27.45

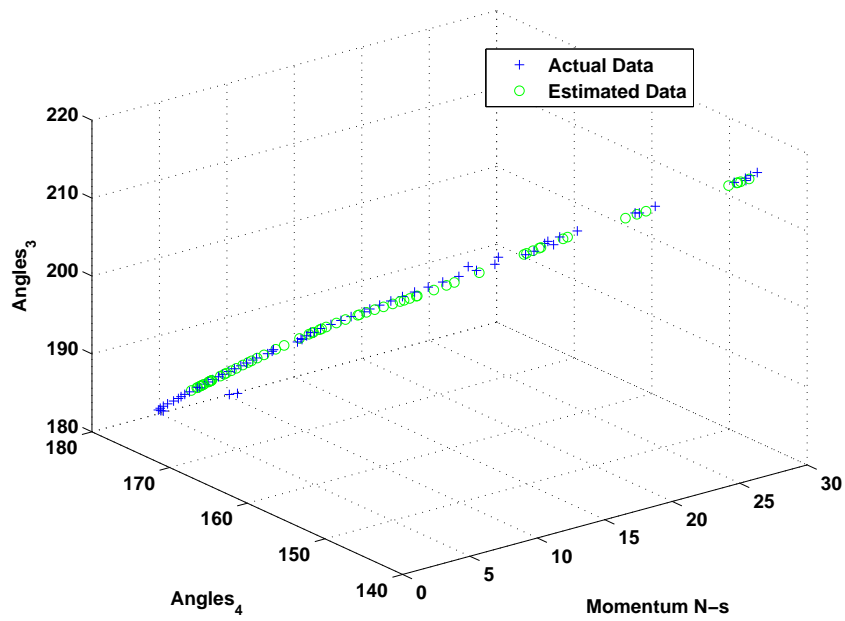
Table 5.3: The error between desired and actual moment at the center of gravity of the square object for Figure 5.2(a)

Joint Angles		Actual Moment(AM)	Desired Moment(DM)	Error ( $ DM - AM $ )
$\Theta_4$	$\Theta_3$			
157.14	202.74	-7.207	-7.489	0.282
156.97	203.90	-7.924	-7.8222	0.102
155.53	203.63	-8.196	-8.846	0.65
149.88	209.96	-13.599	-17.069	3.47





(a)



(b)

Figure 5.2: Analyzing data using back-propagation algorithm (a) momentum versus joint angles of the one link (b) momentum versus joint angles of the both two links

### 5.1.2 Second Goal of the Controller: Determining the initial condition of the robot preshape towards triggering a desired moment distribution on a given object

In the second experiment, given a hand preshape, the controller decides upon the initial position, orientation and aperture of the manipulator to yield the desired moment on the object approached. Figure 5.3 represents six different samples of the training data set for different position, orientation and aperture of hand preshaping. The controller has been trained with 16 different hand preshapes. The input to the controller is again desired moment vector directed around  $z$ -axis, object shape and location and initial robot hand preshape. The output vector is represented by  $Y = [P_x P_y P_z \Phi AP]$  where  $P_x, P_y$  and  $P_z$  are the position of the manipulator, is the orientation of hand preshapes and  $AP$  is the aperture between the fingertips. The desired moment distribution on the object just before landing of the robot hand is given in Figure 5.4(a). As an example of best and worse hand preshaping of velocity magnitude contour is determined from the controller shown in Figure 5.4(b)-5.4(c). If the initial position and orientation of the hand preshaping with different aperture vary, different moment distribution on the object surfaces, thus different motion tendencies is obtained. If we plot the momentum distribution on top and bottom surfaces of the object, we obtain Figure 5.5 indicating that desired moment patterns comparing with the actual ones for each worse and best hand preshaping is completely different. Figure 5.6 demonstrates the error vector based on the Euclidean distance between the actual and the desired output vectors. The minimum difference vector implies the hand preshaping that begins to optimally lands on an object. For this case, the best approximation of given hand preshaped is achieved on the seventh sample.

Another experiment is carried out to analyze the effect of moment patterns generated from fingers landing on a cubic object in 3D case. In this case, the desired moment patterns on the cubic object are shown in Figure 5.7(a). In this experiment, we want to investigate from where optimally a cylindrical hand preshaping should begin closing fingers towards object surfaces so as to generate desired moment distribution leading to motion tendencies of the object. The controller determines the initial position, orientation and aperture of given hand preshape which is in this particular case

cylindrical according to desired moment distribution of Figure 5.7(a). The controller output is given in Figure 5.7(b). The actual moment distribution on the object surface for optimal hand preshape assigned from the controller is given in Figure 5.7(b). From the figure the slight difference between moment patterns can be assessed by the reader which is the error actual.

Another experiment of three dimensional case for pinch grasping is given Figure 5.8. Three fingers, including index finger, middle finger and thumb are used to land on object surface. The desired moment distribution on the object surfaces is given Figure 5.8(a). The actual moment distribution on the object surfaces a given in Figure 5.8(b) for pinch grasping is completely different than the cylindrical grasping. Approaching through the object surface with different hand preshape yields different moment distribution, meaning that object provides different motion tendencies.

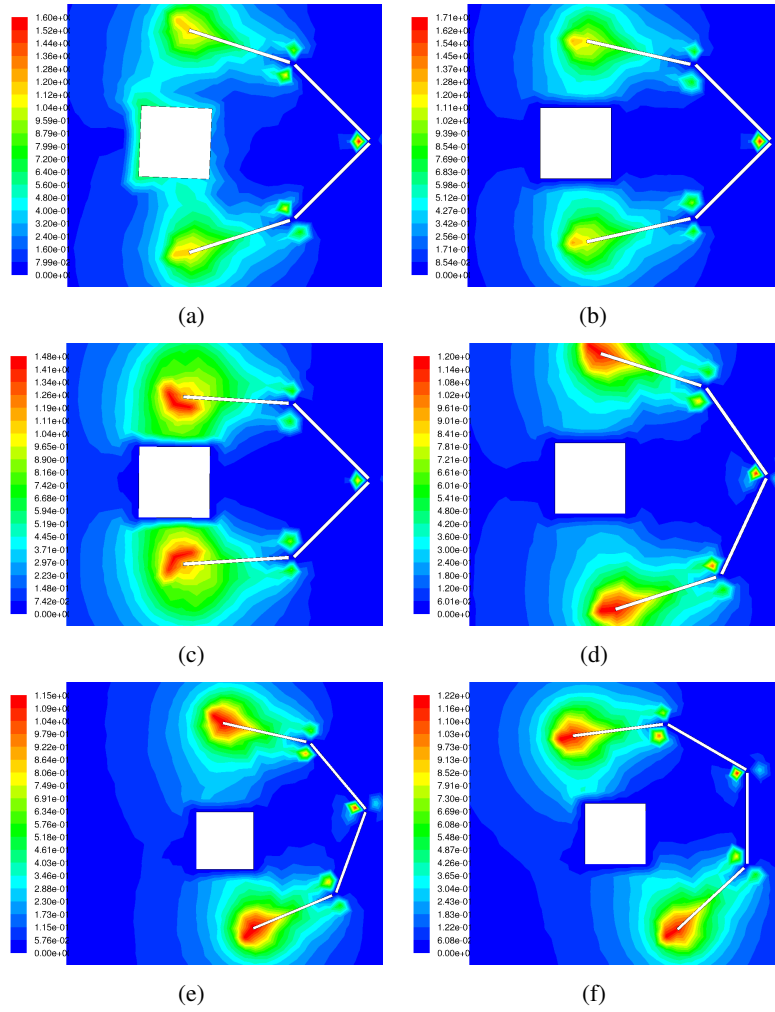
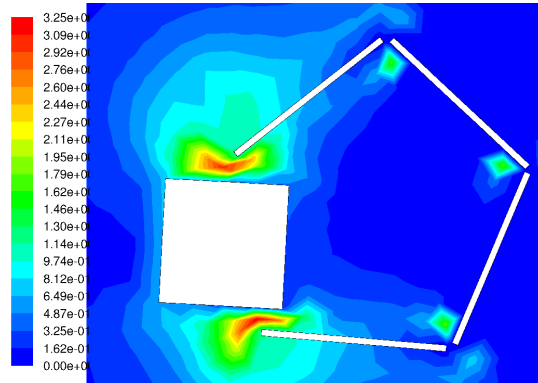
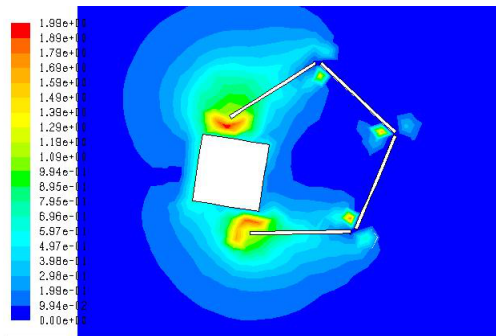


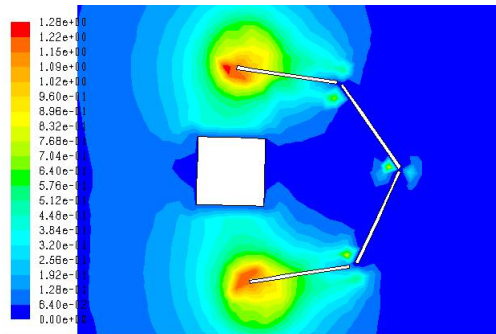
Figure 5.3: Different orientation, preshape and aperture of fingers landing on the object



(a)

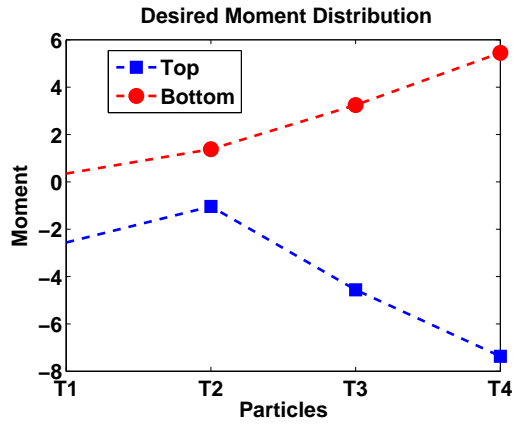


(b)

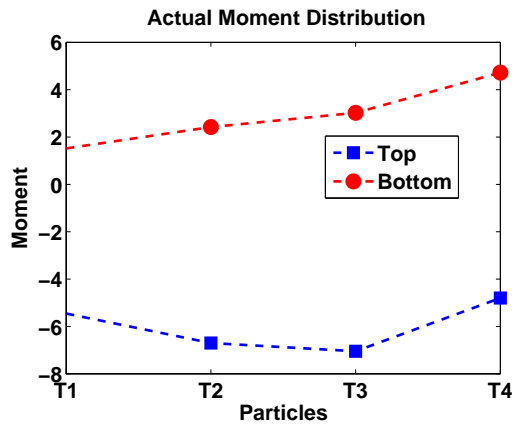


(c)

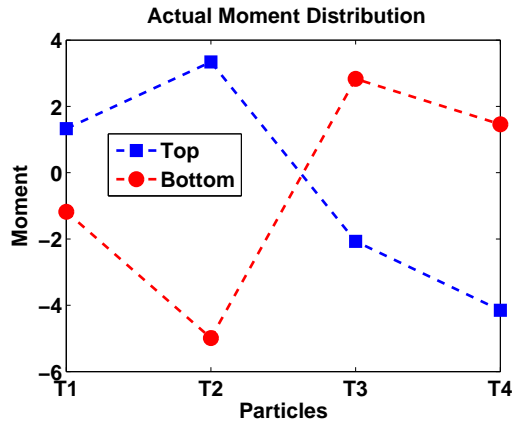
Figure 5.4: Velocity magnitude contour for square object (a) desired moment distribution (b) actual moment distribution of best preshape (c) actual moment distribution of worse preshape



(a)



(b)



(c)

Figure 5.5: Momentum distribution on top and bottom surfaces of the object (a) desired moment distribution (b) actual moment distribution of best preshape (c) actual moment distribution of worse preshape

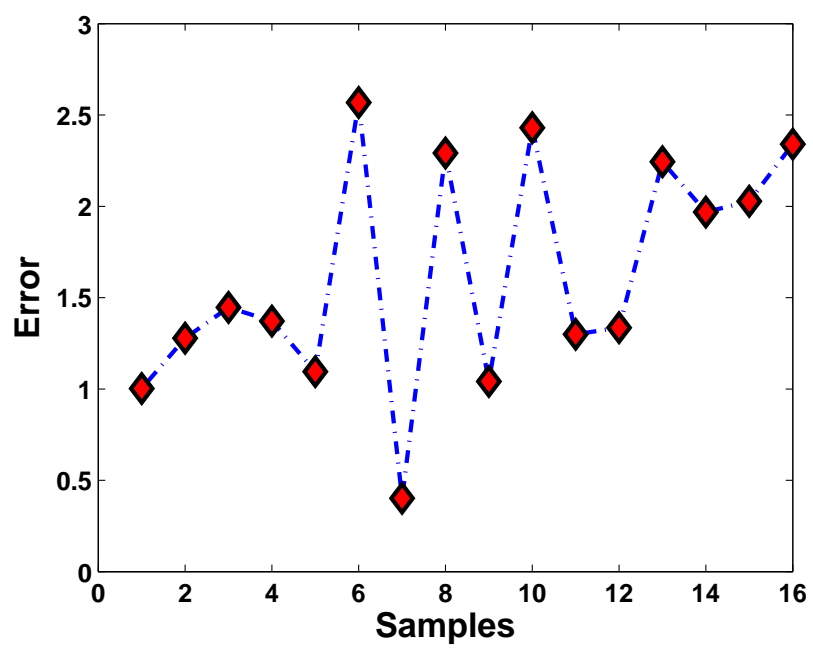
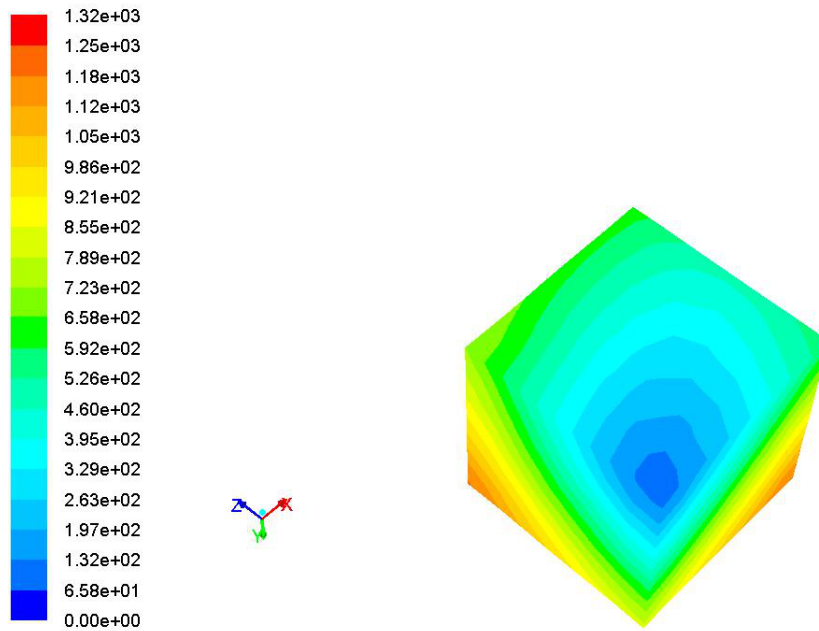
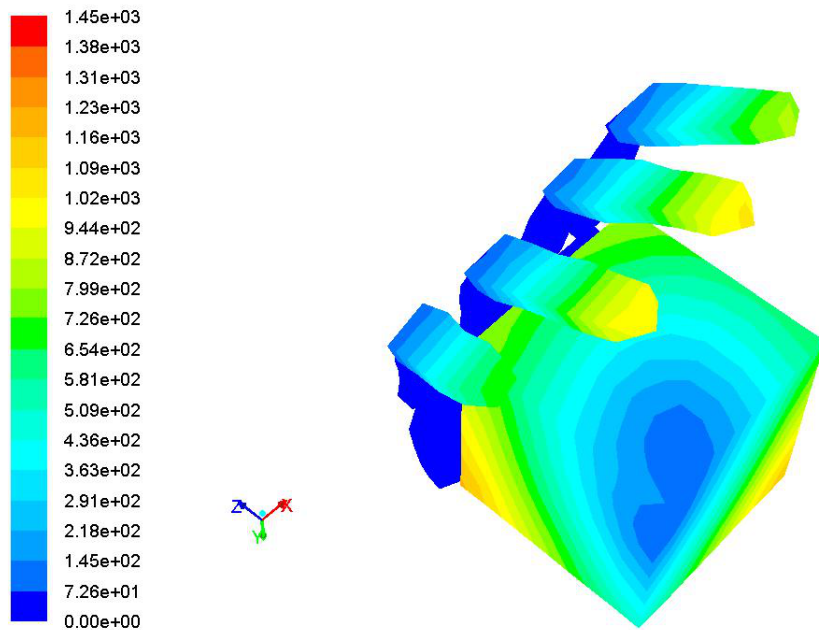


Figure 5.6: Error between the actual and desired output vectors



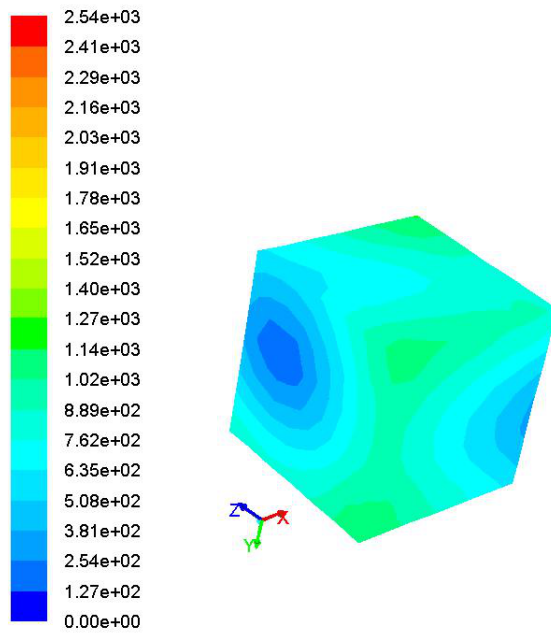
(a)



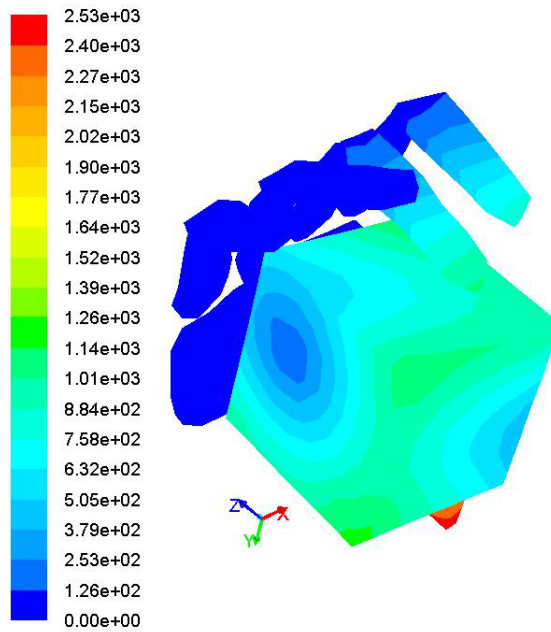
(b)

Figure 5.7: 3d velocity magnitude contour for cylindrical grasp (a) desired velocity magnitude contour motion tendencies of the object (b) actual velocity magnitude contour





(a)



(b)

Figure 5.8: 3d velocity magnitude contour for pinch grasp (a) desired velocity magnitude contour (b) actual velocity magnitude contour

## CHAPTER 6

### DIPPING FINGERS INTO THE WATER TOWARDS A FULLY IMMERSED OBJECT

This chapter enlarges the focus of this thesis work by analyzing of problems of robot hand dipping into the water, with the fingertips moving into the fluid environment towards an object fully immersed in suspension in the water. We investigate the effect of momentum transfer phenomena for dipping the fingers into the water towards an immersed object in shallow water. This work is inspired from the study of water entry of a free-falling solid object and motivated by the fact that for realizing the main aim of the thesis work which focuses on fully immersed robot hand approach onto fully immersed object, the robot hand has first to dip into the water. We assume that fingers are free falling down on a tank filled with water. The velocity of the finger particles increases due to gravitational forces during the falling process. When the fingers touch the water surface, the momentum transfer from the fingers to the water occurs that leads to strong deformation of water surfaces. Dipping fingers into water towards an immersed object, the deformation of the fluid particles increases that transfer momentum from the fluid environment to object the surface. This momentum transfer phenomena lead to modification of object orientation and position at this initial stage of approach evenbefore contacting the object for manipulating it. For that purpose, we propose a new fluidics based methodology to determine a continuum of momentum transfer from the finger particles to the fluid environment particles, then from these particles to object surfaces based on the solid fluid interactions. We model fingers as particles in a solidified environment while the medium affected by the approach of a hand preshape that is closing upon an object, is modeled as a compressible fluid where momentum is propagated until hitting the surface object modeled as a so-

lidified particle medium. Smoothed particle hydrodynamics model (SPH) is used to simulate the general dynamic of fluid flows and momentum transfer between particles of different media. The fingers of the robotic hand are modeled by solidified fluid particles interacting with incompressible surrounding fluids in which fully immersed objects are defined as rigid-body solidified fluid particles. The developed model has been applied, in this chapter, to the simulation of various simple planar robot hand preshaping and the generated momentum transfer profiles of an object surface have been analyzed.

## 6.1 Problem Definition

Our major aim in this section is to generate a single model for the continuum of a hand preshape dipping into water towards an object to create an initial object motion tendency based on the impact forces and torques. These motion tendencies should then be suitable for the proper initiation of the grasping task. The aim is motivated by human like behavior where we preshape and land on an object to initiate a certain grasping behavior without losing the continuum, reducing the energy loss during transfer from "preshaping to grasping" phases, without resetting between the two phases.

In our work, we catch the continuum between preshaped hand impact and initiation of grasping task within the single model of fluid dynamics. The specifications of our problem are :

- Robotic fingers, object, and medium between hand fingers are all modeled as a finite number of particles. Particles form a strongly connected network for which we simplify the number of connected neighbors to each particle by taking only those falling within a finite disc centered at that particle.
- Robotic fingers and objects are modeled as a solidified fluid medium while the volume squeezed by robot fingertips upon entry of the water medium closing upon an object is modeled as a compressible fluid medium.
- We require a meshless approximation of fluid dynamics for simplified com-

putation, where Smoothed Particle Hydrodynamic (SPH) has proven to meet perfectly our approximation needs, which are preliminary 1) not to be obliged to select a grid 2) to be able to constrain the neighborhood of a given particle to particles over finites disc around that particle. This is achieved by the smoothing function of SPH.

## 6.2 Smoothed Particle Hydrodynamics (SPH)Fundamentals

Smoothed Particle Hydrodynamics is a particle based computational method for simulating fluid flows which is mesh free Lagrangian method. The basic fundamental principle of the SPH is an interpolation procedure where an approximation function (Kernel function) is constructed in such a way that it approximates the integration over a finite domain surrounding each particle. This integral approximation is computed over a finite number of particles carrying the discretized fluid metrics of density, pressure, and velocity. The combination of this particle based approximation and the SPH Lagrangian formulation leads to model based quantifications of internal interactions between particles. The SPH methodology has powerful features in handling complex fluid motions including physical effects of fluids such as those under external forces.

We will describe the fundamentals of SPH by introducing its approximated governing equations, representing physical principles, such as conservation of mass and momentum. These governing equations of fluid dynamics are described by a set of differential Navier-Stoke equations in Lagrangian form;

$$\frac{1}{\rho} \frac{dp}{dt} + \nabla \cdot u = 0 \quad (6.1)$$

$$\frac{du}{dt} = -\frac{1}{\rho} \nabla P + g \quad (6.2)$$

where  $\rho$  is the density,  $P$  the pressure,  $u$  the velocity,  $g$  the gravitational acceleration and  $\nabla$  the gradient operator, . The first differential equation (6.1), which is the conservation of mass in Lagrangian form, is represented by density of fluid continuum in

the control volume. The mass contained in the control volume remain constant over time. The momentum equation (6.2) is composed of two force terms; pressure gradient and body forces without considering the viscosity which resists to deformation of fluid flows. The changes of acceleration for each particle occur due to acting external forces (body forces) on the entire of fluid particles. In our case, the external force term is obtained from the closing hand fingers transmitted to the medium.

The integral interpolation of any function  $f(x)$ , approximating it to a finite neighborhood activation domain, is defined as:

$$f(x) = \int_{\Omega} f(x')W(x - x', h)dx'; \quad (6.3)$$

where  $\Omega$  is a 2D disc with a radius equal to  $2h$ ,  $x$  is the position of the center particle,  $x'$  is the position of the neighbor particles of the center particle  $x$  inside disc and  $h$  is the smoothing length which determines the range of particle interaction within a finite neighborhood defining the disc.  $W$  is the smoothing kernel function which has following three properties [99],

- Normalization condition

$$\int W(x - x', h)dx' = 1 \quad (6.4)$$

- Boundary condition

$$\lim_{h \rightarrow 0} W(x - x', h) = \delta(x - x') \quad (6.5)$$

as the neighbor domain limit goes to zero

- Definition of the activation upper limit

$$W(x - x', h) = 0 \quad \text{when } |x - x'| > 2h \quad (6.6)$$

where support domain of smoothing function is  $|x - x'| < 2h$

The smoothing function  $W$  is generally chosen as a Gaussian kernel function in hydrodynamic calculations due to its smoothness and accuracy. The kernel function applied in our study is represented by

$$W(R, h) = \begin{cases} \frac{1}{\pi h^2} e^{-R^2} & R_{ij} \leq 2h \\ 0 & \text{otherwise} \end{cases} \quad (6.7)$$

and  $R_{ij} = \frac{r}{h} = \frac{|x_i - x_j|}{h}$ , where  $R$  is the distance between two particles  $i$  and  $j$  normalized by the smoothing length, and  $r$  is the distance between two particles  $i$  and  $j$ .  $x_i$  and  $x_j$  represent the 2D positions of the  $i$ -th and  $j$ -th particles respectively.

Continuous integration in fluid activities is converted to a discretized form based on the particle approximation in the support domain  $\Omega_i$  by the following equation,

$$f(x_i) = \sum_{j \in \Omega_i} \frac{m_j}{\rho_j} W(x_i - x_j, h) \quad (6.8)$$

where  $m_j$  is the mass and  $\rho_j$  is the density of particle  $j$ . The summation is over particles located within the disc of radius  $2h$  centered at  $x_i$

The approximation of particle density is written in the form of

$$\rho_i = \sum_j^N m_j W(|x_i - x_j|, h) \quad (6.9)$$

where  $\rho$  is density,  $N$  is the number of particles interacting with particle  $i$  in the support domain, and  $m_j$  is the mass of  $j$ -th particle.  $W$  is the interpolation kernel function represented in equation (6.7).

The pressure gradient can be discretized using its symmetric form as

$$\left(\frac{1}{\rho} \nabla \cdot P\right)_i = \sum_j m_j \left( \frac{P_i}{\rho_i^2} + \frac{P_j}{\rho_j^2} + \Pi_{ij} \right) \nabla_i W_{ij} \quad (6.10)$$

where  $P$  is the pressure,  $\rho$  is the density,  $\nabla_i W_{ij}$  is the gradient of the kernel with respect to the position of the particle  $i$  and  $\Pi$  is the artificial viscosity. Artificial viscosity is

added in the momentum equation in order to increase the numerical stability of the approximation and is given in the following form,

$$\Pi_{ij} = \begin{cases} \frac{\beta \cdot \mu_{ij}^2}{\bar{\rho}_{ij}} & \vec{u}_{ij} \cdot \vec{x}_{ij} < 0 \\ 0 & \vec{u}_{ij} \cdot \vec{x}_{ij} \geq 0 \end{cases} \quad (6.11)$$

where  $\beta$  is a constant that we consider 1 in our work and the other variables are defined as:

$$\mu_{ij} = \frac{h_{ij} \vec{u}_{ij} \cdot \vec{x}_{ij}}{r^2 + \eta^2}, \quad \vec{u}_{ij} = u_i - u_j, \quad \bar{\rho}_{ij} = \frac{1}{2}(\rho_i + \rho_j), \quad h_{ij} = \frac{1}{2}(h_i + h_j), \quad \eta^2 = 0.01 h_{ij}^2, \quad (6.12)$$

where  $\vec{x}_{ij}$  is the position difference vector of i-th and j-th particles,  $\vec{u}_{ij}$  is the velocity difference vector of i-th and j-th particles,  $\bar{\rho}_{ij}$  the average density of the particles,  $h_{ij}$  is the average of smoothing length of the particles,  $\eta$  is the constant which is used to prevent singularities of constant  $\mu_{ij}$  and  $r$  is the distance between two particles  $i$  and  $j$ .

Finally, the relationship between pressure and density in compressible fluids are expressed in the following manner

$$P_i = \beta \left[ \left( \frac{\rho_i}{\rho_0} \right)^\gamma - 1 \right] \quad (6.13)$$

where  $\gamma$  is a constant that is often used in astrophysics and  $\beta$  refers to stiffness constant that limits the maximum changes of the density and  $\rho_0$  is the nominal density value.

### 6.3 Modeling Simple Two Fingers Preshapes

In the proof of concept work upon which this work stands, we consider the modeling of simple 2D pinching preshapes of robot grippers as shown in Figure 6.1.

The point O denotes the wrist.  $l_{01}$  and  $l_{02}$  are the lengths of respective fingers.  $\theta$  represents the pinching joint angle. The point of P1 and P2 denote the respective end positions  $(x_{01}, y_{01})$  and  $(x_{02}, y_{02})$  of the links.

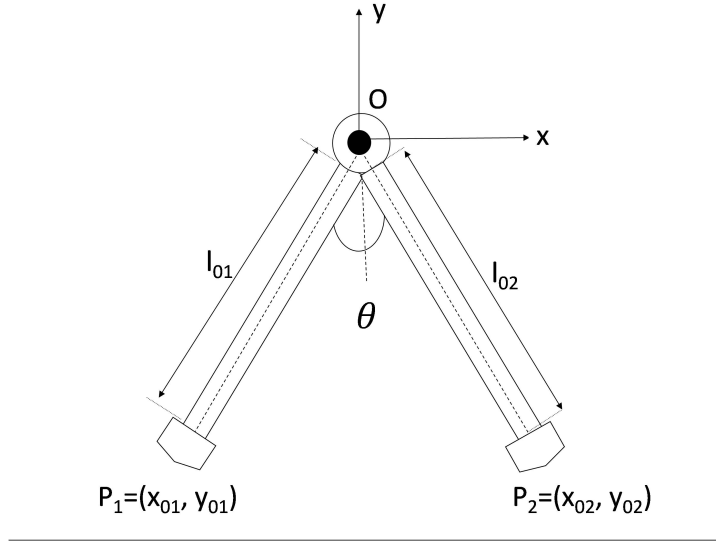


Figure 6.1: 1 DOF planar gripper

Motivated from a totally different work in the literature, referred as [100], we assume now that each link is composed of  $n$  numbers of particles. Each particle location is represented by  $p_k$ . The relative position of each particle to the center  $q_k$  of the link and the inertia  $I$  of the fingers are calculated by

$$p_k = [p_1, p_2, p_3, \dots, p_n] \quad (6.14)$$

$$q_k = p_k - p_c \quad \text{where } p_c = 0 \quad (6.15)$$

$$I = \sum_{k=1}^n |q_k|^2 \quad (6.16)$$

where  $p_c$  represents the center of the link taken as reference point.

The translational ( $T$ ) and rotational ( $R$ ) velocities of the fingers are calculated as

$$T = \frac{1}{n} \sum_{k=1}^n u_k \quad (6.17)$$

$$R = \frac{1}{I} \sum_{k=1}^n u_k x q_k \quad (6.18)$$



where we represent the velocity  $u_k$  of each particle on the links which is calculated by

$$u_k = T + q_k x R \quad (6.19)$$

In the above equation  $x$  denotes the cross product operation. As a result of the above model, we are able to generate and track the motions of the swarm of particle modeled as a rigid-body without deformation.

### 6.3.1 Modeling Solid Objects

Solid object is also composed of fluid particles. The solid 2D object modeled as a swarm particle in a solidified medium is represented as a black solid block of particles in Figure 6.5. These particles are treated as fixed particle that is located in frozen fluidic environment. The velocities of the particles are thus, all set to zero in order to represent the boundary without deforming. In our work, the rectangular object with uniform distribution of particles on its perimeter is used in the simulation. The number of the particles of the solid object is determined experimentally and can be changed. The motion tendency of the object is generated from the momentum transfer from the fingers to the perimeter particles expressed according to center of gravity.

### 6.3.2 Modeling our solid fluid interaction

In this section, we look into boundary conditions of the SPH method in order to model solid fluid interactions of fingers to medium, to object interactions. The fluid flows represented by particle trajectories caused by robot fingers pressing onto the medium are defined by reflection across boundaries in a way adopted from mirror particle approach of reference [100], [101]. In our adopted approach, as the solidified fluid particles of the fingers moves down through the medium, the particles are mirrored across the boundary of the medium when the distance between the particles of the fingertips and boundary particles is less than  $0.1h$ . These mirrored particles in the medium are called "Ghost Particles" shown in Figure 6.2 . In other words, the velocities of the fluid particles or ghost particles are transmitted from the solid particle velocities.

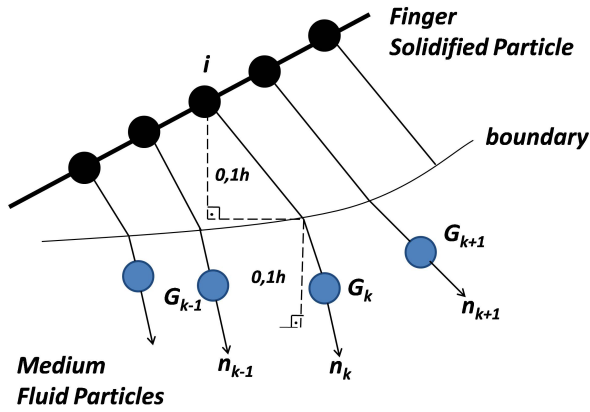


Figure 6.2: The velocity vector for  $i - th$  solidified particle on fingers

Consider solidified fluid particles  $i$  with velocity  $v_i$ . The particle velocity vector is decomposed as a sum of two vectors such as  $v_i^x$  and  $v_i^y$ . If the distance between the particle  $i$  and boundary particles less than  $0.1h$ , interaction begins between the finger and fluid medium and the velocity of particle  $i$  is transferred to the ghost particles. The velocity relationship of the ghost particles indexed as  $G_k$  are determined by the following equations

$$v_{Gk}^n = -v_i^x \quad (6.20)$$

$$v_{Gk}^t = -v_i^y \quad (6.21)$$

where  $v_i$  is the velocity of the solidified particle  $i$ ,  $v_{Gk}^n$  and  $v_{Gk}^t$  is the normal and tangential velocities of the mirrored particle in the medium. This representation is used for the link on the left side of the gripper.

## 6.4 Simulations

In this section, we investigate the proof of concept of our novel approach based on simulation results. We analyze here the momentum transfer from gripper to medium particles to object relevant side on its perimeter. The numerical simulation is inspired from water entry problem of free falling object of reference [100].

2-D compressible SPH is used in the experiments. The total width and height of the 2D fluidic environment is considered as 1 because the initial particle spacing is  $\Delta x = 0.02$ . In total, 2601 fluidic particles are used for generating compressible medium in the numerical simulation. The initial velocities of the particles are all set to zero.  $\gamma$  is a constant typically around 7, stiffness constant  $\beta$  is 1 and nominal density used for water that is  $\rho_o = 1000\text{kg}/\text{m}^3$  in equation (6.13). The joint angle of the robotic fingers is variable for different pinching preshapes. The number of the particle used for rectangular object is 2700 which are represented as a 27 by 100 array.

Each particle has neighboring particles falling within a distance kernel range  $2h$ , the radius of the kernel function being 0.5. The calculation of the distance between particles is updated at every step. Because of huge number of the particles, the computational time cost of the simulation increase significantly. In order to simplify this computational burden, we generate particle connection list identifying the neighbor particle in order to reduce the time cost of the simulation. Particles are stored in cartesian grid cells each having a side length  $2h$  in the list. In order to find the neighbor particles of a given particle  $i$ , we need to search the particles located in its cell as well as in the eight cells around it represented in Figure 6.3. This procedure is used for neighbor search algorithm. By the help of this procedure, the dimension of the interaction list of the particles is reduced leading to a considerable decrease of CPU time.

Figure 6.4 gives the algorithm flow chart of our approach that achieves within a single model the continuum between preshaping and grasp through the momentum transfer. The flow chart starts the initialization parameters of the particle. The initial velocities of all particles are set to zero. An example of initial positions of the robotic fingers,

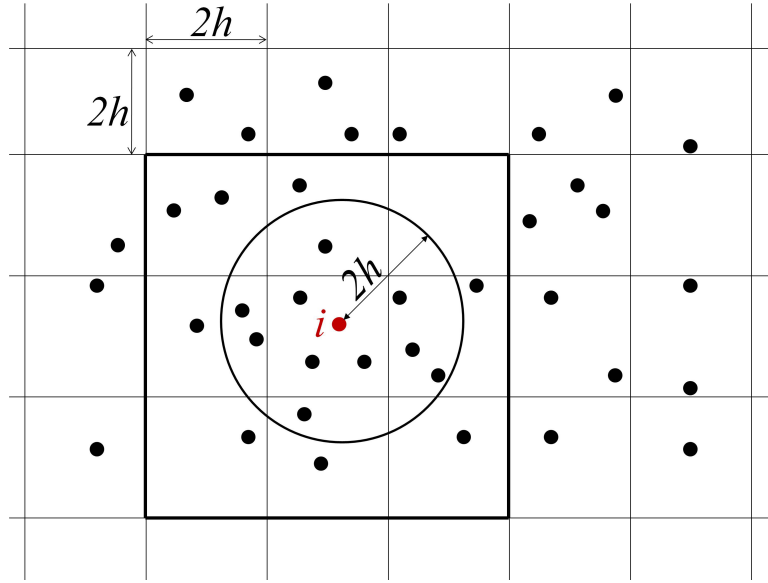


Figure 6.3: Grid based listing neighbor particles

fluid particles, and object are shown in Figure 6.5. No interactions between fingers and medium exist yet in the Figure 6.5(a). As for all initialization, the parameters of medium do not change until the onset of interaction between the solid and fluid particles. The position of the grippers moves down into the medium for the initialization of grasp where robot grippers clip into the fluid medium in a pinching preshape as in Figure. 6.5(d). The momentum transfer from the grippers to the fluidic environment is achieved by the body forces of the gripper in the impacted fluid medium ( Equation 6.2) . The intermediate velocity and position of the medium particles are computed using,

$$u_t = u_{t-\Delta t} + \Delta u \quad (6.22)$$

$$(6.23)$$

$$x_t = x_{t-\Delta t} + \Delta t.u \quad (6.24)$$

where  $u$  is the velocity and  $x$  is the position of the medium particle and  $\Delta t$  represents the time step of the simulation. The visualization of the simulation is used for check-

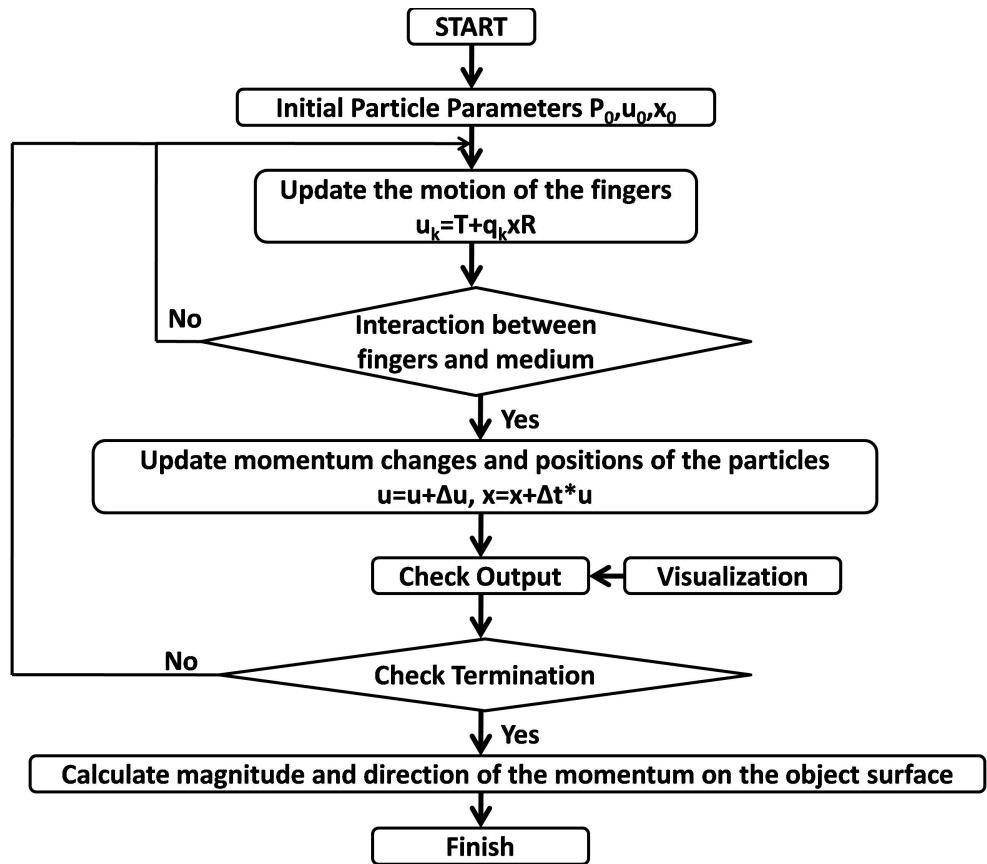


Figure 6.4: Flow chart of Compressible SPH Program

ing motion of particles under the momentum transfer. At the end of the simulation runs, the magnitude and direction of the momentum around a particle on the object side is calculated and displayed as in Figure 6.7.

In the first scenario represented at different steps of the iterations in Figure 6.5 is based on the hand preshape which is a pinching with an angle of  $80^{\circ}$ . The effect of external forces from the fingers to fluidic medium is generated at the instant of first interaction with the medium as shown Figure 6.5(b). Incrementing the time step, the fingers move down into the medium in Figure 6.5(c). The simulation ends when the momentum changes of the particles on the object side are generated as in Figure 6.5(d). Figure 6.6 gives the velocity field of Figure 6.5(d) in terms of magnitude and direction of the fluid motions associated with each particle of the object side. Then the momentum magnitude and phase of each particle of the interacting side of the object is transformed into the momentum with respect to the object center of gravity

seen in Figure 6.7(b), Figure 6.8 and Figure 6.9. The resultant momentum of this distribution at the center of gravity of the object is the sum of all momenta, + or - according to the direction of moving the object to the counterclockwise or clockwise. The resultant generates the object motion tendencies given also in figures 8c and 8f. In Figure 6.7(b), the resultant is almost null and the object has almost no tendency to rotate either to left or right.

Two different initializations of gripper medium interactions based on momentum transfer between the particles are represented in the following two scenarios displayed as Figure 6.8 and Figure 6.9. Fingers approaches to the right side of the object with an angle  $80^\circ$  in Figure 6.8(a) and left side of the object with an angle  $10^\circ$  in Figure 6.9(a). Figure 6.8(b) and Figure 6.9(b) show the maximum momentum changes at the edge of the object. Figure 6.8(d) and Figure 6.9(c) represent the momenta of the edge particles with respect to the object center of gravity. The horizontal axis shows the momentum contribution of each particle on the object side, to the motion of object around the center of gravity. Momentum hitting the object to right is taken as negative (-) and the reverse, positive (+). Fingers is hitting to left and right edge of the object with different preshapes to generate motion tendencies around the center of gravity as also shown in Figure 6.9(d) and Figure 6.8(d).

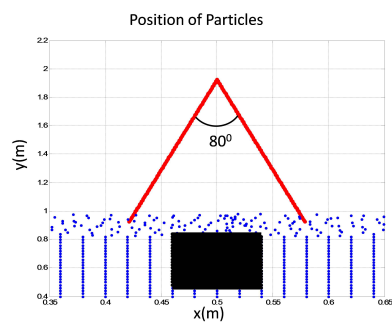
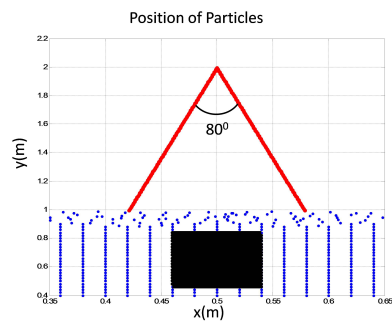
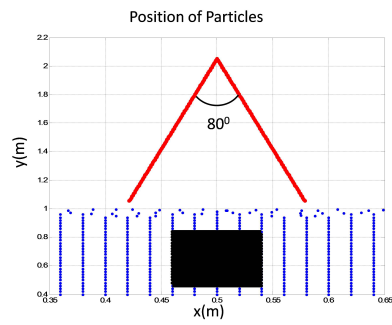
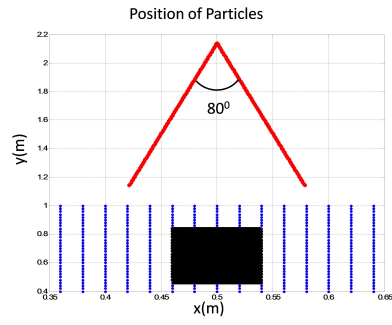


Figure 6.5: Fluidic environment including fluid particles represented by blue dots, robotic fingers red lines, objects black dots. It shows the particle positions during the fingers entry. The angle between the gripper  $\theta$  is equal  $80^\circ$

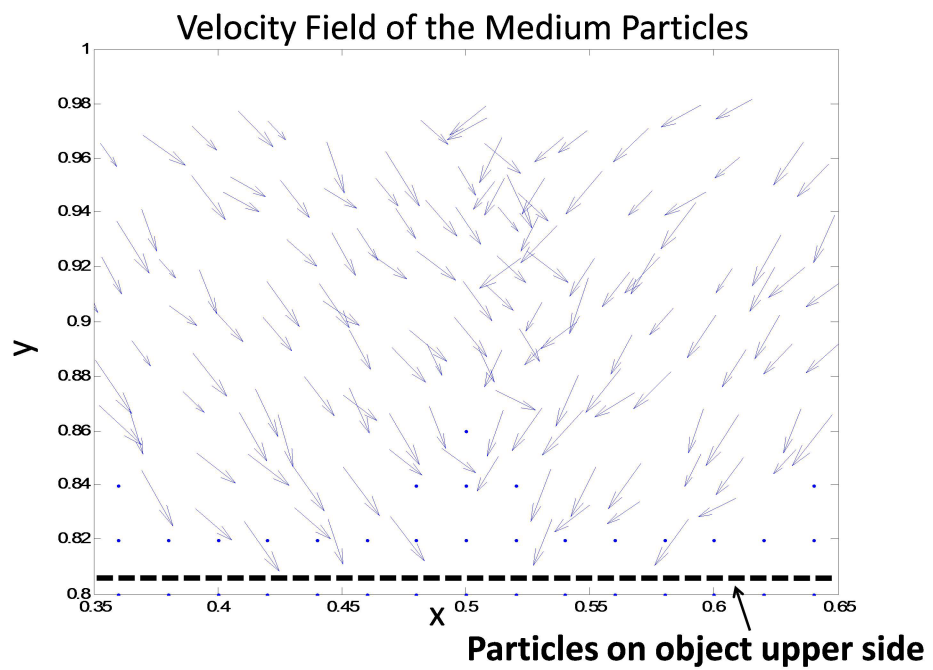
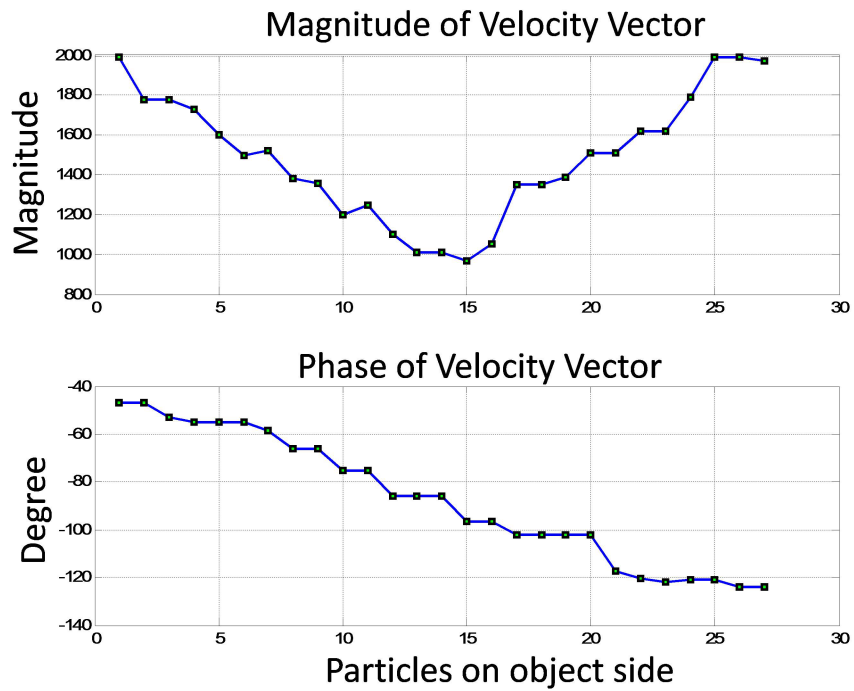
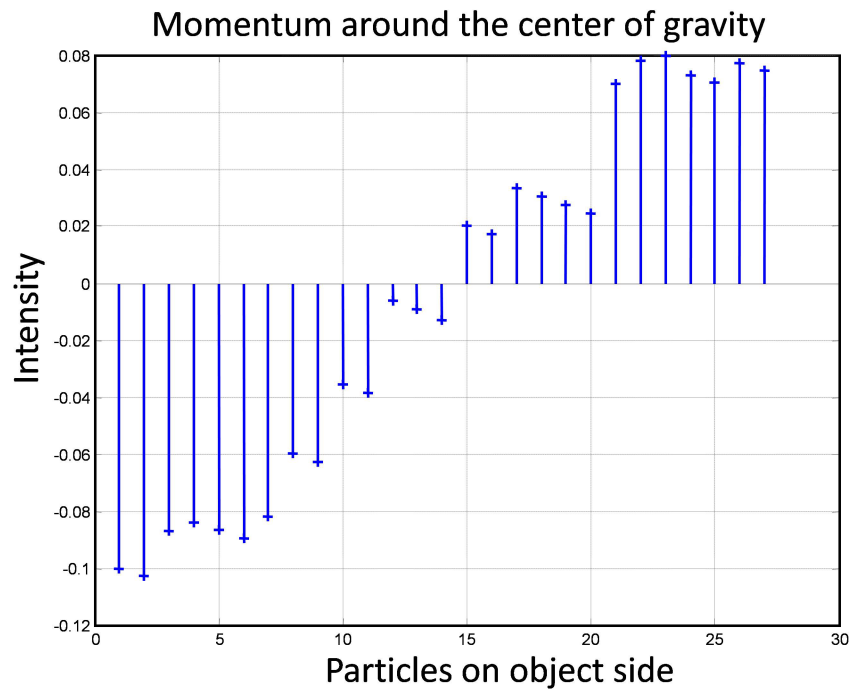


Figure 6.6: shows velocity fields of the particle upper side of the object at the end of the simulation.



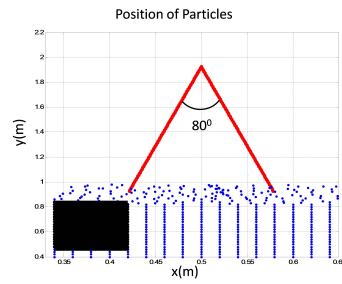


(a)

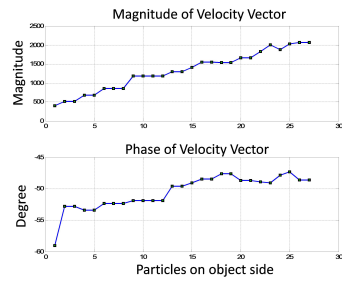


(b)

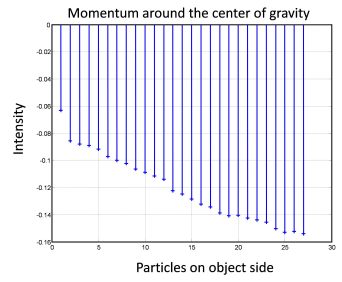
Figure 6.7: (a) shows the magnitude and phase distribution of the velocity vectors applied on horizontal edge of the object. (b) shows the momentum around the center of gravity for each particle upper side of object



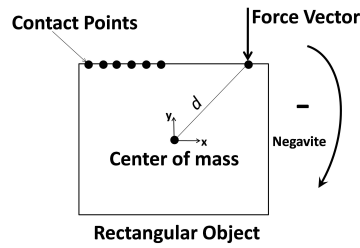
(a)



(b)

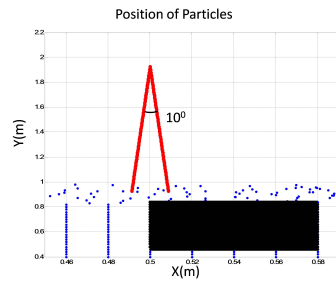


(c)

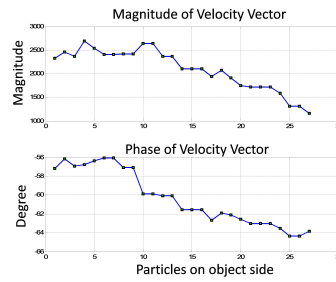


(d)

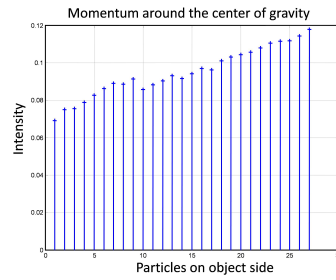
Figure 6.8: Particle positions, phase, and magnitude of the velocity vectors and momentum around the center of gravity for different preshapes and position of the rectangular object. (a) Joint angle between the fingers is  $80^\circ$  (b) shows the magnitude and phase distribution of the velocity vector on the object side(c) shows the momentum distribution around the center of gravity for each particle on the object side



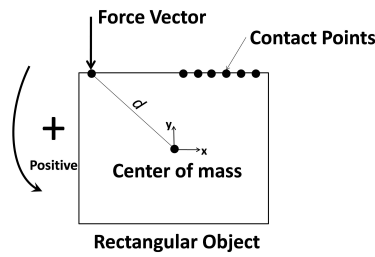
(a)



(b)



(c)



(d)

Figure 6.9: Particle positions, phase, and magnitude of the velocity vectors and momentum around the center of gravity for different preshapes and position of the rectangular object. (a) Joint angle between the fingers is  $10^\circ$  (b) shows the magnitude and phase distribution of the velocity vector on the object side.(c) shows the momentum distribution around the center of gravity for each particle on the object side

## 6.5 Conclusions

In this chapter, we have proposed a new approach to investigate the continuum of the momentum transfer phenomena for dipping fingertip into the fluid medium towards a fully immersed an object. Our concept is based upon the fact that the initial effect of the impact forces and torques on the object can be modeled by using a momentum transfer from the solidified swarm of robot fingers to the fluid medium and then from fluid medium to the solidified fluid swarm modeling the object to be grasped. We modeled the momentum transfer in fingers, medium and object that leads to a motion tendency of an object upon landing on it. We have demonstrated in this work that different simple 2D preshapes differing in their pinching effects, have different momentum transfers on the surface of the object, and thus lead to different motion tendencies of the object. These motion tendencies should then be adequate for the initialization of grasping task. If for example the hitting to the left of the object in Figure 6.9(c) is not the motion required by grasping task that is for example a rotation in the y axis around its center of gravity of the object, then we have to approach the object with a 2D preshape having a pinching angle as given in scenario one in this work because as seen Figure 6.7(b), the object does not tilt to the right or left and stands almost still. This is suitable of initiating stability a rotation in the y axis of the object. If the object is being hit to the right or left as in Figure 6.8 and Figure 6.9, there would be a motion tendency to the right or left along an axis perpendicular to the work surface (the z axis). Wanting also to turn the grasped object around its y axis while the object has a motion tendency in the z axis, there would be an energy loss, requiring more effort to stably rotate it around its y axis.

## CHAPTER 7

### CONCLUSION and FUTURE WORK

In this dissertation, a new computational model based on fluid dynamics have been developed for investigating the continuum between robot preshapes and grasping in order to analyze the initial effect of impact force patterns generated from the fingers to medium and then from the medium to the object to be grasped. The grasping and manipulation phase of multi-fingered robot hand is initialized by adjusting appropriate hand preshaping imply the controlled adjustments of suitable finger configuration according to the object contact position for achieving stable grasping. The initial motion tendencies of the object are caused by the momentum transfer generated from the fingers approaching on the object. The momentum transfer phenomena is modeled based on computational fluid dynamics to determine the continuity of the fluid particles in underwater. These motion tendencies should then be adequate for the initialization of grasping task.

We also model the dipping of the robot fingers (Chapter 6) into the water moving towards an immerse object in shallow water and demonstrate also the continuum of momentum transfer based on fluid dynamics by using finite volume method and Smoothed Particular Hydrodynamics(SPH) in order to provide visual simulations. Simulations results demonstrate that the motion tendency of object vary for different hand preshape since each preshape land on the object with different momentum distribution. Solid-fluid interaction model is used to transfer momenta from fingers to the fluid medium. Moreover, simulations not only demonstrate the motion tendency of object but also the deformation of the object during the approach of the robot hand just due to momentum transfer within the fluid medium whenever the rigidity of particle connections that model object surfaces is relaxed (Chapter 4). Besides all robot

fingers entering into the water are also considered and they demonstrate the momentum transfer to the object being approached immersed in shallow water (Chapter 6).

This dissertation is summarized as follows, details of which are introduced throughout the thesis.

- Appropriate hand preshaping is a crucial issue during the approach of the object since we aim at also using the motion tendency during approach towards the manipulation task just after landing on the object. The aim is to minimize losses in this manipulation task by handling the approach, the landing and the early manipulation phases as a continuum. The need for this continuum is best demonstrated underwater provides also the controller designed to achieve the best preshape and initial conditions of the approach to generate a desired moment distribution on the object. This desired distribution is the fact that desired motion tendency to be used in the early phase of a manipulation task.
- Considering the relationship between hand preshapes and momentum transfer phenomena, we investigate which type of hand preshape and from where this preshape should start, taking which orientation in order to be suitable for the initiation of the manipulation task upon landing on an object. Towards this aim this thesis has demonstrated our method on several examples including different hand preshapes and type of objects with variable cross sections. Simulation results have found to support the need for properly initiating accuracy the continuity between preshaped approaches and landing an object for manipulation. It was shown that object motion tendencies can be only be controlled by suitable preshapes that are properly initiated in the medium based on position, orientation and aperture.
- If the object is deformable, the preshaped approach of a robot hand can also trigger a deformation. Our method modeling robot fingers and object as solidified fluidic element poses a rigidity parameter that can be relaxed for demonstrations an compliant underwater grasps. This thesis also demonstrated the effect of robot hand approaches and grasping on flexible fingers as well as object deformations when enabled by a suitable change in rigidity. Different cases of compliance are also analyzed within the balance of this thesis. One of the

advantages of finger compliance is that hand can better adapt to the grasped object surface reducing the complexity of grasp control of the robot in terms of stability and disturbance handling and easing constraints on contact models on the object.

- We developed a neuro-controller (Chapter 5) that decides upon the hand preshape to be used for landing on the object, so that a desired moment distribution is created on the object during the approach. This decision is then carried out by initiating that hand preshape from a given initial position and orientation. The controller also determines, in the case that a given hand preshape has to be adopted, what is the initial position, orientation and aperture of that given hand preshape so that a desired moment distribution is generated upon approach until the landing of the fingers on the object surfaces.

## **7.1 Future Work**

It is my hope that our proposed approach will be inspired by the further study on grasping an object by multi-fingered robot hand. There are still a lot of problems to be solved in grasping problem. Some topics arising from the thesis that deserve further studies are summarized below:

- In my opinion, our proposed approaches can be applied in underwater grasping and satellite manipulation. Determining optimal initialization for free floating objects with sliding and rolling contacts is absolutely necessary for achieving stable grasping. When the dexterous robot hand is used for these problems, it will be important to study how to optimize the hand preshaping in order to initialize motion tendencies.
- The problem of object deformation due to the applied forces generated from the fingers is interesting topic during the grasping process. Moreover, finger deformation and its grasping ability can be studied further because new generation robotic hands are inspired by human beings and aimed to gain human dexterity. Hence, soft finger model of human fingers will be modeled to adapt the robotic system in daily tasks.

- The continuity model of momentum transfer can also be applied multi-hand assembly underwater and in space for trajectory planning during the approaching phase.
- The development of the sensors is required to realize and implement our proposed approaches into practical application. This might reveal different problems and research in the different areas.
- Our approaches can be used to determine object shapes in the case of the grasping an object in poor visible environment. Some interesting problem arises in the field of object recognition considering the momentum distribution around the object surfaces.



## REFERENCES

- [1] Okamura A.M., Smaby N. and Cutkosky M.R. "An Overview of Dexterous Manipulation", *IEEE International Conference on Robotics and Automation*, pp. 225-262, 2000.
- [2] Supuk T., Kodek T., and Bajd, T., "Estimation of hand preshaping during human grasping", *Medical Engineering and Physics*, 2005;27(9):790-797.
- [3] Miller A.T., S.Knoop H.C., and Allen P., "Automatic grasp planning using shape primitives", *IEEE Intl. Conference on Robotics and Automation*, 2008 pp.1824-1829.
- [4] Chris F., Gurvits L. , and Li Z., "Near-optimal nonholonomic motion planning for a system of coupled rigid bodies", *Automatic Control, IEEE Transactions on* 39.3 (1994): 450-463.
- [5] Bicchi A., "Hands for dexterous manipulation and robust grasping: A difficult road toward simplicity.", *Robotics and Automation, IEEE Transactions on* 16.6 (2000): 652-662.
- [6] Wren D. and Fisher RB., "Dextrous hand grasping strategies using preshapes and digit trajectories", *IEEE International Conference on Systems, Man and Cybernetics*, 1995:910-915.
- [7] Bard C, Troccaz J and Vercelli G., "Shape analysis and hand preshaping for grasping", *IEEE/RSJ International Workshop on Intelligent Robots and Systems*, 1991;(91):64-69.
- [8] Baysal C.V. and Erkmen A.M., "Preshape induced grasp controller for dextrous manipulation with a multifingered robot hand", *IEEE International Conference on Mechatronics*, vol., pp. 78- 83, 3-5 June 2004.
- [9] Erkmen A.M., Erkmen I. and Tekkaya, E., "Optimal Initialization of Manipulation Dynamics by Vorticity Model of Robot Hand Preshaping. PartI: Vorticity Modeling ", *Journal of Robotic Systems*, 17, (2000), p.199-212.
- [10] Jeannerod, M., "The timing of natural prehension movements", *Journal of Motor Behavior*, Vol 16(3), Sep 1984, 235-254.
- [11] Iberall T. and MacKenzie C. L., "Opposition space and human prehension", In S. T. Venkataraman and T. Iberall editors, *Dexterous Robot Hands*, chapter 2, pages 32-54. Springer-Verlag, Berlin, 1990.
- [12] Jeannerod, M., "The formation of finger grip during prehension. A cortically mediated visuomotor pattern.", *Behavioural Brain Research* 19.2 (1986): 99-116.

- [13] Castiello U., "The neuroscience of grasping", *Nature Reviews Neuroscience*, 2005;6(9):726-36.
- [14] Wing AM, Turton A and Fraser C., "Grasp size and accuracy of approach in reaching.", *J Mot Behav*, vol.18, pp.245-260,1986.
- [15] Paulignan Y. , MacKenzie C. , Marteniuk R., and Jeannerod M., " Selective perturbation of visual input during prehension movements", *Experimental Brain Research* , 83(3):502-512, 1991.
- [16] Haggard P. and Wing A.M., " Coordination of hand aperture with the spatial path of hand transport.", *Exp Brain Res*, vol.118, pp. 286-292, 1998.
- [17] Iberall T., and Andrew H.F. "Neural network models for selecting hand shapes." *Hand and brain. Academic Press*, San Diego (1996): 243-264.
- [18] G. Schlesinger, "Der Mechanische Aufbau der Kunstlichen Glieder. In: M. Borchardt et al (Eds.)", *Ersatzglieder und Arbeitshilfen fur Kriedgsbeschadigte und Unfallverletzte. Berlin: Springer*, 321-699. 1919.
- [19] Napier J.R. , " The prehensile movement of the human hand", *Journal of bone and Joint Surgery* ", vol.38, pp.902-913, 1956.
- [20] D. Lyons. "A simple set of grasps for a dextrous hand". *In Proc. Int. Conf. on Robotics and Automation (ICRA)*, pages 588-593. IEEE, March 1985.
- [21] Cutkosky M.R. ,"On Grasp Choice Grasp Models and the Design of Hands for Manufacturing Tasks", *IEEE Transactions on Robotics*, 1989;5(3).
- [22] Cutkosky M.R. and Howe R.D. , "Human grasp choice and robotic grasp analysis". *In S. T. Venkataraman and T. Iberall, editors, Dexterous Robot Hands*, chapter 1, pages 5- 31. Springer- Verlag, Berlin, 1990.
- [23] Cutkosky M. R. and Wright P. K., "Modeling manufacturing grips and correlations with the design of robotic hands." *In Proc. Int. Conf. on Robotics and Automation (ICRA)*, volume 3, pages 1533-1539. IEEE, April 1986.
- [24] Iberall T.," Human prehension and dexterous robot hands", *International Journal of Robotics Research*, 16: 285-299, 1997.
- [25] Iberall T and Arbib MA., " Schemas for the control of hand movements: an essay on cortical localization", *In: Goodale MA Vision and action: the control of grasping*, pp 163 - 180
- [26] Arbib M., Iberall T and Lyons D.," Schemas that integrate vision and touch for hand control",. *In Arbib M and Hansen A (Eds), Vision, Brain and Cooperative Communication*, Cambridge, MA: MIT Press, 1985.
- [27] T. Iberall. "The nature of human prehension: Three dextrous hands in one", *IEEE. In Proc. Int. Conf. on Robotics and Automation (ICRA)*, pages 396-401, Raleigh, NC, 1987.
- [28] T. Iberall, G. Bingham, and M. A. Arbib. "Opposition space as a structuring concept for the analysis of skilled hand movements", In H. Heuer and C. Fromm, editors, *Generation and Modulation of Action Patterns, Exp Brain Res Series 15*, pages 158-173. Springer, Berlin Heidelberg New York, 1986

- [29] T. Iberall and D. M. Lyons., "Towards perceptual robotics"., *IEEE. In International Conference on Systems, Man, and Cybernetics*, pages 147-157, Halifax, Nova Scotia, October 1984.
- [30] Bicchi A., and Kumar V., "Robotic Grasping and Contact: Review", *IEEE International Conference Robotic and Automation*, 348-353 ,2000
- [31] C. Melchiorri and M. Kaneko, "Robot Hands" , *Springer Handbook of Robotics*, Part 15 pages 345-363
- [32] Fukuda H., Fukumura N., Katayama M., and Uno Y., "Relation between Object Recognition and Formation of Hand Shape : A Computational Approach to Human Grasping Movements", *Systems and Computers in Japan*, 2000;31(12):11-22.
- [33] M. Jeannerod, M. A. Arbib, G. Rizzolatti and H. Sakata, "Grasping objects: the cortical mechanisms of visuomotor transformation", *Trends in Neurosciences* , Volume 18, Issue 7, July 1995, Pages 314-320.
- [34] Hoff B., and Arbib M. A. , " Models of Trajectory Formation and Temporal Interaction of Reach and Grasp." *Journal of Motor Behavior*, 25(3): 175-192.
- [35] Arbib MA., Iberall T., and Lyons D., "Neural network model integrating visual and somatic information", *Exp. Brain Research*, 1985; 10:111-129.
- [36] E. Oztop and M. Kawato," Models for the control of grasping", *Sensorimotor Control of Grasping: Physiology and Pathophysiology*, Cambridge University Press ,2009.
- [37] Smeets J.B. and Brenner E. " A new view on grasping." *Motor control*, 1999;3(3):237-71.
- [38] Flash T., and Hogan, N. " The coordination of arm movements: an experimentally confirmed mathematical model ",*Journal of Neuroscience*, 5:1688-1703, 1985.
- [39] Frank R., *Real Robot Hand Grasping using Simulation-Based Optimization of Portable Strategies*, Phd Thesis, May 2007
- [40] Tung, C. and Avi C.K. "Automatic learning of assembly tasks using a dataglove system." *IEEE/RSJ International Conference on Intelligent Robots and Systems*, 1995.
- [41] Sturman, David J., and David Zeltzer. "A survey of glove-based input." *IEEE Computer Graphics and Applications*, (1994): 30-39.
- [42] Chang L.Y., Pollard N.S., Mitchell T. M., and Xing, E.P., "Feature selection for grasp recognition from optical markers." *IEEE/RSJ International Conference on Intelligent Robots and Systems*, 2007.
- [43] Stilman M., Koichi N., Satoshi K., and James J.K. "Planning and executing navigation among movable obstacles.", *Advanced Robotics*, 21, no. 14 (2007): 1617-1634.

- [44] Ozyer B., and Oztop E., "Task dependent human-like grasping," *8th IEEE-RAS International Conference on Humanoid Robots, 2008*, pp.227-232, 1-3 Dec. 2008.
- [45] Ekvall S., and Kragic D. "Interactive grasp learning based on human demonstration",*IEEE International Conference on Robotics and Automation*,pp. 3519-3524 , Vol.4, 2004.
- [46] Rohling R.N. and Hollerbach J.M. " Optimized fingertip mapping for teleoperation of dextrous robot hands", *IEEE International Conference on Robotics and Automation*, 1993:769-775.
- [47] Argall B.D., Chernova S., Veloso M. and Browning B.," A survey of robot learning from demonstration ", *Robotics and Autonomous Systems*, 2009;57(5):469-483.
- [48] Kang S.B., Ikeuchi K., Member S., " Toward Automatic Robot Instruction From Perception Mapping Human Grasps to Manipulator Grasps ", *IEEE Transactions on Robotics*, vol.13, pp. 81-95.
- [49] Tegin J., Ekvall S., Kragic D., Wikander J. and Iliev B., " Demonstration-based learning and control for automatic grasping ", *Intelligent Service Robotics*, 2008;2(1):23-30.
- [50] Markus H., Tim B., and Jianwei Z., "Learning of demonstrated Grasping Skills by stereoscopic tracking of human hand configuration" , *IEEE International Conference on Robotics and Automation*, pp. 2796-2800, 2006.
- [51] Kroemer O., Detry R., Piater J. and Peters J.," Active learning using mean shift optimization for robot grasping", *IEEE/RSJ International Conference on Intelligent Robots and Systems*, 2009:2610-2615.
- [52] Ekvall S. and Kragic D., "Learning Task Models from Multiple Human Demonstrations ", *The 15th IEEE International Symposium on Robot and Human Interactive Communication*, 2006:358-363.
- [53] Kaneko M., Hino Y. and Tsuji T. " On three phases for achieving enveloping grasps-inspired by human grasping",*International Conference on Robotics and Automation*, 1997;(April):385-390.
- [54] Zhu X, Ding H, Member S, Wang J and Member S., " Grasp analysis and synthesis based on a new quantitative measure ", *IEEE Transactions on Robotics and Automation*, 2003;19(6):942-953.
- [55] Pollard N.S., and Lozano-Perez T.; , "Grasp stability and feasibility for an arm with an articulated hand ," *IEEE International Conference on Robotics and Automation* , pp.1581-1585 vol.3, 13-18 May 1990.
- [56] Ascari L, Bertocchi U, Corradi P, Laschi C, "Dario P. Bio-inspired grasp control in a robotic hand with massive sensorial input", *Biological cybernetics*, 2009;100(2):109-28.
- [57] T. Yoshikawa and K. Nagai, "Manipulating and grasping forces in manipulation by multifingered robot hands," *IEEE Trans. Robot. Automat.*,vol. 7, no. 1, pp. 67-77, Feb. 1991.

- [58] Zribi M, Chen J. and Mahmoud M.S., "Coordination and Control of Multi-fingered Robot Hands with Rolling and Sliding Contacts", *Journal of Intelligent and Robotic Systems*, 1999:125-149.
- [59] Montana, D.J., "Contact stability for two-fingered grasps," *IEEE Transactions on Robotics and Automation* , vol.8, no.4, pp.421-430, Aug 1992.
- [60] K. Salisbury and B. Roth, "Kinematic and force analysis of articulated mechanical hands," *ASME J. Mech. Transm. Automat. Design*, vol. 105, pp. 35-41, Mar. 1983.
- [61] B. Barkat, S. Zeghloul and J.P. Gazeau, "Optimization of grasping forces in handling of brittle objects ", *Robotics and Autonomous Systems*, pp. 460-468, vol. 57, no. 4, 2009.
- [62] Hyodo S., Kubo R. and Ohnishi K., "A Stable Grasping and Manipulating Control Method Based on Grasp Plane", *IECON 2006 - 32nd Annual Conference on IEEE Industrial Electronics*, 2006:4030-4035.
- [63] Nguyen V-D., "Constructing force-closure grasps", *IEEE International Conference on Robotics and Automation*, pp. 1368-1373, 1986.
- [64] Bing-Ran Z., and Wen-Han Q., "A general dynamic force distribution algorithm for multifingered grasping," *IEEE Transactions on Systems, Man, and Cybernetics, Part B: Cybernetics* , vol.30, no.1, pp.185-192, Feb 2000.
- [65] K. Salisbury and B. Roth, "Kinematic and force analysis of articulated mechanical hands," *ASME J. Mech. Transm. Automat. Design*, vol. 105, pp. 35-41, Mar. 1983.
- [66] M. Y. Wang and D. M. Pelinescu, "Optimizing fixture layout in a point-set domain," *IEEE Trans. Robot. Autom.*, vol. 17, no. 3, pp. 312-323, Jun. 2001.
- [67] Watanabe T. and Yoshikawa T., "Grasping Optimization Using a Required External Force Set," *IEEE Transactions on Automation Science and Engineering*, vol.4, no.1, pp.52-66, Jan. 2007.
- [68] Buss M., Faybusovich L. and Moore J.B., "Recursive algorithms for real-time grasping force optimization," *IEEE International Conference on Robotics and Automation* , vol.1, pp.682-687 , 20-25 Apr 1997.
- [69] M. Buss, L. Faybusovich, and J., "Moore, Dikin-type algorithms for dextrous grasping force optimization", *International Journal of Robotics Research*, vol.17, pp.831-839 ,1998.
- [70] Buss M, Hashimoto H and Moore JB., "Dextrous hand grasping force optimization", *IEEE Transactions on Robotics and Automation*, 1996;12(3):406-418.
- [71] Zheng X.Z., Nakashima R., and Yoshikawa T., "On dynamic control of finger sliding and object motion in manipulation with multifingered hands", *IEEE Transactions on Robotics and Automation*, 2000;16(5):469-481.
- [72] Phoka T. and Pipattanasomporn P., "Niparnan N, Sudsang a. Regrasp Planning of Four-Fingered Hand for Parallel Grasp of a Polygonal Object", *IEEE International Conference on Robotics and Automation 2005*;(April):779-784.

- [73] Chen J and Zribi M. , "Control of Multifingered Robot Hands with Rolling and Sliding Contacts", *The International Journal of Advanced Manufacturing Technology* vol.16 , no.1, pp. 71-77, 2000.
- [74] Cole A. A., Hsu P. and Sastry S.S., "Dynamic control of sliding by robot hands for regrasping", *IEEE Transactions on Robotics and Automation*, 1992;8(1):42-52.
- [75] Erkmen A.M. and Durna M., "Genetic algorithm-based optimal regrasping with the Anthrobot 5-fingered robot hand," *IEEE International Conference on Robotics and Automation*, vol.4, vol.4, pp.3329-3334, 16-20 May 1998.
- [76] Nenchev D.N. and Yoshida K., " Impact Analysis and Post-Impact Motion Control Issues of a Free-Floating Space Robot Subject to a Force Impulse", *IEEE Transactions on Robotics*, 1999;15(3):548-557.
- [77] Dechev N., "Multiple finger, passive adaptive grasp prosthetic hand", *Mechanism and Machine Theory*, 2001;36(10):1157-1173.
- [78] Becker J.C., and Thakor N.V. "A study of the range motion of human fingers with application to anthropomorphic designs", *IEEE Trans. Biomedical Eng.*, vol. 35, pp. 110-116, 1998.
- [79] Delp S. L., Komattu A. V., and Wixson R. L., " Superior displacement of the hip in total joint replacement: Effects of prosthetic neck length, neck-stem angle, and anteversion angle on the moment-generating capacity of the muscles", *Journal of Orthopaedic Research*, vol. 12, pp. 860-870, 1994.
- [80] Yong Cui and Sarkar N., "A unified force control approach to autonomous underwater manipulation," *IEEE International Conference on Robotics and Automation* , pp.1263-1268 vol.2, 2000.
- [81] Lee M. and Choi H.S., "A robust neural controller for underwater robot manipulators", *IEEE Transactions on Neural Networks* , 11(6):1465-70, 2000.
- [82] Utsumi M., Hirabayashi T., and Yoshie M., "Development for teleoperation underwater grasping system in unclear environment", *International Symposium on Underwater Technology*, pp. 349- 353, 2002.
- [83] Garcia, J.C., Fernandez J.J., Sanz P.J. and Marin R., "Increasing autonomy within underwater intervention scenarios: The user interface approach," *4th Annual IEEE Systems Conference*, pp.71-75, 5-8 April 2010.
- [84] Lane D.M., Davies J.B.C., Casalino G., Bartolini, G., Cannata, G., Veruggio, G., Canals M., Smith C., O'Brien D.J., Pickett M., Robinson G., Jones D., Scott E., Ferrara A., Angelletti D., Coccoli M., Bono R., Virgili P., Pallas R., Gracia E., "AMADEUS: advanced manipulation for deep underwater sampling," *Robotics and Automation Magazine*, vol.4, no.4, pp.34-45, Dec 1997.
- [85] Qingxin M., Hua W., Ping L., Liquan W. and Ze H., "Dexterous Underwater Robot Hand: HEU Hand II", *IEEE International Conference on Mechatronics and Automation*, pp.1477-1482, 25-28 June 2006.

- [86] Yoshinada, H.; Yamazaki, T.; Suwa, T.; Naruse, T.; Ueda, H.; , "Seawater hydraulic actuator system for underwater manipulator," *Fifth International Conference on Advanced Robotics*, 1991. , pp.1330-1335 vol.2, 19-22 Jun 1991.
- [87] J. Davies, D. Lane, G. Robinson, D. O'Brien, M. Pickett, M. Sfakiotakis, and B. Deacon, I., "Subsea applications of continuum robots", *Proc. ISUT*, Apr. 15-17, 1998, pp. 363-369.
- [88] Yuh, J., "Design and Control of Autonomous Underwater Robots: A Survey", *Autonomous Robots*, vol.8(1), pp.7-24, 2000.
- [89] M.R.Pac, A.M.Erkmen and I.Erkmen, Control of Robotic Swarm Behaviors based on Smoothed Particle Hydrodynamics, *Proc IEEE/RSJ International Conference on Intelligent Robots and Systems* , 2007.
- [90] Zarzhitsky, D., Spears, D.F., and Spears, W.M., "Swarms for chemical plume tracing", *IEEE Swarm Intelligence Symposium*, pp. 249- 256, 8-10 June 2005
- [91] Shimizu M., Ishiguro A., Kawakatsu T., Masubuchi Y., and Doi M., "Coherent swarming from local interaction by exploiting molecular dynamics and stokesian dynamics methods," *IEEE/RSJ International Conference on Intelligent Robots and Systems*, pp. 1614- 1619 vol.2, 27-31 Oct. 2003.
- [92] W. Kerr, D. Spears, W. Spears, D. Thayer, "Two Formal Gas Models for Multi-Agent Sweeping and Obstacle Avoidance, Formal Approaches to Agent Based Systems," *Lecture Notes in Computer Science*, Springer- Verlag, pp. 111-130, 2004.
- [93] J. R. Perkinson and B. Shafai, "A Decentralized Control Algorithm for Scalable Robotic Swarms Based on Meshfree Particle Hydrodynamics", *In Proceedings of the IASTED International Conference on Robotics and Applications*, 2005, pp. 102-107.
- [94] Tilki U., Erkmen I. and Erkmen M.A., "Imitation of basic hand preshapes by fluid based method: fluidics formation control", *Turkish Journal of Electrical Engineering and Computer Science*, 19, (2011), 221-234.
- [95] B. Ozyer, I. Erkmen and A. Erkmen, "Catching continuum between Preshape and Grasping based on Fluidics", *Proceedings of the ASME 2010 10th Biennial Conference on Engineering System Design and Analysis*, July 12-14, 2010.
- [96] Versteeg H.K and Malalasekera W, "An Introduction to Computational Fluid Dynamics: the finite volume method", *Prentice Hall*, 2007.
- [97] J. Y. Murthy, W.J Minkowycz, E.M. Sparrow and S.R. Mathur, "Survey of Numerical Methods", *Handbook of Numerical Heat Transfer*, (2006).
- [98] Gambit 2.2 Tutorials, 2002
- [99] J. Monaghan, "Smoothed particle hydrodynamics ", *Annu. Rev. Astron, Astrophys*, vol.30(1), pp. 543-574.
- [100] S. Shao, "Incompressible sph simulation of water entry of a free-falling object", *International Journal for Numerical Methods in Fluids*, vol.59(1) pp. 91-115.

- [101] G. Oger, M. Doring, B.A., and P.Ferrant, "Two-dimensional sph simulations of wedge water entries ", *Journal of Computational Physics* , vol. 213(2), pp. 803–822, 2006.



# CURRICULUM VITAE

## PERSONAL INFORMATION

Surname, Name : Özyer, Barış  
Nationality : Turkish (TC)  
Date and Place of Birth : 24 August 1978 , Ankara, TURKEY  
email : bozyer@eee.metu.edu.tr, bozyer@gmail.com

## EDUCATION

Degree	Institution	Year of Graduation
PhD	:METU, Electrical and Electronics Engineering	2012

## WORK EXPERIENCE

Year	Place	Enrollment
2002–Present	: METU, Department of Electrical and Electronics Eng.	Research and Teaching Assistant
2007–2008	: HRCN Laboratory, Japan	Intern

## FOREIGN LANGUAGES

Turkish	Native
English	Advanced
Japanese	Beginner

## PUBLICATIONS

1. B. Ozyer, İ. Erkmen, and A. M. Erkmen *Momentum Transfer From Preshape to Grasping: Initiating underwater the controlled motion tendencies on object to be grasped by the approach of a robot hand preshaped*, submitted to journal
2. B. Ozyer, İ. Erkmen, and A. M. Erkmen, *Momentum Transfer From Preshape to Grasping*, International Conference on Intelligent Robots and Systems (IROS), Workshop: Beyond Robot Grasping - Modern Approaches for Dynamic Manipulation, Oct, 2012
3. B. Ozyer, İ. Erkmen, and A. M. Erkmen, *En uygun robot eli sekli ile yaklaşıarak nesne kavranması*, EEE 20. Sinyal İşleme ve İletişim Uygulamaları Kurultayı, April 2012, Muğla, Turkey.
4. B. Ozyer, İ. Erkmen, and A. M. Erkmen, *Catching continuum between Preshape and Grasping based on Fluidics*, Proceedings of the ASME 2010 10th Biennial Conference on Engineering System Design and Analysis, ESDA 2010 , Istanbul, Turkey, July 12-14, 2010
5. E. Oztop, B. Ozyer, E. Uğur , and M. Kawato, *From human grasping to robot grasping*, Neuroscience Research vol.65 pp.183-183, 2009 (SCI)
6. B. Ozyer, E. Oztop, G. Cheng , and M. Kawato, *Biologically Inspired Grasping*, Neuroscience Research vol.61 pp.815-815, 2008 (SCI)
7. B. Ozyer, E. Oztop *Task Dependent Human Like Grasping*, IEEE 8th IEEE-RAS International Conference on Humanoid Robots pp. 227-232, December 1-3, 2008, Daejeon, Korea